NANOPARTICLE-MEDIATED DELIVERY OF ANTIBODIES AND/OR RNA FOR GENE REGULATION IN TRIPLE-NEGATIVE BREAST CANCER

by

Megan Ngoc Dang

A dissertation submitted to the Faculty of the University of Delaware in partial fulfillment of the requirements for the degree of Doctor of Philosophy in Biomedical Engineering

Fall 2022

NANOPARTICLE-MEDIATED DELIVERY OF ANTIBODIES AND/OR RNA FOR GENE REGULATION IN TRIPLE-NEGATIVE BREAST CANCER

by

Megan Ngoc Dang

Approved: _____
Kristi Kiick, Ph.D.
Chair of the Department of Biomedical Engineering

Approved: _____
Levi Thompson, Ph.D.
Dean of the College of Engineering

Approved: _____
Louis F. Rossi, Ph.D.
Vice Provost for Graduate and Professional Education and
Dean of the Graduate College

I certify that I have read this dissertation and that in my opinion it meets the academic and professional standard required by the University as a dissertation for the degree of Doctor of Philosophy.

Signed: _____

Emily S. Day, Ph.D.
Professor in charge of dissertation

I certify that I have read this dissertation and that in my opinion it meets the academic and professional standard required by the University as a dissertation for the degree of Doctor of Philosophy.

Signed: _____

Millicent O. Sullivan, Ph.D.
Member of dissertation committee

I certify that I have read this dissertation and that in my opinion it meets the academic and professional standard required by the University as a dissertation for the degree of Doctor of Philosophy.

Signed: _____

Catherine A. Fromen, Ph.D.
Member of dissertation committee

I certify that I have read this dissertation and that in my opinion it meets the academic and professional standard required by the University as a dissertation for the degree of Doctor of Philosophy.

Signed: _____

April M. Kloxin, Ph.D.
Member of dissertation committee

ACKNOWLEDGEMENTS

Thank you first and foremost to my advisor, Emily. I am truly grateful that you have always believed in me from the beginning. Especially at the start I was so timid and unsure, but as time went by, I realized how much you were there to help guide and support me as a scientist and an individual. There's been so many times where you've had my back and I can't thank you enough for these past 5 years. I appreciate your enthusiasm for my personal and professional growth – it goes a long way! You've taught me to take the wins and be proud of my accomplishments. I will miss having such a strong advocate and hope to have that moving forward. Next thank you to Jil, Danielle, Jason, Chintan, Ritu, Shoaib, Maggie, and Benjamin for being such a great group of scientists from who I have had the privilege to learn from. A special thank you to Rachel R. for taking me under your wing 5 years back and trusting me to help you wrap up some of your studies as I got the change to train with you. To think I'm now where you were standing! A huge thank you to the day to day lab crew mates I have privilege to call my colleague and friends: Kejian, Jenna, Mackenzie, N'Dea, Elise, Eric, Sara. I honestly count my blessings on the fact we had each other during the covid shutdowns and through our time now. Jenna, for being there whenever things are tough and I need to process my thoughts out loud. Mackenzie, for being the best cubbie mate ever! N'dea, for always getting us up and social. Elise, I'm so glad we have bonded over books, the k-universe, and everything in between! So glad Karrie and you always invite me over on the whim. Sara, I hope you find a fellow cat lover. Eric, I appreciate all the small conversations making me come out of my

introvert shell. Kejian, I'm forever grateful for your willingness to learn and help us out in the lab and for having random chats in between. John and Catherine, I consider you guys as my adopted lab mates from DTP to APBio! Thank you to others within the BME department including Shantanu, Zeinab, Rachel G., Katie, Brielle, George, Alexis, Max, Jamie, Meghan and colleagues I have connect with through CBI – particularly Dr. Grimes for another platform to share my work over the years. Stephanie, thank you for your enthusiasm and coordinating fun events for us all! To my committee members, I appreciate all the time you have given to me in hearing my work and providing invaluable feedback. Thank you for the nuggets of encouragement through my career – it may have seemed small, but they boosted my confidence and excitement. Thank you to undergraduates Carolina Gomez Casas, Sejal, Suri, Elizabeth Pappas, Liza Guner, and Gianna Stigliano. I'm so glad to have mentee such amazing trainees and all the best for your futures. Special shout-out to Carolina and Sejal. You both started with me early in your undergraduate careers and stuck with me through out. Lab was a lot more fun with you guys around and I can't wait to see what research you guys will accomplish in graduate school! To the OLAM staff: Gwen, thank you so much for working closely with me as a figured out how to be a mouse surgeon. Christine and Laura, thank you so much for your time in taking care of the mice on the daily. To other UD/DBI staff: Yuhan, thank you for showing me the ICP-MS. Shannon, for getting TEM images. Sylvain, for always being willing to go through the multiphoton imaging with me every time I attempt to visualize nanoshells. To the DnD crew: Wade, Dan, Michael, Ellen, John, Ryan, Andrew, Michael thank you for taking in Saorise/Horseshoe for the past 3 years – we saved Humblewood! Special thanks to Wade for all of the game nights, Ellen for random movie nights and

Dan for feeding into my need to get kittens friends. To Cindy and Min. I joke that we became friends because we were all short so the first few days of classes we were always walking behind everyone else. Cindy, you have seen me through it all, the bad, the good, the ugly. To all the future spontaneous futures to come. Min, I'm so so happy to have lived with you for the past 4 years! Thank you for all the random food deliveries and late night talks. To the Fab5 cousin crew: Chi Tu, Chi Gia Linh, Tue, and Bao. Seriously, I don't know what I would have done without you all in 2020. I couldn't ask for better peeps to take holiday trips or dress up for Halloween. To the Counsel: Faith, Ebony, Ruth, Noriko, Emma. Thank you for being my Maryland homebase. Special shout-out to Faith for inspiring me to go for my PhD and being such a good listener for all of my struggles and success through this time! Ebony, we never fail to pick up the phone for each other and I can't be more grateful to have such a steady friend in my life. Now it's my turn to return the favor and I'll be there for your PhD journey! To my other lifelong friends: Jessica, Becky, Emilia. Jessica, thank you for being my go for car phone calls and your friendship for 10+ years now! Becky, who would have thought we'd be where we are now today? Thank you for being down to catch up for even short periods of time! Emilia, nothing beats the time we spent as roommates and I'm so grateful for our annual NYC trips. Last but not least to my family. Ba Mẹ Bảo cám ơn rất nhiều. Thank you for loving me unconditionally and making sure I was supported and am still am day to day. It means the world to me knowing I can always rely on you, and I can't express my thanks enough. Ba, for always feeling proud of me and supporting all my accomplishments. Me, for showering me with love given through food. Bao, for being there to chat about literally everything and being supportive of all my decisions.

TABLE OF CONTENTS

LIST OF TABLES xii
LIST OF FIGURES xiii
ABSTRACT xxii

Chapter

1 INTRODUCTION 1

1.1 A Brief Introduction to Cancer History of Triple-Negative Breast Cancer 2

1.1.1 Introduction to Triple-Negative Breast Cancer 3
1.1.2 Current Treatment Strategies for Triple-Negative Breast Cancer 6
1.1.3 miR-34a and Wnt Signaling Pathway as Therapeutic Targets for Triple-Negative Breast Cancer 9

1.2 Nanotechnology in Cancer Nanomedicine 13

1.2.1 Passive versus Targeting Nanoparticles 14
1.2.2 Photoresponsive Nanoparticles for Cancer Therapy 15
1.2.3 Nanoparticle Based Delivery of RNAs 17
1.2.4 Antibody-Mediated Nanoparticle Delivery 19

1.3 Introduction to Gold Nanoshells 21

1.3.1 Structure and Photoreactive Capabilities 23
1.3.2 Development of Antibody and/or RNA Nanoshell Delivery Platforms 24

2 MATERIALS AND METHODS FOR NANOPARTICLE SYNTHESIS & CHARACTERIZATION 26

2.1 Introduction 26
2.2 Nanoshell Preparation & Synthesis 26
2.3 Nanoshell Functionalization with methoxy-poly(ethylene) glycol (mPEG), Antibodies, and RNA 28

2.3.1 Methoxy poly(ethylene) glycol Attachment to Nanoshells 28
2.3.2 miRNA Loaded Nanoshell Conjugation 28
2.3.3 Antibody and siRNA Loaded Nanoshell Conjugation 29

2.4 Characterization Methods of Antibody and/or RNA Loaded Nanoshells 32

2.4.1 UV-Vis Spectroscopy of NP Conjugates 32
2.4.2 Electron Microscopy of NP Conjugates 33
2.4.3 Dynamic Light Scattering & Zeta Potential Characterization 33
2.4.4 Quantifying RNA Loading on NP Conjugates 33
2.4.5 Quantifying Antibody Loading on NP Conjugates 35

3 PHOTORESPONSIVE miR-34a/NANOSHELL CONJUGATES ENABLE LIGHT-TRIGGERED GENE REGULATION TO IMPAIR THE FUNCTION OF TRIPLE-NEGATIVE BREAST CANCER CELLS 37

3.1 Introduction 37
3.2 Materials and Methods 41

3.2.1 Nanoshell Synthesis and Coating with miRNA and mPEG-SH . 41
3.2.2 miRNA/Nanoshell Conjugate Characterization 42
3.2.3 Evaluation of miRNA/Nanoshell Stability 42
3.2.4 Characterization of miRNA Release Upon Pulsed Nanosecond Laser Irradiation 42
3.2.5 Cell Culture and Laser Irradiation Setup for Cell Experiments .. 45
3.2.6 Transfection of Cells with miR-34a to Validate Concentration Required for Gene and Functional Impact 46
3.2.7 Transfection of Cells with Released miRNA and EdU Analysis of Cell Proliferation 47
3.2.8 Taqman qPCR Analysis of miR-34a Expression in Cells Treated with miRNA/NS and CW versus Pulsed NIR Light 49
3.2.9 qRT-PCR Analysis of mRNA Expression in Cells Treated with miRNA/NS and Light 51
3.2.10 Western Blot Evaluation of Protein Expression 52
3.2.11 alamarBlue^{TM} Metabolic Activity Assay 54
3.2.12 EdU Proliferation Assay 54
3.2.13 Transwell Migration Assay 55

3.3 Results and Discussion 56

3.3.1 Optimization of miRNA Loading 56
3.3.2 miRNA/NS Conjugate Characterization 57
3.3.3 miRNA/NS Stability Evaluation 59

3.3.4 Characterization of miRNA Release from NS after CW and ns Pulsed Laser Irradiation 59
3.3.5 Transfection of Cells Comparing Released and Native miRNA Through EdU Proliferative Analysis 61
3.3.6 Analysis of miR-34a Delivery and Target Gene Regulation in NP Treated TNBC Cells Following CW and Pulsed Laser Irradiation 62
3.3.7 Analysis of TNBC Cell Metabolic Activity and Proliferation After Treatment with miRNA/NS and Pulsed NIR Light. 66
3.3.8 Analysis of MDA-MB-231 cell migration in response to light-triggered miRNA delivery. 70

3.4 Conclusions 72

4 ANTIBODY AND siRNA NANOCARRIERS FOR WNT SIGNALING INHIBITION IN TRIPLE-NEGATIVE BREAST CANCER 75

4.1 Introduction 75
4.2 Materials and Methods 78

4.2.1 Nanoshell Synthesis and Coating with Antibodies and siRNA... 78

4.2.1.1 Optimizing Loading Based on Biomolecule Order of Addition, Salt Concentration, and mPEG-SH Concentration 80
4.2.1.2 Optimizing Loading Based on Salt Concentrations 81
4.2.1.3 Optimizing Loading Based on mPEG-SH Concentration 81
4.2.1.4 Optimizing Loading Based on Initial Number of Antibodies Added 82

4.2.2 Antibody and/or siRNA Conjugate Characterization 82
4.2.3 Cell Culture and NP Treatment Setup for Cell Experiments 83
4.2.4 Validation of siRNA Gene Knockdown in MDA-MB-231 Cells 84
4.2.5 Binding Avidity of Wnt Inhibitory NPs *via* Multiphoton Microscopy 85
4.2.6 Analysis of Cy5-Labeled NP Cellular Uptake *via* Flow Cytometry 86
4.2.7 qPCR Analysis of mRNA Expression in Cells Treated with Wnt Inhibitory NPs 87
4.2.8 Edu Proliferation Assay 87
4.2.9 Transwell Migration Assay 88
4.2.10 Spheroid Formation Assay 89

4.3 Results and Discussion 91

4.3.1 Wnt Inhibitory NP Loading Optimization 91
4.3.2 Wnt Inhibitory NP Characterization 95
4.3.3 Binding Affinity of Wnt Inhibitory NPs *via* Multiphoton Microscopy 96
4.3.4 Cellular Uptake of Cy5-labeled Wnt Inhibitory NPs 97
4.3.5 Assessment of Downstream mRNA Wnt Genes *via* qPCR-RT 100
4.3.6 Analysis of Cellular Proliferation Following NP Treatment 102
4.3.7 Analysis of Cellular Migration Following NP Treatment 104
4.3.8 Analysis of Spheroid Formation Following NP Treatment 106

4.4 Conclusions 107

5 DESIGNING WNT INHIBITORY NANOPARTICLES FOR TREATMENT OF TUMORS IN SPONTANEOUS METASTATIC BREAST CANCER MODEL 110

5.1 Introduction 110
5.2 Materials and Methods 112

5.2.1 Cell Culture and Experimental Setups 112
5.2.2 Validating FZD7 and β-catenin Expression Levels in 4T1 113
5.2.3 Nanoshell Synthesis and Coating with Antibodies and siRNA. 114
5.2.4 Antibody and/or siRNA Conjugate Characterization 115
5.2.5 Analysis of Cellular Proliferation Following NP Treatment 116
5.2.6 Modeling Spontaneous Metastatic Tumor Growth 116
5.2.7 Monitoring Tumor Growth *via* Caliper Measurements and IVIS Imaging 119
5.2.8 Designing Therapeutic Study to Treat Primary Tumor and Metastatic Growth 120
5.2.9 Quantifying Gold Content in Tissue Samples *via* ICPMS 121
5.2.10 Assessing mRNA Gene Knockdown in Extracted Tumor Samples *via* qPCR-RT 121

5.3 Results and Discussion 122

5.3.1 Validating FZD7 Receptor and β-catenin Expression Levels in TNBC Murine Cell Lines 122
5.3.2 Wnt Inhibitory NP Loading Optimization 123
5.3.3 Wnt Inhibitory NP Characterization 124
5.3.4 Analysis of Cellular Proliferation Following NP Treatment 125
5.3.5 Monitoring Primary and Metastatic Tumor Growth in Balb/C Mice 126

5.3.6 Evaluation of Therapeutic Impact on Primary, Recurrent, and Metastatic Tumor Burden 129
5.3.7 Biodistribution Quantification of Gold Content 132

5.4 Conclusions 136

6 CONCLUSIONS AND FUTURE DIRECTIONS 138

6.1 Introduction 138
6.2 Overview of the Work Presented 139
6.3 Future Directions 141

6.3.1 Maximizing the Light-Triggered Release of miRNA from Nanoshells 142
6.3.2 Understanding the Impact of Wnt Inhibitory NPs in Multiple Murine Models 144

REFERENCES 147

Appendix

A INSTITUTIONAL ANIMAL CARE AND USE COMMITTEE FORMS ... 160
B PERMISSIONS TO SELF-AUTHORED PAPERS 162

LIST OF TABLES

Table 1. miRNA sequences utilized. 41

Table 2. Primer sequences used for real time qRT-PCR studies. 47

Table 3. Parameters for Taqman PCR Analysis of miR-34a Expression in Cells. (**A**) U6 and miR-34a primer sequences ordered from ThermoFisher for the Taqman™ MicroRNA Assay. (**B,C**) Thermocycler and LightCycler parameters for reverse transcription and PCR amplification. 51

Table 4. siRNA sequences utilized. 80

Table 5. Primer sequences used for real time qRT-PCR studies, listed from 5' to 3' end. 85

Table 6. Primer sequences used for real time qRT-PCR studies. 114

Table 7. siRNA sequences utilized. 115

LIST OF FIGURES

Figure 1. Hallmarks of Cancer. Illustration of the ten hallmarks of cancer as defined by Hanahan and Weinberg. [21] The Wnt signaling pathway plays a critical role in each of these hallmarks. 4

Figure 2. Spread of Metastatic Cancer. Extravasation of circulating tumor cells from the primary tumor site through the blood vasculature towards metastatic secondary locations.[30] 6

Figure 3. miRNA Regulation and RNA Interference. Scheme of miRNA biogenesis and mechanism of gene regulation through RNAi.[6] 10

Figure 4. miR-34a and p53 Pathway. Scheme of miR-34a dysregulation affecting the p53 apoptotic pathway. 12

Figure 5. Wnt Signaling Pathway. Adapted scheme of hyperactive Wnt Signaling Pathway activated by the abundance of Wnt ligands binding to overexpressed FZD7 receptors on the cellular membrane.[57] 13

Figure 6. Nanoshells and Near Infrared Window. Adapted scheme depicting NIR window I with an overlayed NS absorbance spectrum (orange).[89] . 16

Figure 7. Barriers to RNA Delivery. Scheme depicting the biological barriers that RNA nanocarriers must overcome.[6] 19

Figure 8. Timeline of mAbs FDA Approvals. Adapted graph depicting the number of FDA approved mAbs overtime.[8] 20

Figure 9. Benefits of Gold Nanoshells. Graphic depicting the advantages of gold NS exploited in the context of this dissertation. 23

Figure 10. Gold Nanoshell Tunability and Absorbance Spectrum. Graphs showing the tenability of gold NS synthesis to control the peak plasmon resonance peak.[86] 24

Figure 11. Nanoparticle Platforms Designed In Context of This Dissertation. Graphic depicting the two main nanocarrier platforms designed and the outline of the main three scopes of this dissertation. 25

Figure 12. Nanoshell Formation. TEM images of seed growth as the colloid coats the aminated silica cores overtime starting with a) the initial gold colloid deposition to f) with complete growth of the metallic NS.[121] 27

Figure 13. Functionalization of Gold Nanoshells with miRNA Duplexes. Adapted scheme of miRNA conjugation onto gold NS.[124] 29

Figure 14. Functionalization of Gold Nanoshells with Antibody and siRNA. 32

Figure 15. OliGreen™ Assay Quantification of RNA Duplexes on NPs. Adapted schematic representing the procedure to quantify siRNA duplexes on gold NPs.[125] 34

Figure 16. Light-triggered release of miR-34a from nanoshells in TNBC cells. Following miRNA/NS uptake by TNBC cells, the cells are irradiated with a ns pulsed NIR laser, which induces release of the miRNA duplexes from the gold surface of the NPs. RISC recognizes the released miRNA duplexes, initiating gene regulation. When tumor-suppressive miR-34a is delivered into TNBC cells by this mechanism, the metabolic activity, proliferation, and migration of TNBC cells are reduced. Portions of this figure were produced with permission using Servier Medical ART templates, which are licensed under a Creative Commons Attribution 3.0 Unported License from Servier Medical Art; https://smart.servier.com.[124] 40

Figure 17. Scheme of Irradiation Setups to Characterize miRNA Release from NS and Impacts of Photoactivated Gene Regulation on Treated Cells. (**A**) Gel electrophoresis analysis was used to assess the structure of miRNA released from NS after irradiation with 810 nm ns pulsed light. After light exposure, the NPs were pelleted and the supernatant containing the released RNA was collected for gel electrophoresis. (**B**) Thermal readings of miRNA/NS were recorded every 2 minutes throughout irradiation to monitor bulk solution temperature changes. Portions of this figure were produced with permission using (1) Servier Medical ART templates, licensed under a Creative Commons Attribution 3.0 Unported License from Servier Medical Art; https://smart.servier.com and (2) Shutterstock Images, licensed under a Standard Image License from Shutterstock; http://shutterstock.com.[124] 44

Figure 18. General Setup of Cells Treated with NPs Being Laser Irradiated. Cells were placed on a hotplate during irradiation. D is the distance between the laser and the cells/NPs which was adjusted to ensure the laser beam covered the necessary surface area and that the appropriate laser density was being applied.[124] 46

Figure 19. Validating Function of Light-Triggered Release miRNA. Adapted scheme depicting the functionality examination of miR-34a released from NS. to validate that released miR-34a retains its functionality by transfecting TNBC cells with equal concentrations of native or released miRNA and the resultant cell proliferation was measured.[124] .. 48

Figure 20. Schematic of NP Treatment and NS-Pulsed Laser Irradiation to Assess Cell Migration 48 Hours Post Irradiation. GFP expressing cells were reseeded into transwell inserts with a porous membrane to assess the numbers of cells that migrated across the membrane.[124] 55

Figure 21. Optimizing miRNA Loading on Nanoshells. (**A**) Increasing amount of initial nmol of miRNA was added to a mL of NS to determine the saturation point of maximum loading. (**B**) Prepping NS with varying concentrations of surfactant Tween-20 impacts end loading of miRNA. (**C**) Increasing salt aging concentrations provide ion screening in order for miRNA duplexes to load more efficiently onto NS. (**D**) Timing of passivating NS with mPEG competes with the loading of miRNA. n = 1 (technical triplicates when quantifying loading, values shown are the average and the standard deviation of the triplicates).[124] 57

Figure 22. Synthesis and Characterization of miRNA/NS Conjugates. (**A**) Transmission electron micrograph of miR-co/NS. (**B**) Plasmon resonant extinction spectra comparing miRNA/NS conjugates to bare NS with peak extinction at 810 nm. (**C**) Hydrodynamic diameters (black outline) and zeta potential measurements (gray outline) of miRNA/NS conjugates and bare NS. (**D**) OliGreen^{TM} analysis of miRNA loading on both miR-34a/NS and miR-co/NS. n = 12.[124] 58

Figure 23. miRNA/NS Stability in Various Buffers. (**A**) Extinction spectra of miR-34a/NS conjugates in various buffers after 0 and 60 minutes of incubation. (**B**) Hydrodynamic diameter of miR-34a/NS conjugates in various buffer conditions after 0 and 60 minutes of incubation. n = 2.[124] 59

Figure 24. Characterization of miRNA release from NSs after CW and ns pulsed laser irradiation. (**A**) Heating profile of solutions of miRNA/NS conjugates irradiated at various power densities. (**B**) Percent of duplexed miRNA remaining bound to NS post-irradiation at different power densities. Results are from n = 3 different batches of NPs that were irradiated for temperature measurements and duplex quantification. (**C**) Gel electrophoresis of stock miRNA duplexes, sense strands, and antisense strands compared to miRNA released from NS upon irradiation with ns pulsed light at varying power densities. n = 3.[124] 61

Figure 25. Function of Released miR-34a Compared to Native miR-34a. Normalized count of proliferating cells in samples transfected with native or released miRNA at 50 nM and 100 nM doses. Results are from n = 3 biological replicates with different batches of collected miRNA for transfection. *p<0.05 and #p<0.1 by one-way ANOVA with posthoc Tukey.[124] 62

Figure 26. Relative miR-34a Expression in Cells Following Nanoparticle and CW or Pulsed Laser Treatment. Results are from n = 3 biological replicates. Not significant by one-way ANOVA with posthoc Tukey-Kramer.[124] 63

Figure 27. Relative mRNA Expression of miR-34a Target Genes. qPCR-RT assessment of mRNA expression levels in MDA-MB-231 cells following NP and ns pulsed laser treatment. Results are from n = 3 biological replicates for all genes. Not significant by one-way ANOVA with posthoc Tukey-Kramer.[124] 64

Figure 28. Validation of miRNA Transfection Effects on miR-34a Target Genes. qRT-PCR analysis of the mRNA expression of several genes in MDA-MB-231 cells that were transfected with miR-34a or miR-co for 48 hours n = 1 (technical triplicates when running PCR plates).[124] .. 65

Figure 29. Analysis of Protein Expression of MDA-MB-231 Cells 24 Hours After Pulsed Laser Irradiation. (**A**) Representative Western blot showing Sirt1 (3 isoforms), Bcl2, and β-actin protein expression following NP and ns pulsed laser treatment. Results are from n = 3 biological replicates for all proteins. (**B**) Quantitative densitometry analysis of the Western blots. Not significant by one-way ANOVA with posthoc Tukey-Kramer.[124] 65

Figure 30. Analysis of Protein Expression of MDA-MB-231 Cells 48 Hours After Pulsed Laser Irradiation. (**A**) Representative Western immunoblotting showing Sirt1 (3 isoforms), Bcl2, and β-actin expression following NP and laser treatment. (**B**) Quantitative analysis of the Western blots. Not significant by one-way ANOVA with posthoc Tukey-Kramer.[124] 66

Figure 31. Cellular Metabolic Activity Assessment Following NP and Laser Treatment. Adapted graphics depicting metabolic activity assessment. (**A**) Normalized metabolic activity of MDA-MB-231 cells following NP and comparing two modes of laser treatments assessed *via* an alamarBlue™ Assay. (**B**) Functionality assessment *via* TFX. MDA-MB-231 cells were transfected with an increasing dosage of miRNA concentrations of 25, 50, and 100nM and accessed for metabolic activity following 96 hours *via* an alamarBlue™. **p<0.001 and *p<0.01 by one-way ANOVA with posthoc Tukey-Kramer.[124] 67

Figure 32. Cell Proliferation Assessment Following NP and Laser Treatment. Adapted graphics depicting cell proliferation assessment. (**A**) Normalized count of proliferating MDA-MB-231 cells following NP and ns-pulsed laser treatment at varying laser power densities assessed *via* an EdU Proliferation Assay. (**B**) MDA-MB-231 cells were transfected with an increasing dosage of miRNA concentrations of 25, 50, and 100nM and accessed for proliferation following 96 hours *via* an EdU Proliferation Assay. #p<0.1, *p<0.05, and **p<0.01 by one-way ANOVA with posthoc Tukey-Kramer.[124] 69

Figure 33. Analysis of MDA-MB-231 Cell Migration in Response to Light-Triggered miRNA Delivery. (**A**) Normalized count of migrated MDA-MB-231 cells following NP and laser treatment assess. (**B**) Zoomed in sections of representative fluorescent images of the migrated GFP cells. #p<0.1 by one-way ANOVA with posthoc Tukey. Scalebar = 1 mm.[124] 71

Figure 34. Qualitative Analysis of Migrated GFP-cells. Migration assay at timepoints 48, 72, 96, and 120 hours reseeding. *p<0.05 and #p<0.1 by one-way ANOVA with posthoc Tukey-Kramer.[124] 72

Figure 35. Scheme of NPs for Regulation of the Wnt Signaling Pathway. Wnt inhibitory NPs designed to target the signaling pathway at multiple levels including extracellularly through receptor inhibition and intracellularly through mRNA cleavage. 78

Figure 36. Schematic of NP Treatment to Assess Cell Migration. GFP-expressing MDA-MB-231 cells were incubated with NPs for 72 – 96 hours, then reseeded into transwell inserts with a porous membrane to assess the numbers of cells that migrated across the membrane over the following 24-72 hours. 89

Figure 37. Schematic of NP Treatment to Assess Spheroid Formation. At 24 – 72 hours post NP incubation MDA-MB-231 cells were reseeded in spheroid forming media in U-bottom plates with ultra-low attachment surfaces to assess the ability of the cells to form loose or compact spheroids over the course of one week. At the end of this time frame, the metabolic activity of the individual spheroids was assessed using an Alamar Blue assay. 90

Figure 38. Optimizing Biomolecule Loading on NPs by Order of Biomolecule Addition. Optimization of (**A**) antibody and (**B**) siRNA loading onto gold NS when considering the order of molecule addition: stripes (1) = antibody added first and solid (2) = siRNA added first. (a/b) low/high NaCl concentration, (i/ii) low/high mPEG concentration. n = 2 (technical triplicates when quantifying loading). 92

Figure 39. Optimizing Biomolecule Loading on NPs by Adjusting Salt Aging Concentrations. Comparing (**A**) antibody and (**B**) siRNA loading of FZD7-NS, Combo-NS, and βcat-NS when keeping antibody, siRNA, and mPEG concentration constant and adjusting the NaCl concentrations (in parentheses). n = 3. 93

Figure 40. Optimizing Biomolecule Loading on NPs by Adjusting mPEG Concentrations. Comparing (**A**) antibody and (**B**) siRNA loading of FZD7-NS, Combo-NS, and βcat-NS when keeping antibody, siRNA, and NaCl concentration constant and adjusting the mPEG concentrations. n = 3. 94

Figure 41. Finetuning Antibody Loading of FZD7-NS and Combo-NS. Anti-FZD7 loading was adjusted by increasing initial addition antibodies for FZD7-NS. Confirming equivalent (**A**) antibody and (**B**) siRNA loading with new set parameters for Combo-NS in comparison to the monotherapeutic NPs. n = 3. 95

Figure 42. Wnt Inhibitory NP Characterization. Final characterization of the Wnt Inhibitory NP platforms assessed *via* DLS and Zeta Potential. Additional recap of the FZD7 antibody and β-catenin siRNA loading on NS in table format. n = 11 – 19. 96

Figure 43. NP Cellular Binding Affinity. Multiphoton images of NP binding to MDA-MB-231 or MCF10A cells. Two images were taken with each biological replicate (n = 3). Scalebar = 20 μm. 97

Figure 44. NP Cy5 Fluorescence. Cy5 fluorescence raw values of NPs tagged with Cy5 labeled mPEG. n = 3. 98

Figure 45. NP Cellular Uptake *via* Flow Cytometry. (**A**) Cellular uptake of NPs at an OD of 1 after 1 hour assessed *via* flow cytometry. (**B**) Representative flow graphs. n = 4. *p<0.1 and **p<0.01 by one-way ANOVA with posthoc Tukey-Kramer. 99

Figure 46. NP Cellular Uptake Over Time. Additional Cy5 labeled NP uptake *via* flow cytometry after 4 and 8 hours of NP incubation. n = 1 (technical triplicates when running flow samples). 99

Figure 47. **NP Cellular Uptake *via* Flow Cytometry At A Higher Dose.** NP uptake when treated with twice as high concentration of NPs. n = 3.... 100

Figure 48. Validation of mRNA Knockdown in Wnt Related Genes. MDA-MB-231 cells were transfected with β-catenin siRNA at 50 nm and assessed for mRNA expression levels after 48 and 72 hours. n = 2 (technical triplicates when running PCR plates). 101

Figure 49. Relative mRNA expression of Wnt target genes in MDA-MB-231 cells following NP treatment. Results are from n = 3 biological replicates for all genes. Not significant by one-way ANOVA with posthoc Tukey-Kramer. 102

Figure 50. Assessment of Cell Proliferation Following NP Treatment. Normalized count of proliferating MDA-MB-231 cells following NP treatment assessed *via* an EdU Proliferation Assay after 96 hours. #p<0.1 and *p<0.05 by one-way ANOVA with posthoc Tukey-Kramer. 103

Figure 51. Analysis of MDA-MB-231 Cell Migration in Response to NP Treatment. (**A**) Normalized count of migrated MDA-MB-231 cells following NP incubation for 96 hours. (**B**) Representative fluorescent images of the migrated GFP cells. Not significant by one-way ANOVA with posthoc Tukey-Kramer. Scalebar = 1 mm**.** 105

Figure 52. Optimizing Seeding Densities and Impact on Cell Migration. Normalized count of migrated MDA-MB-231 cells following NP treatment incubation for 72 hours. Not significant by one-way ANOVA with posthoc Tukey-Kramer. Scalebar = 1 mm**.** 106

Figure 53. Analysis of MDA-MB-231 Spheroid Formation in Response to NP Treatment. (**A**) Metabolic activity assessment of spheroids after a week of formation. (**B/C**) Representative brightfield images of the spheroids formed after a week. Out of the biological replicates there were two types of spheres from. One was the lack of spheroid formation (top row) and two was the decrease in compact formation (bottom row). n = 4. #p<0.1 and **p<0.01 by one-way ANOVA with posthoc Tukey-Kramer. Scalebar = 200 μm..... 107

Figure 54. **4th Inguinal Mammary Fat Pad.** Simplified mice anatomy for visualization of the 4th inguinal mammary fat pad, surgical site, and IP injection site. 117

Figure 55. NP Regimen for Treatment of Spontaneous Metastatic Tumor Model. Scheme depicting the initial tumor inoculation, start of NP treatment, removal of the primary tumor, two different therapeutic dose regimens, and the end dates of the study. 120

Figure 56. Validation of FZD7 Receptor and β-catenin mRNA Expression Levels in 4T1 Cells. (**A**) Immunocytochemistry analysis of cancerous 4T1 and breast epithelial cell line EpH4-Ev were evaluated for extracellular FZD7 expression levels. n = 3. Scalebar = 25μm. (**B**) Validation of β-catenin mRNA Knockdown. 4T1 cells were transfected with β-catenin siRNA *via* transfection delivery for qPCR-RT analysis of mRNA expression levels. n = 3. 123

Figure 57. Loading Optimization of Multiple Wnt Biomolecules on NPs. Optimization of (**A**) antibody and (**B**) siRNA loading on gold NS depending on mPEG-SH concentration added. n = 3..... 124

Figure 58. Wnt Inhibitory NP Characterization. Final characterization of the Wnt Inhibitory NP platforms assessed *via* Litesizer measurements and loading assays for biomolecule loading. n = 12 – 16. 125

Figure 59. Assessment of Cell Proliferation Following NP Treatment. Normalized count of proliferating 4T1 cells following NP treatment at OD1 assessed *via* an EdU Proliferation Assay after 48 hours**.** n = 3. Not significant by one-way ANOVA with posthoc Tukey-Kramer..... 126

Figure 60. Primary Tumor Growth Overtime in the Mammary Fat Pad. Tumor volumes were recorded *via* caliper measures after initial cell inoculation of **(A)** 5K **(B)** 10K **(C)** 50K **(D)** 100K into the mammary fat pad. n = 1 – 3 mice per group (several mice did not take tumors – each color within the graphs indicates an individual mouse of the same experimental group). 127

Figure 61. Evaluation of Primary Tumor and Lung Metastatic Growth. Monitoring tumor growth following initial cell inoculation of **(A)** 10K **(B)** 20K **(C)** 50K in the mammary fat pad. Primary tumors were removed at around 200 – 400 mm^3 and lung metastatic signal was monitored *via* IVIS imaging. (+) = start date of lung metastatic signal. n = 3 mice per group..... 128

Figure 62. Primary Tumor Growth in the Mammary Fat Pad. (**A**) Change in tumor volume over time. (**B**) Change in primary tumor volume upon removal starting from initial NP injection. *p<0.05 by one-way ANOVA with posthoc Tukey. n = 12 – 14..... 129

Figure 63. Change in Recurrent Tumor Growth. Primary tumors were surgically removed on day 14 and tumor regrowth was monitored starting a week after for treatment (**A**) schedule 1 (**B**) schedule 2. n = 6 – 7. 130

Figure 64. Lung Metastatic Analysis *via* IVIS Imaging. Comparison of treatment (**A**) schedule 1 and (**B**) schedule 2 with (**i**) average radiance taken, (**ii**) days until lung metastases signal appears, and (**iii**) percentage of mice that did not form metastasis by the end of the study. n = 6 – 7..... 132

Figure 65. ICP-MS Quantification of Gold Content in Tumors and Metastatic Organs. (**A**) Primary Tumor (**B**) Lungs and Recurrent Tumors of treatment (**i**) schedule 1 and (**ii**) schedule 2. #p<0.1, *p<0.05, **p<0.01 by one-way ANOVA with posthoc Tukey. n = 12 – 14 (primary tumor) ; 6 – 7 (lungs and secondary tumor). 133

Figure 66. ICP-MS Quantification of Gold Content in Clearance Organs Liver and Spleen. Treatment (**A**) schedule 1and (**B**) schedule 2. 134

Figure 67. ICP-MS Quantification of Gold Content in Other Remaining Organs. Treatment (**A**) schedule 1and (B) schedule 2. n = 6 – 7. 135

Figure 68. qPCR-RT Analysis of β-catenin mRNA Expression Levels in Excised Tumors. Assessment of β-catenin mRNA expression levels in excised primary tumors on day 14 and recurrent tumors at the end of the study. n = 6 – 7. 136

ABSTRACT

Triple-negative breast cancer (TNBC) is an aggressive disease that is unsusceptible to most current targeted or hormonal therapies because it lacks expression of the three receptors these therapies target: the estrogen, progesterone, and human epidermal growth factor 2. Consequently, patients with TNBC suffer from earlier relapse, increased rates of metastasis, and lower survival rates than patients with other forms of breast cancer. New treatment strategies must be developed to improve the prognosis for TNBC patients, and the research described here seeks to meet this need through targeted gene regulation. TNBC progression is driven by both loss of expression of the tumor suppressive microRNA miR-34a and by overactivity of the Wnt signaling pathway, which appears in the form of elevated Frizzled7 receptor expression and elevated β-catenin protein expression. The aberrant expression of miR-34a, Frizzled7, and β-catenin leads to increased translation of numerous oncogenes that are downstream of these molecules. Hence, increasing miR-34a expression through the delivery of miRNA mimics or decreasing β-catenin expression through delivery of small interfering RNAs (siRNAs) would profoundly impair TNBC progression. Unfortunately, naked RNA molecules cannot be used therapeutically because they are unstable in biological fluids, exhibit unfavorable pharmacokinetics, and cannot passively enter cells. To overcome these issues, various nanocarriers have been designed to protect RNAs from degradation and deliver them into target cells to initiate gene regulation. However, most reported systems lack specificity, leading to off-target effects. This dissertation addresses the need for selective gene regulation by

developing two different NP platforms that use photoactivation or antibody targeting to provide TNBC cell-specific gene regulation. The first platform uses light-responsive nanoparticles called nanoshells (NS) as a carrier for miR-34a mimics. Chapter 3 demonstrates that these conjugates can hold the miRNA inactive until it is released from the NS surface on-demand with light activation. The second platform consists of NS coated with β-catenin siRNA molecules and Frizzled7 antibodies. Here, the antibodies both target TNBC cells and block Wnt ligand/Frizzled7 receptor interactions to suppress the signaling pathway at both the receptor and effector level. Chapter 4 examines the effectiveness of these Wnt inhibitory siRNA/antibody nanocarriers *in vitro*, while Chapter 5 demonstrates their utility *in vivo.* This research is both innovative and impactful because it develops and validates two distinct nanocarrier platforms to treat TNBC through high precision gene regulation. With further development, these and other RNA nanocarrier platforms have substantial potential to transform TNBC patient care.

Chapter 1

INTRODUCTION

Cancer is the leading cause of death globally and mortality rates peaked in the 1900s.[1] Since then, cancer incidence and death rates have declined because of shifts in healthier decision making, advances in detection methods that enable earlier diagnosis, and improvements in therapy. However, cancer still collectively stands as one of the top causes of death globally.[2–4] This underscores the need for continued development of advanced treatment options. The overall arching goal of this dissertation was to develop novel nanoparticle (NP)-based treatments for cancer, particularly TNBC. This chapter provides an overview of cancer and the biology of TNBC, discusses the historic evolution, and advantages of NP therapeutics, and introduces concepts that inspired development of the NP platforms presented in this dissertation. **Chapter 2** details the synthesis and characterization of the NP formulations, and **Chapters 3 – 5** describe the impact of the specific NP therapeutics on TNBC both *in vitro* and *in vivo*. Throughout this work, silica core/gold shell NPs known as "nanoshells" (NS) were used as the core nanocarrier to enable the treatment of TNBC through either (1) light-triggered release of gene regulatory microRNA (miRNA) molecules, or (2) co-delivery of gene-silencing small-interfering RNAs (siRNAs) and antagonistic antibodies that provide both cell-specific targeting and signaling inhibition. Finally, **Chapter 6** discusses future directions for the nanotechnology field building upon this current work. The introduction provided in **Chapter 1** contains adaptations from the following co-authored publications.

1) Valcourt *et al.* Nano Research (2018); 11(10), 4999–5016[5]

2) Kapadia *et al.* Journal of Applied Polymer Science (2019); 48651[6]

3) Valcourt *et al.* Annals of Biomedical Engineering (2019); 48(7):1864-1884[7]

4) Dang *et al.* Current Opinion in Biomedical Engineering (2021); 19, 100295[8]

1.1 A Brief Introduction to Cancer History of Triple-Negative Breast Cancer

Cancer is a disease characterized by uncontrolled cell growth and metastatic spread to distant sites in the body that can result in death without proper diagnosis and treatment.[9] On the global scale, cancer is a major public health issue and is the second leading cause of death within the United States.[2] It is estimated that in 2022 within the US there will be approximately 1.9 million new cancer cases and 609 thousand cancer deaths.[10] The likelihood of developing cancer increases greatly with age, and 80% of people diagnosed with cancer are 55 years of age or older.[3] Additionally, risk factors such as tobacco use and excess body weight can further increase the chances of cancer.[3] In fact, cancer-related deaths peaked in the 1990s as a consequence of the smoking epidemic within the US.[1] Beyond lifestyle factors, inherited genetic mutations and infectious agents can also initiate the development of cancer. Fortunately, over the past three decades, cancer rates have dropped by 32% mostly due to reductions in smoking, behavioral changes, improvements in screening and detection, and treatment advancements.[3] It is noted that in 2020, due to the ongoing coronavirus pandemic, the diagnosis and treatment of cancer was adversely affected because of reduced access to health care settings.[2] Overall, the decline in the cancer death rates is largely driven by progress in managing the four most common cancer types – lung, colorectal, breast, and prostate.[11] This dissertation focuses a specific subset of breast cancer known as TNBC, introduced below.

1.1.1 Introduction to Triple-Negative Breast Cancer

Breast cancer accounts for the majority of all cancers worldwide, with a remarkable 2.26 million cases and 685 thousand deaths in 2020.[12] Breast cancer is a highly heterogenous disease with multiple subtypes that are defined by the expression of two hormone receptors (HR), which include estrogen receptor (ER) and progesterone receptor (PR), and human epidermal growth factor receptor 2 (HER2).[4] From these three receptors yield four distinct breast cancer subtypes: HR+/HER2+, HR+/HER2-, HR-/HER2+, and HR-/HER-. The last subtype which expresses none of the cell surface receptors is classified as TNBC, which accounts for approximately 15% of all breast cancer cases.[13–17] TNBC is a particularly aggressive subtype that exhibits rapid tumor growth, higher recurrence, and poorer prognosis than other forms of breast cancer.[18]

It is critical to understand the mechanisms of cancer biology and tumor progression to design more effective therapeutics. In the 2000s, Hanahan and Weinberg defined six hallmarks of cancer: sustaining proliferative signaling, evading growth suppressors, resisting cell death, enabling replicative immortality, inducing angiogenesis, and activating invasion & metastasis[19]. In 2011, four additional characteristics were added to the established hallmarks: reprogramming of energy metabolism, evading immune destruction, genome instability & mutation, and tumor-promoting inflammation.[20] Altogether cancer is characterized by these defining ten hallmarks (**Figure 1)**. Below the relevance of these hallmarks to TNBC are discussed along with a discussion of how they informed the design of the NP platforms explored in this thesis.

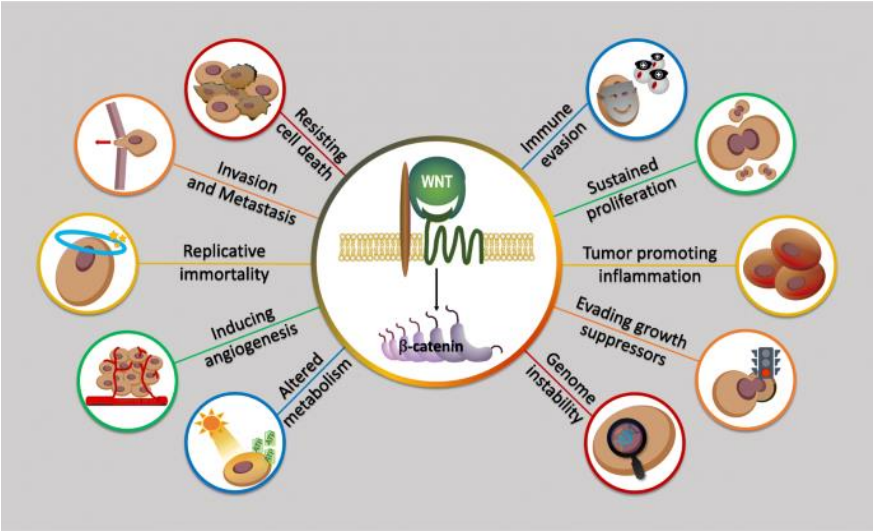

Figure 1. Hallmarks of Cancer. Illustration of the ten hallmarks of cancer as defined by Hanahan and Weinberg.[21] The Wnt signaling pathway plays a critical role in each of these hallmarks.

One cancer hallmark that is abundant in TNBC cells is genomic instability and mutations. Normal breast cells are self-regulated by tumor suppressor genes that help control cell function, maintain division, control DNA mistakes, and regulate apoptosis. Genomic instability disrupts the cellular mechanisms that ordinarily maintain proper cell division and death, allowing cancer cells to grow uncontrollably.[9] Of note, the p53 apoptotic signaling pathway that is regulated by the miR-34a tumor suppressor gene is dysregulated in TNBC and contributes to tumor formation.[22] **Chapter 3** presents a novel approach to restore miR-34a levels in TNBC cells through light-triggered miRNA release from NS.

Genomic instability also causes cancer cells to have abnormal gene expression levels compared to healthy cells, which in turn causes aberrant oncogenic cell signaling that supports tumorigenesis. One signaling pathway that is overactive in

TNBC is the Wnt signaling pathway, which is characterized by overexpression of Frizzled7 (FZD7) surface receptors and intracellular β-catenin molecules.[23,24] Overabundant Wnt signaling has been shown to play a role in each of the hallmarks of cancer (**Figure 1**), making it an important target for therapeutic manipulation.[25] **Chapters 4 & 5** introduce a new NP-based strategy to suppress the Wnt signaling pathway at both the FZD7 receptor and β-catenin effector level to reduce tumor progression

Aberrant miR-34a expression and dysregulated Wnt signaling are also both implicated in sustaining proliferative signaling, another hallmark of cancer.[23,26] The proliferation of healthy breast cells is strictly maintained to preserve homeostasis, however in cancer, cells acquire dysregulated proliferation capabilities to continuously divide. This uncontrolled proliferation is due to either lack of tumor-suppressive genes like miR-34a, or increased levels or activity of specific oncogenes like β-catenin. In this thesis, TNBC cell proliferation in response to NP treatment is evaluated to affirm the efficacy of the therapy

A third cancer hallmark that is studied in this thesis is metastasis. Metastasis is a multi-step process, wherein cancer cells from the primary breast location locally invade the surrounding tissue and blood vessels. The circulating tumor cells then extravasate into distant tissues to form secondary or metastatic tumors (**Figure 2**). TNBC is particularly aggressive, with a propensity to form metastases in lungs, brain, and bone. This presents a significant clinical challenge as metastatic spread is the primary cause of death for TNBC patients.[27] Relevant to this thesis, hyperactive Wnt signaling has been shown to drive TNBC spread to the lungs.[28,29] Therefore, we

explore in **Chapters 5 & 6** whether Wnt inhibitory NPs can reduce lung metastasis in murine TNBC models.

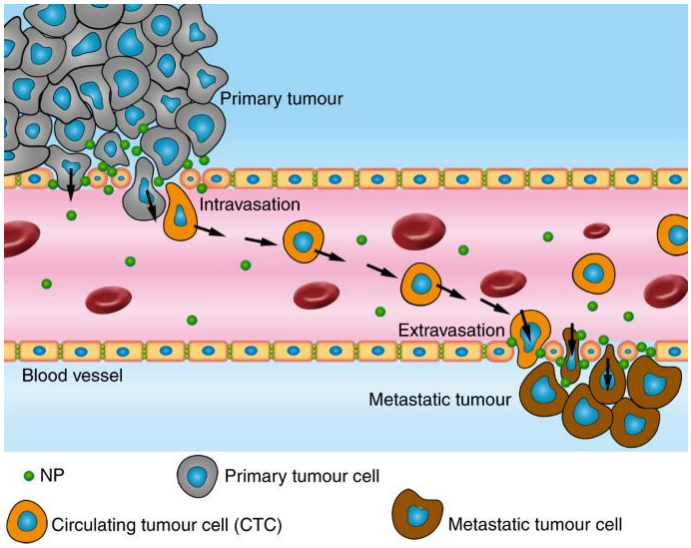

Figure 2. Spread of Metastatic Cancer. Extravasation of circulating tumor cells from the primary tumor site through the blood vasculature towards metastatic secondary locations.[30]

Overall, many clinical therapeutics used to treat cancer focus on blocking rapidly dividing cancer cells by homing in on the hallmark characteristics. The following section describes the current treatment strategies for TNBC and discusses the limitations this dissertation aims to overcome.

1.1.2 Current Treatment Strategies for Triple-Negative Breast Cancer

The standard-of-care for cancer treatment has traditionally included chemotherapy, radiation, and surgery, which has remained unchanged over the past several decades.[31] Although they can be highly effective for certain cancers,

depending on the stage of the disease, the end success also depends on the cancer's heterogeneity. In respect to breast cancer and TNBC, whose heterogeneity as implicated above contribute to the more aggressive cancerous nature, these treatments alone or even in combination often are not sufficient. Below, we briefly outline each of these therapies and general limitations that hinder their overall success.

Surgery procedures seek to directly remove the primary tumor mass, along with any sizable secondary masses, directly from the original organ. While this can be effective at earlier stages of tumor progression, this type of mass removal leaves the site susceptible to local recurrence in the case of later-stage clearance. Moreover, such a procedure is highly invasive and it difficult to ensure thorough removal of the tumor masses. And as alluded to, regarding later-stage cancers where circulating cancer cells or metastatic legions play a role, surgery is not precise enough to remove those components of tumor progression.[28] Additional to the invasive nature of surgery, stress factors from surgical procedures have been correlated with elevated metastatic rates. Thus, with TNBC, which is highly metastatic, surgery is typically not sufficient, unless when utilized for other less aggressive breast cancer subtypes detected and diagnosed at earlier stages of progression.[13,32] As a result, for early-stage TNBC, breast-conserving surgery or mastectomy with an evaluation of the lymph nodes and for larger tumors or if circulating cancer cells are find in the lymphatic system, radiation follows the initial surgery. In some cases, chemotherapy is given following surgery to reduce the chances of recurrence.[33]

Radiation therapy utilizes high-energy rays to destroy cancer cells.[34] Again, this sort of therapy would require identifying the tumor sites for effective treatment. In relation to breast cancer there are two main types of radiation: external bean radiation

therapy and brachytherapy. As mentioned above, radiation is typically used following breast tumor removal surgeries and additionally can be applied to metastatic spread, such as the bones and brain. Alternatively, chemotherapy involves anti-cancer drugs administered *via* intravenously or orally. While such drugs are highly effective in killing cancerous cells, chemotherapy typically lacks specificity and consequently can attack healthy cells resulting in significant adverse effects. In current standard-of-care, chemotherapies can be used prior or after surgical breast cancer removal. After surgery, adjuvant chemotherapy is typically utilized to kill off any remaining cancer cells that either may have been missed during the surgeries or have spread from the primary site.[35] Prior to surgery, neoadjuvant chemotherapy may be suggested to shrink the tumor for a less extensive surgery. Chemotherapeutics available on the market for metastatic breast cancers include Paclitaxel, Abraxane, Doxil, Cisplatin, amongst others.[36]

In addition to chemotherapy there are another class of targeted drug therapies for breast cancer. Clinically these involve hormone-targeting therapeutics that utilize monoclonal antibodies or kinase inhibitors. These can be used alone or in conjunction with chemotherapeutics, which are classified as antibody-drug conjugates. Available on the market are Trastuxumab, Lapatinib, Palbociclib, Alpelisib, amongst others.[37] While such targeted therapeutics eliminate the non-specific killing of healthy breast cells, the hormone or protein targeting treatments listed above require the expression of related receptors, HR+ or HER2+.[38] Due to its lack of the common receptors, TNBC is unsusceptible to most targeted or hormonal therapies currently available that leverage the receptor expressions. On the market currently, there is one available antibody-drug conjugate treatment, Sacituzumab Govitecan, that is an composed of an

antibody targeting the human trophoblast cell-surface antigen 2 (Trop-2) and coupled to SN-38 (topoisomerase I inhibitor)[39] There is room for improvement and the market for continue development of therapeutics for TNBC.[40]

Specifically, the advancement of targeted therapeutics has been of focus to specifically halt cellular pathways involved in disease progression. Additionally, while gene therapeutics have yet to enter the market for TNBC treatment, much work has been done preclinically focused on regulating genes either by silencing target genes or replacement gene therapy. This has come to the forefront of potential therapeutics in light of the coronavirus pandemic and the delivery of mRNA technology *via* the COVID-19 vaccine. This dissertation will describe platforms focused on targeted gene therapeutics with the goal of expanding upon the available potential treatments that are direly needed for TNBC to improve patient survival.

1.1.3 miR-34a and Wnt Signaling Pathway as Therapeutic Targets for Triple-Negative Breast Cancer

To design alternative therapeutics for TNBC, it is important to identify potential signaling pathways for therapeutic manipulation. This dissertation exploits TNBC's aberrant expression of miR-34a and β-catenin, which are part of the p53 and Wnt signaling pathways respectively. These pathways are introduced in detail individually below.

miRNAs regulate the expression of gene networks as small, non-coding RNA molecules (**Figure 3**).[41,42] miRNAs are formed in the nucleus. There, they are initially transcribed by RNA polymerase II, producing primary miRNAs (pri-miRNAs) that include a hairpin structure.[43] The pri-miRNA is then cleaved by Dosha at the ends to create 70 base pair (bp) long preliminary miRNAs (pre-miRNAs) with an imperfect

stem-loop structure which are exported from the nucleus into the cytoplasm.[44,45] Within the cytoplasm, RNase III endonuclease Dicer removes the terminal loop to create 22 bp mature double-stranded miRNA duplexes.[45,46] Upon completion in the cytoplasm, the miRNA-induced silencing complex (miRISC) recognizes the duplexed miRNA and incorporates it into the complex to initiate the gene silencing mechanism. Here miRISC processes the mature duplexed miRNA in which the passenger strand or miRNA* strand is typically degraded while the guide or miRNA strand is kept. From here, miRISC guides the loaded miRNA stand to its corresponding messenger RNA (mRNA) for either perfect or imperfect complementary base pairing. This results in either degradation or translational repression respectively of the target mRNA, which inhibits the translation of downstream proteins.

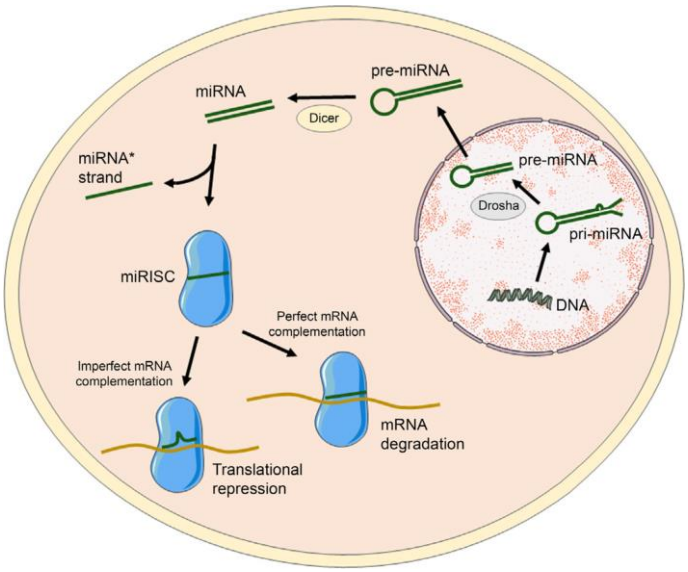

Figure 3. miRNA Regulation and RNA Interference. Scheme of miRNA biogenesis and mechanism of gene regulation through RNAi.[6]

In 2007 the miR-34 family was identified as the first miRNA genes to be directly regulated by p53.[22,47,48] Recent studies have revealed that TNBC typically exhibits down-regulation of the tumor suppressive miRNA, miR-34a.[49] Several studies have implicated miR-34a as a master regulator of TNBC progression through regulating genes such as Sirt-1 and Bcl-2 that are known to play a critical role in cancer (**Figure 4**).[50] As a result, the loss of miR-34a expression increases TNBC cell migration and invasion,[26] and TNBC patients with low miR-34a expression exhibit worse overall survival.[51] Accordingly, restoring miR-34a expression levels through intracellular delivery of synthetic miRNA duplexes is a promising strategy to combat TNBC through RNAi-mediated gene regulation. To that note, MRX34, a liposomal miR-34a mimic formulation, has been initiated in Phase I human clinical trials for a miRNA-based cancer therapy most recently in 2020.[52] However, this system lacks specificity, which may result in off-target gene regulation. Additionally, the delivery of miRNA, and all other nucleic acid, is hindered by many different biological barriers explained in detailed the following sections. Due to this, nanocarriers are necessary to harness the potential of RNA therapeutics, along with other nucleic acids. **Chapter 3** introduces a new system that can enable on-demand miR-34a release from NPs to yield high precision gene regulation.

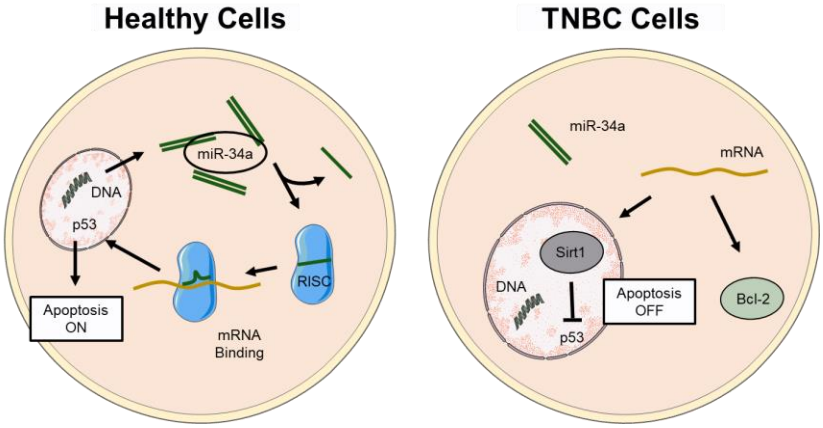

Figure 4. miR-34a and p53 Pathway. Scheme of miR-34a dysregulation affecting the p53 apoptotic pathway.

While miR-34a expression is lost in TNBC, Wnt signaling is hyperactive in TNBC and correlated with poor disease outcomes. As Wnt signaling is known to regulate development and stemness, it is perhaps unsurprising that it also plays a large role in carcinogenesis and has been identified as a driving force behind breast carcinoma.[53] In healthy cells, the canonical Wnt signaling pathway is kept in balance by a destruction complex that marks β-catenin for degradation. In TNBC cells, Wnt signaling is activated when extracellular Wnt ligands bind FZD7 receptors that are overexpressed on the cells' surface (**Figure 5**). This allows β-catenin to stabilize and accumulate in the cytoplasm. Following translocation to the nucleus, β-catenin forms an active complex to initiate the transcription of multiple genes including Axin2, cyclin D1, and c-Myc.[54] Axin2 is a universal indicator of Wnt activity while cyclin D1 and c-Myc are downstream Wnt targets that promote cell proliferation, migration, and invasion.[23,24] Many other oncogenes are also regulated by Wnt signaling, and so this signaling pathway has become another critical target for therapeutic manipulation of TNBC. As a result, Wnt signaling inhibitors have been investigated in clinical trials

for several types of cancer, such as the development of two antibodies that antagonize FZD7 receptors that are also being investigated in combination with chemotherapeutics.[55,56] Due to the potential in targeting the Wnt signaling pathway, **Chapter 4 & 5** focuses on inhibiting the Wnt through multiple levels by delivering both targeting antibodies and siRNA therapeutics *in vitro* and *in vivo*.

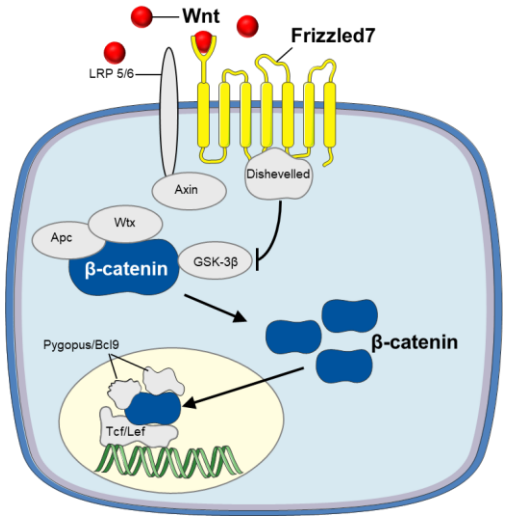

Figure 5. Wnt Signaling Pathway. Adapted scheme of hyperactive Wnt Signaling Pathway activated by the abundance of Wnt ligands binding to overexpressed FZD7 receptors on the cellular membrane.[57]

1.2 Nanotechnology in Cancer Nanomedicine

Nanotechnology provides many advantages over conventional cancer treatment strategies, such as surgery, radiation, and chemotherapeutic.[58–61] Furthermore, nanotechnology could further enhance the effectiveness of the current standard-of-care.[62,63] The main advantages of cancer nanotechnology are the ability to increase biodistribution of therapeutics to the desired site, which would in hand increase therapeutic efficacy and decrease adverse side effects which are one of the main issues

with current treatments.[64,65] NPs have significant potential for the field of medicine due to their unique physicochemical properties, which include tunable size, high reactivity, large surface area to mass ratio, capability for surface modification, potential for optical visualization, and ability to control drug release.[66] As a result, NPs have been utilized as diagnostic tools[67–70], labeling & tracking agents[71–73], and drug carriers.[74,75]

1.2.1 Passive versus Targeting Nanoparticles

NP delivery to cancer cells and solid tumors occurs through two main mechanisms: passive and active targeting.[76] Through passive targeting, NPs inherently accumulate at the tumor sites *via* the enhanced permeability and retention effect.[77] This mechanism exploits the leaky vasculature and disorganized lymphatic system within the tumor microenvironment allowing for higher accumulation of NPs at the tumor site. Historically, polyethylene glycol (PEG) has been used as the ideal stealth agent on NPs to increase circulation time and stability in comparison to uncoated NPs, which is the main mechanism driving passive tumor accumulation for various NP platforms.[78] Passive NPs delivery takes advantageous of the enhanced permeability and retention (EPR) effect, in which therapeutics accumulate in tissues that are characterized with increased vascular permeability, such as inflammation or cancer sites.[77,79,80] Passive NPs are exploited in **Chapter 3** of this dissertation, which utilized NPs for gene regulation of cancer cells through photoresponsive release.

An alternative to passive NPs are active delivery in which the surface of NPs can be modified with targeting agents, which include antibodies, peptides, or other small molecules, to further increase cancer cell specific binding and uptake upon passive accumulation at the tumor sites.[5] This is known as active targeting, where

targeting mechanisms can help decrease non-specific binding to off target healthy cells, overall enhancing the pharmacokinetics and biodistribution of NPs versus the bare counterparts. More recent developments in the realm of targeting nanomedicine including cell membrane wrapped NPs as opposed to bioconjugated NPs.[5] In brief, these NPs utilize homotypic recognition from the cell membrane used to wrap the NPs to the corresponding cancer cells for enhanced cellular binding and uptake. Targeting NPs is exploited in **Chapter 4 & 5** of this dissertation, which utilized NPs for antibody-mediated gene delivery of siRNA for treatment of TNBC *in vitro* and *in vivo*.

1.2.2 Photoresponsive Nanoparticles for Cancer Therapy

Gold NPs have unique optical properties that have been exploited for various applications including diagnostic and imaging purposes.[81] Therapeutically, gold NPs can be utilized for light-activated therapies with various outcomes which include photothermal therapy, photodynamic therapy, or photoresponsive release of therapeutics.[82–84] Briefly, photothermal therapy consists of treating diseases through heat ablation, photodynamic therapy consists of delivering reactive oxygen species, and photoresponsive therapies deliver therapeutics on demand, all of which follow an external stimuli. NP-mediated photoreactive therapy enables selective treatment of tumor tissues while avoiding damage or activation of healthy tissues not in irradiation.[85] Conceptually, plasmonic NPs are delivered into tumors, either by passive or active targeting, and irradiated with laser light, which causes the NPs' conduction band elections to undergo synchronized oscillations that either absorb or scatter the applied light. The absorbed light then either converts to heat, releases reactive oxygen species, or breaks linkages to bond therapeutics.[86]

NPs used in photoreactive applications must account for specific design criteria such as having plasmon resonance tunability, high photothermal conversion efficiency, and simple surface functionalization or encapsulation chemistry. Traditionally, gold-based NPs such as nanoshells (NS), nanorods (NR), nanocages (NC), and nanostars are considered the most common gold-based photothermal transducers.[81] Other polymer-based NPs have similar photothermal capabilities, however, they need to be loaded with additional heat converting molecules.[87] Overall, these NP platforms have optical properties that allow them to be maximally absorbed within the near-infrared region (NIR). Within the NIR window, water and hemoglobins minimally absorb the range of wavelengths, providing an advantage for precision from the NPs that do maximally absorb. The most relevant wavelengths would include either the first (650 – 850nm) or second (950 – 1350nm) NIR windows because at these wavelengths light can safely and deeply penetrate through tissue towards tumor sites embedded with NPS (**Figure 6**).[88]

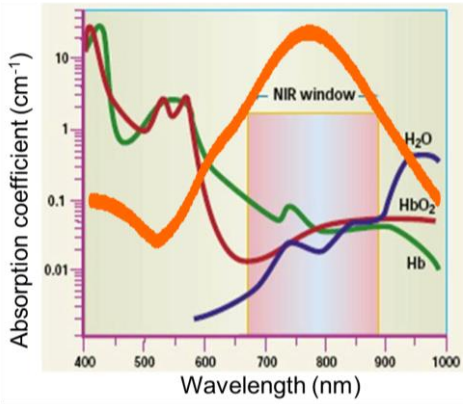

Figure 6. Nanoshells and Near Infrared Window. Adapted scheme depicting NIR window I with an overlayed NS absorbance spectrum (orange).[89]

In addition to NP structure, the mode of light irradiation is important to consider when designing NP platforms for certain desired effects. Historically, continuous wave (CW) lasers have been used primarily for photothermal applications, as the NPs are constantly being activated as the laser is turned on for collective NP heating.[90] Alternatively, pulsed laser irradiation, in which ultrafast pulses of laser light are used to activate NPs are typically used for photoresponsive release of loaded cargo.[91] Pulsed light irradiation of NPs generates a localized energy conversion within the vicinity of the NPs, avoiding heat generation that is time dependent. This capability allows for spatial and temporal control over gene regulation. Since both CW and pulsed lasers cause different responses, it is critical to consider the laser parameters and NP design based on a desired outcome. In **Chapter 3** of this dissertation, CW and pulse laser release of miRNA is compared and the capabilities of a nanosecond pulsed laser versus a more traditional femtosecond laser is evaluated.

1.2.3 Nanoparticle Based Delivery of RNAs

Gene regulation is a technique used to treat diseased cells by using nucleic acids to either replace or inhibit genes that drive the disease progression. This has the most potential for targets that are considered undruggable by small molecule therapeutics due to a lack of an effective binding site. Some of the common nucleic acids utilized include DNA plasmids, CRISPR-Associated Protein 9, RNA therapeutics.[92] For the scope of this dissertation, we will be focused on RNA therapeutics specifically siRNA and miRNA.

siRNAs regulate overexpressed genes *via* RNAi by targeting only a specific downstream mRNA molecule. siRNAs are a class of double stranded RNA around 20 bp in length and are delivered externally to silence downstream target genes through

RNAi.[6] To reiterate the RNAi mechanism described in **Chapter 1.1.3**, cell functions are maintained by regulatory miRNA produced in the nucleus. After exportation into the cytoplasm and additional processing, the mature miRNA is incorporated into RISC. RISC then shuttles the miRNA to relevant mRNA target genes for either degradation or repression depending on the binding complementation of corresponding sequences. Exogenous siRNA duplex sequences are designed with a target mRNA in mind to degrade the mRNA upon perfectly complementary binding. Thus, after delivery into the cytoplasm, duplexed siRNA are recognized and incorporated into RISC. RISC maintains the guide strand and shuttles the siRNA to degrade the relevant mRNA target genes.[93]

Alternatively, miRNA mimics seek to restore the expression of downregulated disease-suppressive miRNA.[43,94] Similarly to siRNA delivery above, exogenous miRNA are delivered into the cytoplasm where they are recognized by RISC and processed through the RNAi mechanism in the same manner. The main difference is due to miRNA being capable of binding to multiple mRNA targets either perfectly complementary or imperfectly. This results in either full degradation or partial repression of the target mRNA sequences.

While RNA therapeutics, and other gene therapies, are highly promising in disease eradication, unmodified naked nucleic acid delivery is not suitable for clinical use due to barriers that include poor stability in biological fluids, unfavorable pharmacokinetics profiles, and limited ability to penetrate across cellular membranes (**Figure 7**).[6] Additionally, in regards to miRNA therapeutics, there is an additional risk factor of wide-spread nonspecific gene regulation, if the miRNA are delivered to other non-specific cells. NP platforms can enhance nucleic acid delivery by overcoming

these barriers regarding stability and effective delivery. Additionally, depending on the design of the NP platform, the release of nucleic acids can be released as desired, whether it is pH activated or initiated from other external stimuli.[95,96] Overall, this dissertation aims to increase favorable delivery of RNA therapeutics through NP platforms. Specifically in **Chapter 3**, we aimed to improve upon the specificity and potency of miRNA delivery through an on-demand light-triggered release NP platform. In **Chapters 4 & 5**, we improved upon the delivery of siRNA *via* NP carriers by co-delivering a targeting antibody.

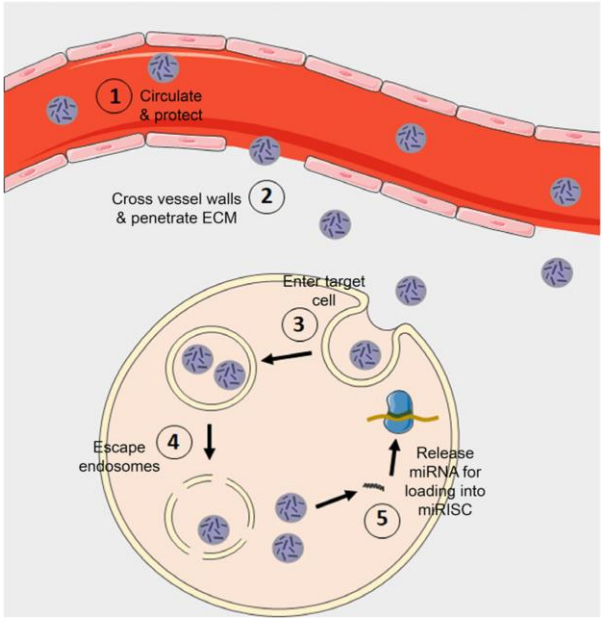

Figure 7. Barriers to RNA Delivery. Scheme depicting the biological barriers that RNA nanocarriers must overcome.[6]

1.2.4 Antibody-Mediated Nanoparticle Delivery

Antibodies are extremely valuable tools in modern medicine due to their ability to target diseased cells through selective antigen binding and thereby regulate cellular

signaling or inhibit cell-cell interactions with high specificity.[97] However, the therapeutic utility of freely delivered antibodies is limited by high production costs, low efficacy, dose-limiting toxicities, and inability to cross the cellular membrane (which hinders antibodies against intracellular targets). To overcome these limitations, researchers have begun to develop nanocarriers that can improve antibodies' delivery efficiency, safety profile, and clinical potential.[98]

Antibodies that can target diseased cells through selective antigen binding and thereby regulate cellular signaling or inhibit cell-cell interactions with high specificity are extremely valuable tools in modern medicine. The monoclonal antibody (mAb) market has grown rapidly in the past decade, with an anticipated valuation of US $137-$200 billion by 2022.[99] Over 120 mAbs have been approved by the Food and Drug Administration (FDA) for treatment of diseases including cancer, autoimmune disorders, and most recently, coronavirus (**Figure 8**).[100] Further, over 2000 numerous mAbs and biosimilars are in preclinical or clinical development, indicating a bright future for antibody therapeutics.[101]

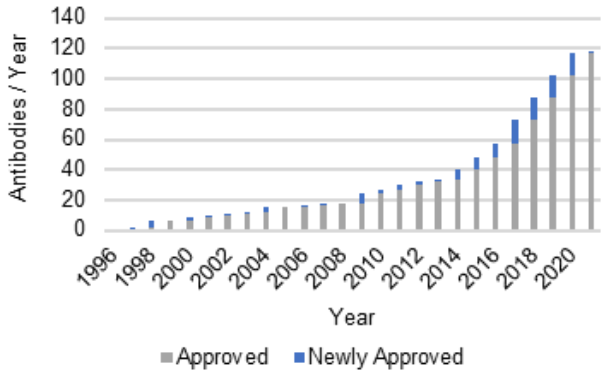

Figure 8. Timeline of mAbs FDA Approvals. Adapted graph depicting the number of FDA approved mAbs overtime.[8]

An antibody's antigen specificity is defined by the variable domains of the Fab (fragment, antigen binding) region within its structure. While polyclonal antibodies bind multiple epitopes on a targeted antigen, mAbs bind a precise epitope, which affords greater specificity, affinity, and biologic effects. However, mAbs are expensive to produce and limited by low efficacy due to poor tissue penetration and inability to cross the cellular membrane.[102,103] To maximize the advantages antibodies provide, technologies such as antibody-drug conjugates are being developed and other methods to enhance mAb stability, delivery, and efficacy are being explored.[102,104]

NP have emerged as promising therapeutic carriers of mAbs because they can improve cargo stability, pharmacokinetics, and delivery into diseased tissues.[105] Nanocarriers can be synthesized from diverse materials, including lipids[106–109], polymers[6,110], and metals[57,111–113], for desirable properties (size, charge, shape, and surface functionality).[105] While most nanocarrier research has focused on delivery of small molecule drugs or nucleic acids, recent studies investigate large protein and antibody nanocarriers.[114,115] Compared to freely delivered antibodies, antibody-NP conjugates have improved efficacy and reduced toxicity owing to the carriers' ability to protect their cargo *in vivo*, provide multivalent binding effects, and more.[105,116] **Chapter 4 & 5** of this dissertation exploits the targeting and repressive functionalities of antibodies towards oncogenic signaling cascades and further inhibits the signaling pathway at the intracellularly level through delivering siRNA.

1.3 Introduction to Gold Nanoshells

In this dissertation, gold NS comprised of silica cores and gold shells are used as the base nanocarrier for two unique platforms designed for various methods of cancer therapy (**Figure 9**). Bare NS are advantageous due to their small size, around

150 nm diameter, which is tunable. More importantly being at this size they enable tumor penetration through passive accumulation means. Additionally, the large surface area provides a platform in which biomolecules can be functionalized for active targeting, gene regulation, or drug purposes. Specifically, the gold surface enables a simple bioconjugation method *via* gold-thiol bonding. This allows scientists to conjugate antibodies, RNA, PEG, amongst other biomolecules without complex methods required. Lastly the unique core:shell structure of NS provides them with unique optical properties in which NS can be engineered to maximally absorb NIR light. This enables NS to be visualized through two photon microscopy and as photothermal transducers NS can be utilized for either heat-based or light-activated therapies.[86,90,91,117,118] Gold NPs have always been a reliable carrier due to their optical visualization and ease of bioconjugation. Consequently, NS have progressed furthest in clinical development in comparison to other gold-base NPs and have shown success in safety assessments in clinical trials.[119,120]

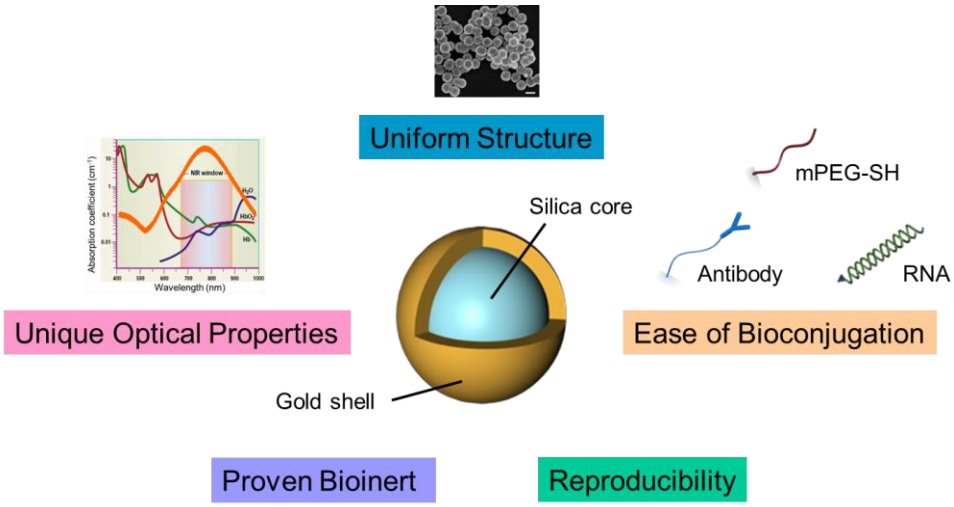

Figure 9. Benefits of Gold Nanoshells. Graphic depicting the advantages of gold NS exploited in the context of this dissertation.

1.3.1 Structure and Photoreactive Capabilities

The specific and design of NS used in this dissertation was carefully chosen for size on the nanoscale, ease of bioconjugation, scalability, and optical capabilities (**Figure 10**). NS are comprised of aminated silica cores, which can range in size, but for the purposes of this work, we chose the 120 nm diameter cores. Gold colloids on the scale of 2 – 3 nm in diameter are then adsorbed to the surface of the aminated silica core, initiating the outer shell formation. Another valuable component of NS is the tunability in shell thickness, which contributes to its optical capabilities. Using the Mie theory, Oldenburg *et al*. showed that the gold shell thickness impacted the light absorbance properties of gold NS.[121] The NS engineered in this dissertation were synthesized with 15 nm thick shells which were characterized by maximal absorbance peaks around 800 nm. Consequently, 180 nm size NS were optical for maximal activation within the NIR window I and could enable optical imaging and phototherapies.

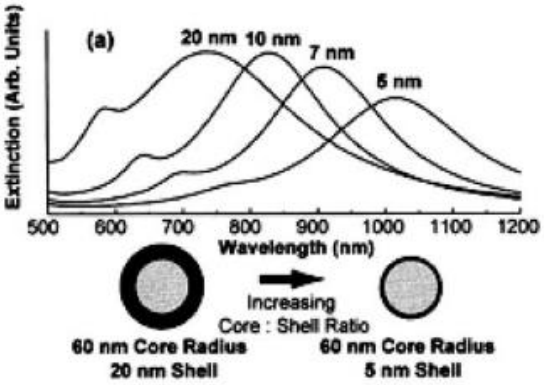

Figure 10. Gold Nanoshell Tunability and Absorbance Spectrum. Graphs showing the tenability of gold NS synthesis to control the peak plasmon resonance peak.[86]

Due to the high scattering profiles of NS, they can be visualized under several imaging modalities, which include optical coherence tomography, darkfield microscopy, and multiphoton microscopy. For the scope of this dissertation, we will primarily utilize multiphoton microscopy, in which NS emit light in response to being activated by a pulse NIR laser specifically tunes their peak plasmon resonance wavelength.[122] Using multiphoton microscopy, targeted NPs can be visualized bound to cancer cells to assess specific binding and update which is described in detail in **Chapter 4**.

1.3.2 Development of Antibody and/or RNA Nanoshell Delivery Platforms

NS were used as the core delivery platform through this dissertation work because of their inherent properties as described above and each chapter following details the synthesis of the base NP along with the design of therapeutic nanocarrier platforms (**Figure 11**). **Chapter 2** describes the methodology to synthesis the base NS and to functionalize them with PEG, antibodies, and RNA therapeutics. In **Chapter 3,**

we exploited the photoreactive properties of NS to deliver miRNA using NIR irradiation for an on-demand release system. The goal of this aim was to increase the delivery and ultimate potency of the miRNA being release once it is at the desired site, within the cytosol for more effective gene replacement therapy. **Chapters 4 & 5** focus on antibody-coated NS for targeted co-delivery of siRNA therapeutics. This co-delivery platform was designed to first demonstrate how multivalent NP binding can increase cellular update and secondly influence oncogenic cell signaling at multiple levels extracellularly and intracellularly. **Chapter 4** focuses on understanding the effects of the co-delivery platform through multiple *in vitro* studies, while **Chapter 5** probes the capabilities of the NP platform in impacting primary tumors and metastasis *in vivo*.

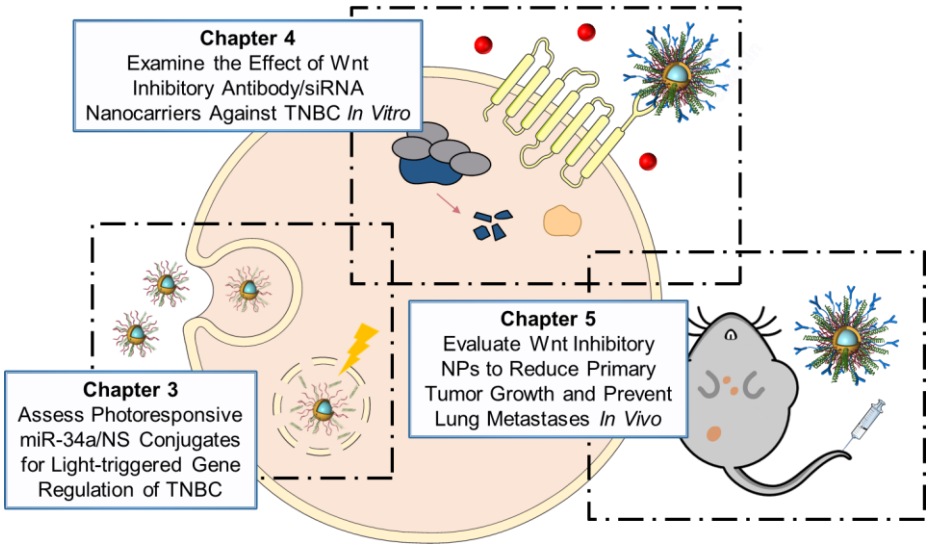

Figure 11. Nanoparticle Platforms Designed In Context of This Dissertation. Graphic depicting the two main nanocarrier platforms designed and the outline of the main three scopes of this dissertation.

Chapter 2

MATERIALS AND METHODS FOR NANOPARTICLE SYNTHESIS & CHARACTERIZATION

2.1 Introduction

This chapter presents the overarching materials and methods used throughout this dissertation for NP synthesis, functionalization, and characterization. Additional materials and methods specific to each chapter are presented later in the respective sections.

2.2 Nanoshell Preparation & Synthesis

NS were synthesized by published methods.[121] First 3-5 nm diameter gold colloids were made by the Duff method[123] from hydrogen tetrachloroaurate (III) hydrate ($HauCl_4$) (VWR), tetrakis(hydroxymethyl)phosphonium chloride (VWR), and 1 N sodium hydroxide (Fisher Scientific). The gold colloid solution was then combined with 120 nm silica spheres functionalized with 3-aminopropyltriethoxysilane (Nanocomposix) and 1 M sodium chloride (NaCl) and rocked for 3-4 days at RT to create "seed" NPs (**Figure 12**). The seed solution was purified twice *via* centrifugation and resuspended in milliQ water to an optical density (OD) of 0.1 at 530 nm. The diluted seed solution was mixed with additional $HAuCl_4$ diluted in potassium chloride followed by addition of a small volume of 37% formaldehyde (VWR). The mixed solution was rapidly agitated to form complete gold shells. Different ratios of the seed, potassium chloride, and 37% formaldehyde were

mixed in small volumes to determine the combination that would produce NS with maximum extinction near 810 nm; this ratio was scaled up to produce the desired volume of NS. Synthesized NS were stored in water at ~$6x10^9$ NS/mL ($OD^{810\ nm} = 2$) at 4°C. Additionally, NS were treated with 0.1% diethyl pyrocarbonate (DEPC) (Sigma) for 3 days rocking at 37°C to render the NS RNase-free. All materials described were purchased or treated with DEPC to be RNase-free prior to use. All NS concentrations were calculated based on Beer's law using the peak extinction (~810 nm) or absorbance measured on a Cary 60 UV-visible spectrophotometer. The modified Beer's Law equation used was NPs/mL = 2.303 * (Absorbance) / [(Cuvette Pathlength) * (Extinction Coefficient) * (π * $Radius^2$)]. Constants: Cuvette Pathlength = 0.01 m, Extinction Coefficient = 4.761, Radius = 74 nm.

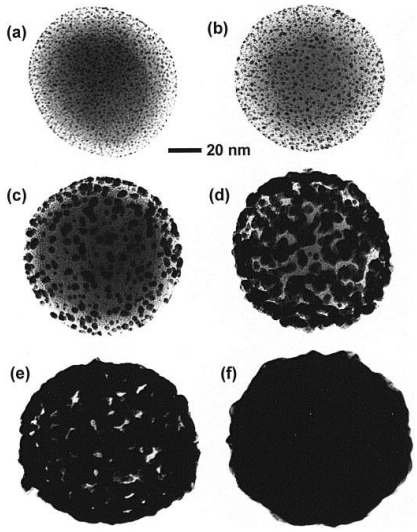

Figure 12. Nanoshell Formation. TEM images of seed growth as the colloid coats the aminated silica cores overtime starting with a) the initial gold colloid deposition to f) with complete growth of the metallic NS.[121]

2.3 Nanoshell Functionalization with methoxy-poly(ethylene) glycol (mPEG), Antibodies, and RNA

Throughout this dissertation, NS were coated with biomolecules (either antibodies and/or RNA duplexes) and passivated with mPEG molecules.

2.3.1 Methoxy poly(ethylene) glycol Attachment to Nanoshells

5 kDa methoxy-poly(ethylene glycol)-thiol (mPEG-SH, Laysan) was added to the NS at a final concentration of 10 μM. After rocking 4 hours at 4°C, the NS solution was purified *via* centrifugation at 500 g for 10 minutes and resuspended in RNase-Free 1X PBS with 100X less volume of the starting NS volume. The miRNA/NS were then stored at 4°C until use. All NS concentrations were calculated based on Beer's law using the peak extinction (~810 nm) measured on a Cary 60 UV-visible spectrophotometer.

2.3.2 miRNA Loaded Nanoshell Conjugation

miRNA oligonucleotides were purchased as single strands from Integrated DNA Technologies. The sense strands were modified with thiol groups on the 3′ end to allow functionalization to the surface of NS. Complementary sense and antisense strands were mixed in duplex buffer (IDT) in equimolar amounts, heated at 95°C for 5 min in a thermomixer, and slowly cooled to 37°C over 1 hour to facilitate duplexing. Duplexed miRNA was aliquoted into one use volumes and stored at -80°C until used for NS conjugation.

NS were diluted to $OD^{810\ nm}$ = 1.5 in milliQ water (**Figure 13**), then 0.2% Tween-20 and 30 mM NaCl were added and incubated with the NS for 5 min at RT. miRNA duplexes were then added to NS at 0.25 or 0.2 nmol miRNA per mL of NS for miR-34a or miR-co sequences, respectively. The solution was vortexed and left to

rock at 4°C for 6 hours. Every 1.5 hours, the solution was briefly vortexed and bath sonicated. At 3 hours, NaCl was added to the solution to increase the NaCl concentration to 160 mM, and at 6 hours the NaCl content was increased to 800 mM. The salt aging step screens charges between duplexes to maximize miRNA loading on NS. The solution was rocked at 4°C for at least 12-14 hours. The NS were then briefly vortexed, and bath sonicated. Next, 5 kDa methoxy-poly(ethylene glycol)-thiol (mPEG-SH, Laysan) was added to the NS at a final concentration of 5 µM. After rocking 4 hours at 4°C, the NS solution was purified *via* centrifugation at 500 g for 5 minutes 3 times, resuspended in RNase-Free 1X PBS with 100X less volume of the starting NS volume. The miRNA/NS were then stored at 4°C until use. All NS concentrations were calculated based on Beer's law using the peak extinction (~810 nm) or absorbance measured on a Cary 60 UV-visible spectrophotometer as described in the nanoshell synthesis section above.

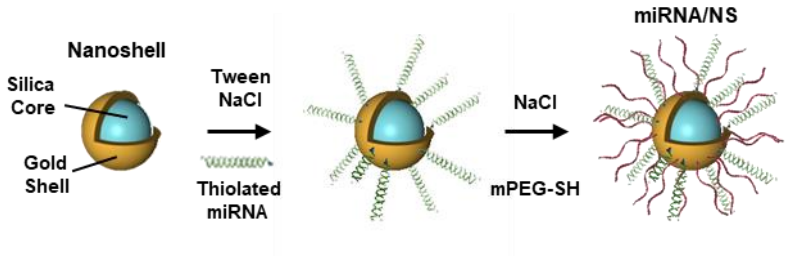

Figure 13. Functionalization of Gold Nanoshells with miRNA Duplexes. Adapted scheme of miRNA conjugation onto gold NS.[124]

2.3.3 Antibody and siRNA Loaded Nanoshell Conjugation

FZD7 antibodies (LSBio) were ordered at 1mg/mL from 100 – 200uL each batch. Upon arrival the antibodies were diluted in sterile 1X PBS at 10X the original

volume to remove the original suspension solution of PBS, 0.02% sodium azide, 50% glycerol, 0.5% BSA. The antibody dilution was reconcentrated and purified using 10 kDA filter centrifugation tubes (Amicon) spun at 8°C 4200rpm for 30 minutes. The final solution was resuspended in 1X PBS to the original volume in order to maintain the original concentration of 1 mg/mL. To non-directionally conjugate antibodies to NS, the FZD7 antibodies were incubated with 5 kDa orthopyridyl disulfide-PEG-succinimidyl valerate (OPSS-PEG-SVA, Laysan Bio) in 100 mM sodium bicarbonate. Volumetrically nine parts OPSS-PEG-SVA in sodium bicarbonate were reacted with one part antibody at a two PEG:one antibody molar ratio, followed by rocking overnight at 4°C. The PEGylated antibodies were aliquoted into one use volumes and stored at -20°C until used for NS conjugation.

β-catenin siRNA oligonucleotides were purchased as single strands from Integrated DNA Technologies. The sense strands were modified with thiol groups on the 3′ end to allow functionalization to the surface of NS. Complementary sense and antisense strands were mixed in duplex buffer (IDT) in equimolar amounts, heated at 95°C for 5 min in a thermomixer, and slowly cooled to 37°C over 1 hour to facilitate duplexing. Duplexed siRNA was aliquoted into one use volumes and stored at -80°C until used for NS conjugation.

PEGylated FZD7 antibodies and duplexed siRNA were left to thaw on ice for ~30 minutes prior to conjugation. NS were diluted to $OD^{810\ nm} = 1.5$ in milliQ water (**Figure 14**) and FZD7-antibodies were added to NS at 1200 or 1000 antibodies per NS for FZD7-NS or Combo-NS respectively. The solution was then vortexed briefly and rocked at 4°C for 1 hours. The solution was then briefly vortexed, and bath sonicated for resuspension. 0.2% Tween-20 and NaCl (at 40 and 12 mM

concentrations for Combo-NS and βcat-NS respectively) were added and incubated with the NS for 5 min at RT.

siRNA duplexes were then added to NS at 0.25 or 0.1 nmol miRNA per mL of NS for Combo-NS and βcat-NS respectively. The solution was vortexed and left to rock at 4°C for 6 hours. Every 1.5 hours the solution was briefly vortexed, and bath sonicated. At 3 hours, NaCl was added to the solution to increase the NaCl concentration to 200 or 60 mM (Combo-NS and βcat-NS respectively), and at 6 hours the NaCl content was increased to 1000 or 300 mM (Combo-NS and βcat-NS respectively). The solution was rocked at 4°C for at least 12-14 hours. The NS were then briefly vortexed, and bath sonicated. Next, 5 kDa methoxy-poly(ethylene glycol)-thiol (mPEG-SH, Laysan) was added to the NS at a final concentration of 10 or 20 μM (details explicitly stated in **Chapters 4 & 5**). After rocking 4 hours at 4°C, the NS solution was purified *via* centrifugation at 500 g for 15 minutes once, followed by two 10 minutes spins at 500g. After removal of the supernatant, the NPs were resuspended in RNase-Free 1X PBS with 100X less volume of the starting NS volume. The antibody and/or siRNA NS conjugates were then stored in LoBIND centrifuge tubes (FisherSci) at 4°C until use. All NS concentrations were calculated based on Beer's law using the peak extinction (~810 nm) measured on a Cary 60 UV-visible spectrophotometer.

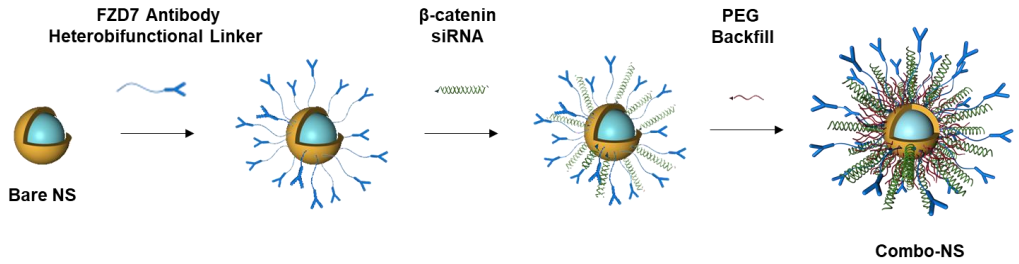

Figure 14. Functionalization of Gold Nanoshells with Antibody and siRNA.

2.4 Characterization Methods of Antibody and/or RNA Loaded Nanoshells

The various NP platforms synthesized were visualized by transmission electron microscopy (TEM) imaging, characterized by dynamic light scattering (DLS) & zeta potential measurements, and quantified for biomolecule loading *via* enzyme-linked immunosorbent assay (ELISA) and OliGreen^{TM} assays as described in detail through the following sections.

2.4.1 UV-Vis Spectroscopy of NP Conjugates

A 100X dilution of the stock NPs were made in molecular grade water to a total of 500uL in volume to be read on the Cary 60 UV-visible spectrophotometer at the peak wavelengths (~810nm) to determine the stock concentration based on optical density (OD). NP dilutions were placed into disposable cuvettes and scanned from 400 – 1100 nm light using a scan rate of 2400 nm/sec and a baseline determined from water was subtracted from the scan. NS concentration was calculated using the peak absorbance and Beer's law. For reference, an optical density (OD) of 1 correspond to $3x10^9$ NPs/mL. NS used for this dissertation were characterized with four distinct UV-Vis features: 1) a narrow plasmon peak at around ~800 nm, 2) a secondary bump at ~600 nm, 3) a trough at ~500 nm, and 4) a peak to trough ratio greater than 3. These

characteristics contribute to the monodisperse, size, and photoreactive properties required for the design of the corresponding nanocarrier platforms.

2.4.2 Electron Microscopy of NP Conjugates

Electron micrographs of the miRNA/NS conjugates were acquired on a Zeiss Libra 120 Transmission Electron Microscope (TEM) at the Delaware Biotechnology Institute. TEM samples were prepared by placing small amounts of NP solutions at $OD^{810\ nm} = 1$ on hydrophilic carbon support films with copper grids in a 400 mesh, followed by a uranyl acetate counter stain. Shannon Modla at the Delaware Biotechnology Institute assisted with TEM sample preparation and imaging. Briefly, images showed monodispersed NPs with a diameter of around 180 – 200 nm.

2.4.3 Dynamic Light Scattering & Zeta Potential Characterization

The hydrodynamic diameter and zeta potential of the miRNA/NS conjugates and bare NS were measured using an Anton Paar Litesizer with at least 3 different batches of NPs diluted in milliQ water. At least 300 µL of NPs at $3x10^9$ NPs/mL ($OD^{810\ nm} = 1$) were used in the Litesizer Uvettes and Omega Cuvettes. Dynamic Light Scatting (DLS) replicates had 60 runs each while the zeta potential replicates included 1000 runs. Briefly, bare nanoshells were about 150 nm in diameter with a charge of around -30 mV. Following biomolecule conjugation, microRNA and antibody and/or siRNA functionalized NPs increased to ~180 – 200 nm in diameter and were more neutral in charge to around -10 mV.

2.4.4 Quantifying RNA Loading on NP Conjugates

RNA loading on NS was quantified using a Quant-iT OliGreen^{TM} ssDNA quantification kit[125] (**Figure 15**). Briefly, RNA loaded NPs were diluted to $OD^{810\ nm}$ =

1, then further diluted with equal volume of 8 M Urea (Sigma). The solution was heated at 45°C and vortexed at 400 rpm for 20 minutes to denature the duplexes. Following this, the NPs were pelleted twice at 1500 x g for 5 minutes, and the supernatant with released antisense strands was collected for quantification. The supernatant was added to a 96-well plate with black walls and bottom in triplicates and the OliGreen™ dye (diluted per manufacturer instructions) was added in equal volume. The plate was excited at 480 nm and fluorescence emission was read at 520 nm using a Biotek Synergy H1 Microplate Reader. The antisense supernatant was compared to a standard curve of antisense strands from 0 – 40 nM. Dividing the number of antisense strands loaded by the number of NS present in the solution revealed the miRNA loading per NS. Briefly, miR-co/NS and miR-34a/NS had approximately 7,300 and 5,500 duplexes on their surface based on the OliGreen™ quantification.

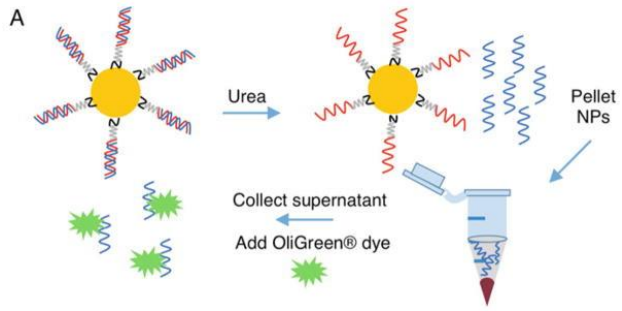

Figure 15. OliGreen™ Assay Quantification of RNA Duplexes on NPs. Adapted schematic representing the procedure to quantify siRNA duplexes on gold NPs.[125]

2.4.5 Quantifying Antibody Loading on NP Conjugates

Antibody loading on NS was quantified using a previously established ELISA assay.[126] Briefly, centrifuge tubes were pre-coated with 1mL of 3% w/v bovine serum albumin in 1X PBS (PBSA) and rocked for 30 minutes at RT. After the blocking incubation, the PBSA was removed *via* aspiration. Meanwhile, antibody loaded NPs and control PEG-NS were diluted to $OD^{810\ nm} = 1$. A stock suspension of secondary HRP-anti rabbit (HRP-AR, Seracare Life Sciences) was prepared to 100 μg/mL in the PBSA. The HRP-AR was then added to the NP suspensions at 10% volumetrically, with an end concentration of 10 μg/mL. The samples were then vortexed and left covered at RT to incubate for 1 hour. Following incubation, the samples were centrifuged at 1500 g for 5 min at RT. 90% of the supernatant was removed, the pellet was dissociated *via* bath sonication, and the samples were resuspended in additional PBSA at the volume originally removed. These three purification steps were repeated two more times. After the last spin step, the samples were resuspended to their original volumes in PBSA. 2.5% of the sample suspension was set aside for antibody quantification (positive samples). 50% of the sample suspension was set aside for UV-Vis analysis in order to quantify the end NP concentration. The remainder sample suspension was spun down once more at 1500 g for 5 min at RT to use the supernatant for background quantification (negative samples). A standard curve was made from the stock 100 μg/mL HRP-AR ranging from 1.9E-4 to 1E-1 μg/mL HRP-AR diluted in 1X PBS. The positive and negative (pos/neg) samples were plated in clear 96 well plates in technical triplicates at a 10X dilution in 1X PBS. The standard curve was plated at the same end volume as the diluted pos/neg samples. 5X volume of 3,3´, 5, 5´- tetramethylbenzidine (TMB Core, BioRad) were added to the samples and standard curve. The plates were left to incubate at RT for 1 minute and then the

reaction was stopped by adding 2 M sulfuric acid at a one-to-one volume to TMB core. The plate was then read at an absorbance of 450 nm using a Biotek Synergy H1 Microplate Reader. The negative sample values were subtracted from the positive samples values to remove background readings and then plotted against the standard curve readings. To calculate the number of antibodies per NS, the number of NS were calculated by reading the absorbance of the 50% NP suspension set aside which was further diluted 2.5X. Dividing the concentration of antibodies loaded by the concentration of NS present in the solution revealed the antibody loading per NS. Briefly, miR-co/NS and miR-34a/NS had approximately 7,300 and 5,500 duplexes on their surface based on the OliGreen^{TM} quantification. Briefly, the antibody loading of Combo-NS and FZD7-NS were ~130 antibodies / NS and siRNA loading of Combo-NS and βcat-NS were ~2400 siRNA / NS.

Chapter 3

PHOTORESPONSIVE miR-34a/NANOSHELL CONJUGATES ENABLE LIGHT-TRIGGERED GENE REGULATION TO IMPAIR THE FUNCTION OF TRIPLE-NEGATIVE BREAST CANCER CELLS

3.1 Introduction

TNBC is an aggressive disease that exhibits more rapid tumor growth, higher recurrence, and poorer prognosis than other forms of breast cancer.[127] TNBC is characterized by absence of the estrogen, progesterone, and human epidermal growth factor 2 receptors, which renders it unsusceptible to traditional targeted or hormonal therapies.[18] Because there is not an effective treatment regimen for TNBC, patients with this disease suffer from earlier relapse, increased rates of metastasis, and lower survival rates.[128–130] New treatment strategies must be developed to improve the prognosis for TNBC patients.

Recent studies have revealed that TNBC typically exhibits down-regulation of the tumor suppressive microRNA, miR-34a.[49,131] This loss of miR-34a expression increases TNBC cell migration and invasion,[26] and TNBC patients with low miR-34a expression exhibit worse overall survival.[51] These observations suggest that restoring miR-34a expression in TNBC cells through the delivery of miR-34a mimics may be a potent strategy to combat TNBC. However, naked miR-34a cannot be administered clinically because, like other nucleic acids, it is unstable in biological fluids, exhibits unfavorable pharmacokinetics, and cannot passively enter cells.[6] Various nanocarriers have been designed to protect miRNA and other nucleic acids from degradation and

deliver them into target cells to initiate gene regulation *via* RNAi.[132–134] However, none of these systems has demonstrated the desired level of potency or specificity. Indeed, most nucleic acid nanocarriers suffer from the inability to distinguish diseased from normal cells, resulting in off-target gene regulation and toxicity because exogenous nucleic acids can activate the innate immune system by engaging toll-like receptors.[135] An ideal delivery system would enable spatiotemporally controlled gene regulation, such that miR-34a is active only in the desired TNBC cells. This would mitigate the potential for undesired immunological side effects. Here, we introduce a system that meets this need.

We, and others, have previously shown that plasmonic NPs, such as NS and nanorods, that are coated with nucleic acids can keep their cargo inactive until it is released from the particle surface on-demand with light.[96,136,137] NS, which are comprised of 120 nm diameter silica cores and 15 nm thick gold shells, are desirable as plasmonic carriers because they maximally absorb tissue-penetrating near infrared (NIR) light and they have already been proven safe in human clinical trials.[81,120,138,139] In our prior work, we showed that NS coated with thiolated siRNA targeting green fluorescent protein (GFP) could silence GFP expression in brain cancer cells *in vitro* only following activation with a femtosecond (fs) pulsed NIR laser.[91] We carefully characterized the mechanism of siRNA release from NS, and found that the release is a temperature-independent process, meaning that the bulk solution temperature does not rise in response to fs pulsed NIR irradiation. This is important because elevated temperatures would risk denaturing the RNA to release single strands rather than full duplexes. Since RISC recognizes duplexes to mediate gene silencing, it is imperative that NIR activation yields full duplex release *via* breakage of the gold-thiol bond

between the NS surface and the RNA. Critically, we confirmed by gel electrophoresis that primarily siRNA duplexes are released from NS following activation with fs-pulsed NIR light, making these conjugates a valuable system for on-demand gene regulation.

In this study, we aimed to demonstrate that NS could enable light-triggered delivery of miR-34a to TNBC cells, resulting in on-demand gene regulation and functional impairment of aggressive cell behaviors. We also aimed to evaluate whether miR-34a release from NS could be achieved with a nanosecond (ns) pulsed laser rather than a fs pulsed laser. Although the fs pulsed laser utilized in our prior work[91] was effective, these systems are expensive and less clinically accessible than ns pulsed lasers. Therefore, we chose to utilize a commercially available ns pulsed LightForce® FXi laser (LiteCure) as the source of NIR irradiation. We hypothesized that miR-34a/NS conjugates would release their cargo upon irradiation with the ns pulsed NIR laser to regulate the expression of miR-34a target genes and impair TNBC cell function (**Figure 16**). The *in vitro* studies presented below validate this hypothesis and demonstrate the immense potential of this system as a tool for spatiotemporally controlled gene regulation of TNBC. This chapter contains sections adapted from Dang *et al.* Nano Letters (2021); 21(1), 68–76.[124]

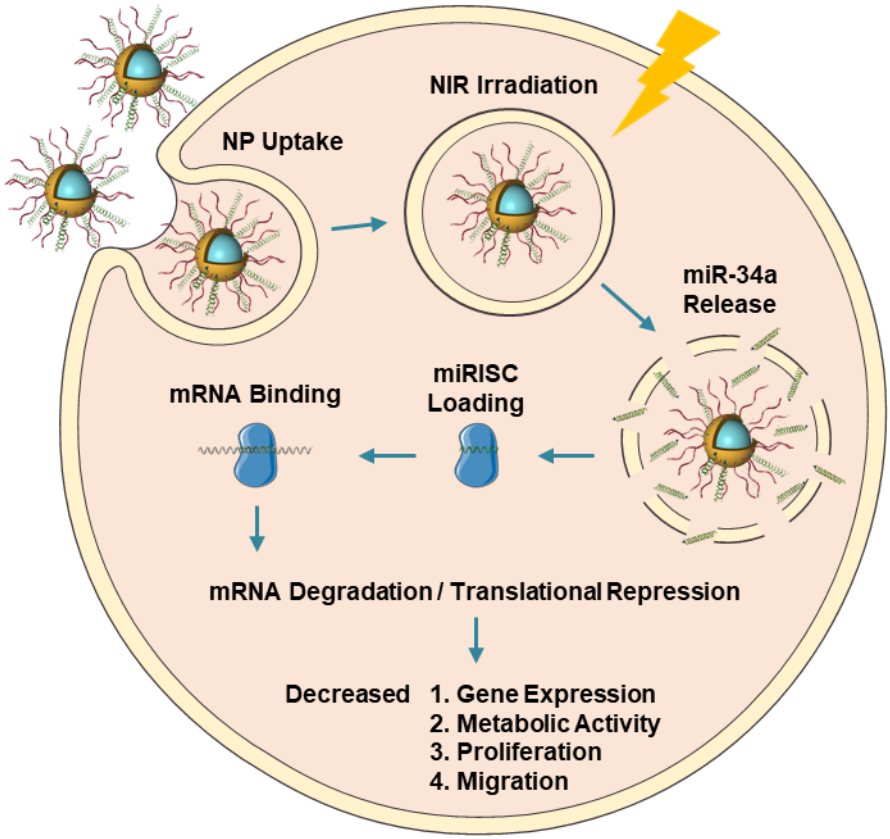

Figure 16. Light-triggered release of miR-34a from nanoshells in TNBC cells. Following miRNA/NS uptake by TNBC cells, the cells are irradiated with a ns pulsed NIR laser, which induces release of the miRNA duplexes from the gold surface of the NPs. RISC recognizes the released miRNA duplexes, initiating gene regulation. When tumor-suppressive miR-34a is delivered into TNBC cells by this mechanism, the metabolic activity, proliferation, and migration of TNBC cells are reduced. Portions of this figure were produced with permission using Servier Medical ART templates, which are licensed under a Creative Commons Attribution 3.0 Unported License from Servier Medical Art; https://smart.servier.com.[124]

3.2 Materials and Methods

3.2.1 Nanoshell Synthesis and Coating with miRNA and mPEG-SH

NS were synthesized according to published methods which were described in detail in **Chapter 2.2**. miRNA oligonucleotides were purchased as single strands from Integrated DNA Technologies (**Table 1**). The sense strands were modified with thiol groups on the 3′ end for ease of functionalization to the surface of the gold NS. Complementary sense and antisense strands were mixed in equimolar amounts and duplexed. NS were diluted to $4.4x10^9$ NS/mL ($OD^{810\ nm}$ = 1.5) in milliQ water and incubated with 0.2% tween, salt aged up to 800 mM, and 0.2 – 0.25 nmol of miRNA, and 5 μM of mPEG-SH which was described in more detail in **Chapter 2.3.2**. In optimizing equivalent loading, we determined how final miRNA loading on the NS is impacted by various parameters, including the initial amount of miRNA, Tween-20 concentration, salt aging conditions, and timing of mPEG addition. NP concentration was determined *via* the absorbance spectrum using the Cary 60 UV-visible spectrophotometer as described in **Chapter 2.4.1.**

miRNA	Sequence
miR-34a sense	5'- ACA ACC AGC UAA GAC ACU GCC A/iSpl 8//iSpl 8//3ThioMC3-D/-3'
miR-34a antisense	5'- UGG CAG UGU CUU AGC UGG UUG U -3'
miR-co sense	5'- AAG UGA UCA AGC ACC GAA GAG /iSpl 8//iSpl 8//3ThioMC3-D/ -3'
miR-co antisense	5'- CUC UUC GGU GCU UGA UCA CUU -3'

Table 1. miRNA sequences utilized.

3.2.2 miRNA/Nanoshell Conjugate Characterization

Electron micrographs of the miRNA/NS conjugates at $3x10^9$ NPs/mL ($OD^{810\ nm} = 1$) were taken on the Zeiss Libra 120 TEM at the Delaware Biotechnology Institute as described in **Chapter 2.4.2**. The hydrodynamic diameter and zeta potential of the miRNA/NS conjugates and bare NS were measured using an Anton Paar Litesizer as described in **Chapter 2.4.3**. miRNA loading on NS was quantified using a Quant-iT OliGreen^{TM} ssDNA quantification kit as described in **Chapter 2.4.4**.

3.2.3 Evaluation of miRNA/Nanoshell Stability

The miR-34a/NS conjugates were also assessed for their stability in various buffer solutions. Specifically, miR-34a/NS were diluted to $OD^{810\ nm} = 1$ in water, PBS at pH 7, or PBS at pH 5.5 at RT. The conjugates were either examined immediately or after 1-hour incubation at 4°C for the water sample and 37°C for the PBS samples. The extinction spectra and hydrodynamic diameters were measured by UV-Visible spectrophotometry and DLS, respectively.

3.2.4 Characterization of miRNA Release Upon Pulsed Nanosecond Laser Irradiation

To determine if solutions of miRNA/NS exhibit temperature changes during CW or ns pulsed irradiation, samples were prepared to $OD^{810\ nm} = 5$ in milliQ water and heated to a starting temperature of 35°C to mimic physiologic conditions. The NP samples were irradiated with a LiteCure FXi laser set to a max pulse of 10K and medium skin (**Figure 17A**). The LiteCure laser is a clinical instrument that has parameters that consider patient-specific considerations, such as skin type. Users can select settings for light, medium, or dark skin based on the Fitzpatrick scale; the medium skin setting was selected for these studies. Importantly, the LiteCure laser

emits both 810 and 980 nm wavelengths, so a bandpass filter (ThorLabs) was used to allow the 810 nm light to pass, while blocking the 980 nm light. The power output of the laser passing through the filter was measured with a power meter and the distance of the laser to the NPs was adjusted to ensure the cuvettes were fully covered and the appropriate laser density was being applied. The NPs were irradiated up to 10 minutes at power densities ranging from 0 to 0.4 W/cm^2 for both CW and ns pulsed laser modes. The temperature of the sample was measured every two minutes with a FLIR A5 Thermal Camera (FLIR) (**Figure 17A**).

The amount of miRNA duplexes remaining bound to the NS post irradiation was measured using the same samples from the temperature experiments. Following irradiation, the NPs were pelleted by centrifugation and the released miRNA was collected with the supernatant; the NS pellet (containing any non-released miRNA) was resuspended in milliQ water. The resuspended NPs were used to quantify the number of antisense strands remaining on the NS using the Quant-iT OliGreen^{TM} ssDNA quantification kit and steps outlined above in **Chapter 2.4.4**. Since the antisense strands are attached to the NS only through their base-pairing to the sense strand, which is physically tethered to the NS by a thiol bond, the number of antisense strands remaining bound post-irradiation indicates the number of duplexes present.

A similar experimental setup was utilized to characterize whether single strands or miRNA duplexes were released from miRNA/NS following ns pulsed irradiation, except that the miRNA/NS were diluted to $OD^{810\ nm} = 2$ in milliQ water to save materials (**Figure 17B**). To examine whether the released miRNA consisted of primarily single strands or duplexes, samples of miRNA/NS in cuvettes were irradiated for up to 30 minutes at the following power densities: 0, 0.20, 0.04, 0.06,

0.15, 0.32, and 0.46 W/cm^2. Post irradiation, the NS were pelleted by centrifugation, and the supernatant containing the released miRNA was collected to run an RNA gel using PAGEr® Gold TBE Precast Gels (Lonza). The gel was loaded with 100 ng of RNA per well, with separate lanes containing stock duplexes, sense strands, antisense strands, and released miRNA. After the gel was run at 150 V for 1 hour, it was stained with SYBR Gold Nucleic Acid Gel Stain (Thermo) for 20 minutes and then imaged using the Ethidium Bromide filter on a UV-Imager.

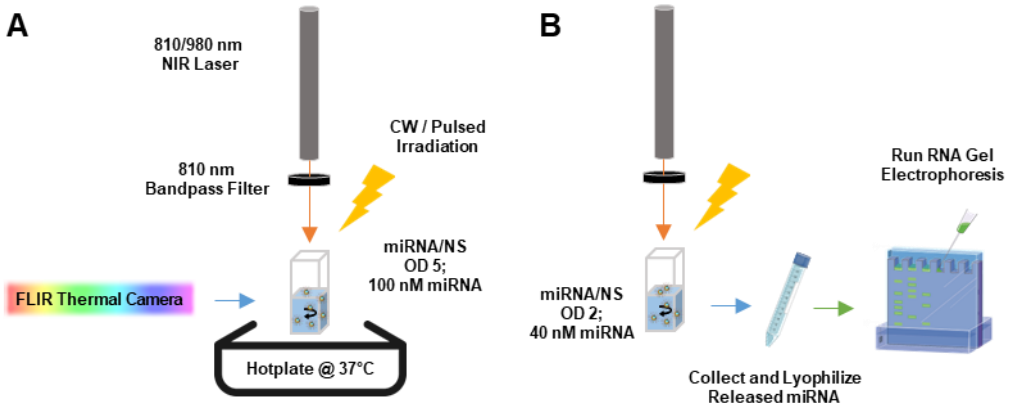

Figure 17. Scheme of Irradiation Setups to Characterize miRNA Release from NS and Impacts of Photoactivated Gene Regulation on Treated Cells. (**A**) Gel electrophoresis analysis was used to assess the structure of miRNA released from NS after irradiation with 810 nm ns pulsed light. After light exposure, the NPs were pelleted and the supernatant containing the released RNA was collected for gel electrophoresis. (**B**) Thermal readings of miRNA/NS were recorded every 2 minutes throughout irradiation to monitor bulk solution temperature changes. Portions of this figure were produced with permission using (1) Servier Medical ART templates, licensed under a Creative Commons Attribution 3.0 Unported License from Servier Medical Art; https://smart.servier.com and (2) Shutterstock Images, licensed under a Standard Image License from Shutterstock; http://shutterstock.com.[124]

3.2.5 Cell Culture and Laser Irradiation Setup for Cell Experiments

MDA-MB-231 TNBC cells purchased from American Type Culture Collection (ATCC) were cultured in Dulbecco's Modified Eagle Medium (DMEM) (VWR) supplemented with 10% fetal bovine serum (FBS) (Gemini Bio) and 1% penicillin-streptomycin (VWR). Cells were cultured in T75 cell culture flasks (VWR), passaged with 0.25% trypsin-EDTA (VWR), and incubated at 37°C in a 5% CO_2 humidified environment. Cells were cultured to 80-90% confluency prior to plating for experiments, used within passage numbers of 40 – 55, and counted using a glass slide hemocytometer for all experiments. GFP-expressing MDA-MB-231 cells (Angio-Proteomie) were cultured with the same conditions.

The general experimental setup used for studies to assess the impact of photo triggered miR-34a delivery on TNBC cells is shown in **Figure 18.** Cells were plated in well plates with complete cell culture media and incubated for at least 20 hours. The cells were then incubated with miR-34a/NS, miR-co/NS, or full media at $1.5X10^{10}$ NP/mL ($OD^{810\ nm} = 5$) for another 20 hours. The cell media was gently pipetted to homogenize the remaining NPs in suspension and the plate(s) were placed into a heat block set to 37°C. The cells were irradiated with the LiteCure FXi laser set to a max pulse of 10K and medium skin. The power was determined by checking the readings with a power meter and adjusting the distance of the laser to the cells to ensure the wells were fully covered and the appropriate laser density was being applied.

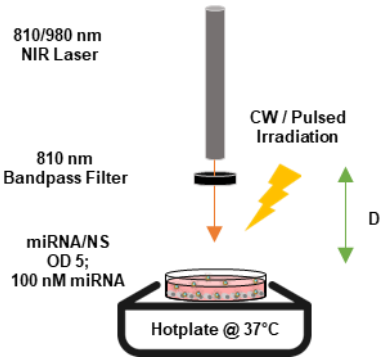

Figure 18. General Setup of Cells Treated with NPs Being Laser Irradiated. Cells were placed on a hotplate during irradiation. D is the distance between the laser and the cells/NPs which was adjusted to ensure the laser beam covered the necessary surface area and that the appropriate laser density was being applied.[124]

3.2.6 Transfection of Cells with miR-34a to Validate Concentration Required for Gene and Functional Impact

The relative expression of these miR-34a target genes was confirmed in MDA-MB-231 *via* cell transfection with 25 nM or 100 nM miR-34a or miR-co using DharmaFect1 (Dharmacon) per manufacturer recommendations. Following 48 hours, RNA was extracted using the Isolate II RNA Mini Kit (Thomas Scientific). Modifications to the protocol include omitting the β-mercaptoethanol addition. RNA concentration was read by reading the sample absorbance at 260 nm using a Take3 Plate on a Synergy H1 plate reader. qRT-PCR was then performed with a concentration of 75 ng RNA/2 uL using the SensiFAST SYBR One-Step Master Mix (Thomas Scientific) on a LightCycler96 (Roche). The mRNA expression levels of each target gene were normalized to that of GUSB and further normalized to no treatment group. Primer sequences are listed in **Table 2**.

Primer	Forward Sequence Reverse Sequence
GUSB	TTTTCTTAGCGCCGCAGA GGGCCTGACTCCCACAG
Bcl2	GACTTCTCCCGCCGCTACC CCCAGTTCACCCCGTCCCT
CCND1	CCTGTCCTACTACCGCCTCA CAGTCCGGGTCACACTTGA
Nanog	AACCTCAGCTACAAACAGGTGA TCTGCGTCACACCATTGCTA
Survivin	CGGTTGCGCTTTCCTTTC TGTTCTTGGCTCTTTCTCTGTCC
Axin2	TTATGCTTTGCACTACGTCCCTCCA CGCAACATGGTCAACCCTAGAC

Table 2. Primer sequences used for real time qRT-PCR studies.

We also assessed cellular metabolic activity 96 hours post transfection of MDA-MB-231 cells with 25, 50, or 100nM of miR-34a or miR-co using DharmaFECT1 as described above to compare the results obtained with those observed for miR-34a/NS + laser treatments. After initial transfection, the cells were incubated for 72-hours then exposed to alamarBlue™ Reagent (Thermo) in complete DMEM media at a 1:100 dilution. The plate was covered and placed back into the cell culture incubator for 4 hours. Following incubation, absorbance was read at 570 nm using the Synergy H1 plate reader. These experiments were performed in triplicate and analyzed using a one-way ANOVA with posthoc Tukey multiple comparisons test.

3.2.7 Transfection of Cells with Released miRNA and EdU Analysis of Cell Proliferation

Prior to examining the direct effects of miR-34a/NS conjugates on TNBC cells, we first performed experiments to confirm that miR-34a retains its functionality following release from NS by ns pulsed irradiation. MDA-MB-231 cells were plated at

10,000 cells/well in a 48-well plate with complete cell culture media and incubated for at least 20 hours. To examine whether the released miRNA retained its functionality, the plated cells were transfected with 50 nM of either released miR-34a/miR-co or native (stock) miR-34a/miR-co using Dharamfect1 (Dharmacon) per manufacturer recommendations (**Figure 19**). Each treatment group had 2 wells each to serve as technical replicates. Following 6 hours, the transfection solution was replaced with antibiotic-free media.

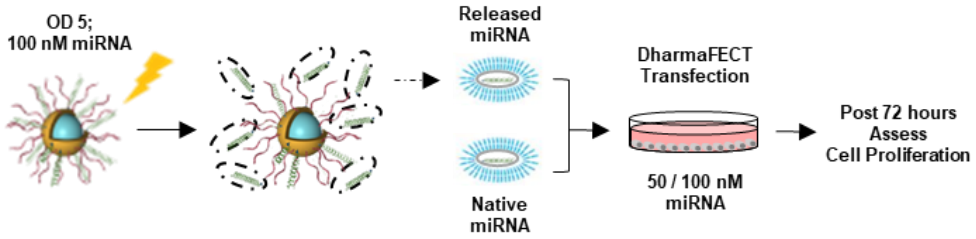

Figure 19. Validating Function of Light-Triggered Release miRNA. Adapted scheme depicting the functionality examination of miR-34a released from NS. to validate that released miR-34a retains its functionality by transfecting TNBC cells with equal concentrations of native or released miRNA and the resultant cell proliferation was measured.[124]

Seventy-two hours after the initial transfection, the cells were assessed for proliferation using the Click-iT^{TM} EdU Cell Proliferation Kit (ThermoFisher). Sixteen hours prior to assessing proliferation (i.e., 56 hours post-transfection), the EdU label was added at 2X equal volume of antibiotic-free media so that the cells were exposed to a final 1X concentration of EdU. At 72 hours, the cells were lifted, pelleted, and fixed with 4% formaldehyde in 1X PBS for 15 minutes. Cells were diluted in 3% bovine serum albumin in 1X PBS (3% PBSA), pelleted and then permeabilized with

0.05% saponin in 1X PBS for 20 minutes. The EdU dye solution, which consisted of Alexa Fluor™ azide, reaction buffer, and reaction additive was made according to the manufacturer's protocol within 15 minutes of use. Alternatively, chromeo 494 azide was used in place of the provided Alexa Fluor™ azide at 5X less volume. Saponin (0.05%) was added to the final dye solution prior to staining cells. Cells were again diluted in 3% PBSA, pelleted and incubated with the EdU dye solution for 30 minutes covered with foil for protection from light. Following this, cells were diluted in 3% PBSA, pelleted, and resuspended in 200 µL of 1X PBS.

The cells were analyzed with an Acea Novocyte 2060 Flow Cytometer at 100 µL/min to a cell cut off at 10,000 cells gated for singlet cells. Cells that were not treated with the initial EdU label were used as an EdU control. Cells were then further gated using the PerCP filter where the cells were excited at 488 nm and detected using the 675/30 nm filter. The parameter set from the EdU control was used to further assess the percentage of cells that were EdU positive or negative. To compare each biological replicate, each treatment group's EdU positive percentage was normalized to the no treatment group (cells that did not receive miRNA/NS or laser exposure). These experiments were performed in triplicate and analyzed by one-way ANOVA with posthoc Tukey multiple comparisons test.

3.2.8 Taqman qPCR Analysis of miR-34a Expression in Cells Treated with miRNA/NS and CW versus Pulsed NIR Light

MDA-MB-231 cells were plated at 10,000 cells/well in 48-well plates prior to treatment with miRNA/NS and the NIR laser. Cells were treated with no NS, miR-co/NS, or miR-34a/NS and irradiated at 0.1 W/cm^2 for 10 min as described in the above **Chapter 3.2.5** with either CW or ns pulsed modes (**Figure 18**). After the cells

were treated and allowed to incubate for one or twenty-four hours, RNA was extracted using the Isolate II RNA Mini Kit (Thomas Scientific). Modifications to the protocol include omitting the β-mercaptoethanol addition. RNA concentration was read by reading the sample absorbance at 260 nm using a Take3 Plate on a Synergy H1 plate reader. Reverse transcription was then performed with a concentration of 20 ng RNA/5 uL using the Taqman miRNA Assay Kit (ThermoFisher) with the sequences listed in **Table 3A** and a reaction volume of 15uL. Reverse transcription was performed in a thermocycler using the parameter values from **Table 3B**. PCR amplification was then performed using the reverse transcriptase RNA and provided Taqman probes in the Taqman MicroRNA Assay Kit on a LightCycler96 (Roche) using the parameter values from **Table 3C**. The miRNA expression levels of miR-34a were normalized to that of U6 and further normalized to the NT – laser group. These experiments were performed in triplicate and analyzed by one-way ANOVA with posthoc Tukey.

A	**Primers for Analysis of miR-34a Expression in Cells**	
Primer	**Accession Number**	**Sequence**
U6 snRNA	NR_004394 (NCBI)	GTGCTCGCTTCGGCAGCACATATACTAAAATTGGA ACGATACAGAGAAGATTAGCATGGCCCCTGCGCAA GGATGACACGCAAATTCGTGAAGCGTTCCATATTTT (Control)
hsa-miR-34a	MI0000268 (miRbase)	UGGCAGUGUCUUAGCUGGUUGU (Mature miRNA)
B	**Thermocycler Parameters for Reverse Transcription**	
Step Type	**Time (min)**	**Temperature (°C)**
Hold	30	16
Hold	30	42
Hold	5	85
Hold	∞	4

C	LightCycler Parameters for Amplification		
Step	**AmpliTaq Gold® Enzyme Activation**	**PCR**	
	Hold	Cycle (40 cycles)	
		Denature	Anneal/Extend
Time	10 min	15 sec	60 sec
Temperature (°C)	95	95	60

Table 3. Parameters for Taqman PCR Analysis of miR-34a Expression in Cells. (**A**) U6 and miR-34a primer sequences ordered from ThermoFisher for the Taqman™ MicroRNA Assay. (**B,C**) Thermocycler and LightCycler parameters for reverse transcription and PCR amplification.

3.2.9 qRT-PCR Analysis of mRNA Expression in Cells Treated with miRNA/NS and Light

MDA-MB-231 cells were plated at 20,000 cells/well in 24-well plates prior to treatment with miRNA/NS and the ns pulsed laser. To ensure enough RNA was collected for downstream analysis, 8 wells were used for each treatment condition, and then the RNA from the 8 samples was combined for analysis. Cells were treated with no NS, miR-co/NS, or miR-34a/NS and irradiated as described in the above **Chapter 3.2.5** (**Figure 18**). After the cells were treated and allowed to incubate, RNA was extracted using the Isolate II RNA Mini Kit (Thomas Scientific). Modifications to the protocol include omitting the β-mercaptoethanol addition. RNA concentration was read by reading the sample absorbance at 260 nm using a Take3 Plate on a Synergy H1 plate reader. qRT-PCR was then performed with a concentration of 75 ng RNA/2 uL using the SensiFAST SYBR One-Step Master Mix (Thomas Scientific) on a LightCycler96 (Roche). The mRNA expression levels of each target gene were normalized to that of GUSB and further normalized to the miR-co/NS – laser group.

Primer sequences are listed in **Table 2** in **Chapter 3.2.6**. These experiments were performed in triplicate and analyzed using a one-way ANOVA with posthoc Tukey.

3.2.10 Western Blot Evaluation of Protein Expression

MDA-MB-231 cells were plated at 20,000 cells/well in 24-well plates prior to treatment with miRNA/NS and the ns pulsed laser. To ensure enough protein was collected for downstream analysis, 4 wells were used for each treatment condition, and then the protein from the 4 wells was combined for Western blot analysis. Cells were treated with no NS, miR-co/NS, or miR-34a/NS and the laser as described in the above **Chapter 3.2.5** (**Figure 18**). Twenty-four and forty-eight-hours post irradiation, cells were lysed with Halt Protease Inhibitor in RIPA buffer at a ratio of 1:100 for at least 15 minutes. The cells were then manually lysed using a pipette tip and collected in 1.5 mL Eppendorf tubes. The lysate was collected, bath sonicated for 1 minute, and pelleted at 12,000 g for 5 minutes at 8°C to remove debris. The lysate supernatant was further concentrated using Spin-X® UF 500 Concentrators (Corning) at 14,000 g for 10 minutes at 8°C. The protein lysate's concentration was determined using the DCTM Protein Assay (Bio-rad) per manufacturers' instructions and compared to a standard curve of 0 – 10% wt BSA/RIPA. The lysate was diluted to at least 30 µg with 1XPBS. Additionally, equal volume of 2X Laemmli's Buffer (Sigma) and lysate were mixed. The lysate mixture was then denatured at 99°C for 20 minutes while vortexing at 400 rpm.

Polyacrylamide Gel Electrophoresis (PAGE) was run using 30 µg of protein sample per well and a prestained protein 11 – 250 kDa ladder (CST). A mini-gel tank (Thermo) was filled with 1X morpholino-ethanesulfonic (MES) sodiumdodecyl sulphate (SDS) running buffer (LifeTech) and set to 120V. The protein was run in 4-

12% Bolt Bis-Tris Plus gels for 75 minutes. Following PAGE, the gel was transferred onto a 0.2 μm pore nitrocellulose membrane using the Power Blotter System (Thermo) set to HIGH MW for 10 minutes. The transferred blot was then blocked in 5% milk diluted in tris buffer saline with 0.1% Tween-20 (TBS-T) for 1-hour rocking at RT. Following the blocking step, the membrane blots were cut right below 32 kDa and right above 57 kDa. The corresponding blots were then incubated with primary antibodies in 5% milk/TBS-T sealed in a plastic sleeve for at least 20 hours rocking at 4°C. The following concentrations were used for the primary antibodies: Sirt1 - 1:500 (Proteintech); Bcl2 - 1:1000 (Proteintech); β-actin - 1:20000 (CST). The next day the blots were washed with TBS-T 3X for 5 minutes rocking at RT. They were then incubated with secondary antibodies, HRP-Rabbit or HRP-Mouse, at a dilution of 1:20,000 for 1 hour covered and rocking at RT. The blots were washed with TBS-T 3X for 5 minutes and an additional wash with just TBS. Finally, the blots were incubated with enhanced chemiluminescence (ECL) solutions (Thermo) per manufacturer's instructions. The blots probed for Sirt1 and Bcl2 were incubated specifically with the SuperSignal West Femto ECL while the blots probed for β-actin were incubated with Pierce ECL Plus Solution. The blots were lastly imaged using a UV-Imager chemiluminescent setting with exposure times ranging from 500 milliseconds to 1 minute. The resultant images were further analyzed in ImageJ for protein quantification. Each target gene was normalized to the corresponding β-actin expression and further normalized to the no treatment group. These experiments were performed in triplicate and analyzed using a one-way ANOVA with posthoc Tukey.

3.2.11 alamarBlue™ Metabolic Activity Assay

To understand the impact of miR-34a/NS and laser treatment on cellular metabolic activity (a measure of viability), MDA-MB-231 cells were plated at 5,000 cells/well in 96-well plates prior to treatment with no NPs, miR-co/NS, or miR-34a/NS and laser irradiated as described in the above **Chapter 3.2.5** (**Figure 18**). Each treatment group contained 3 replicate wells. After NP treatment and laser irradiation, the cells were incubated for 72-hours then exposed to alamarBlue™ Reagent (Thermo) in complete DMEM media at a 1:100 dilution. The plate was covered and placed back into the cell culture incubator for 4 hours. Following incubation, absorbance was read at 570 nm using the Synergy H1 plate reader. These experiments were performed in triplicate and analyzed using a one-way ANOVA with posthoc Tukey.

3.2.12 EdU Proliferation Assay

For studies to assess cell proliferation, MDA-MB-231 cells were plated at 10,000 cells/well in 24-well plates prior to NP and laser treatment. Each treatment group had 2 wells each to serve as technical replicates. Cells were treated with no NS, miR-co/NS, or miR-34a/NS and then irradiated with the laser as described in the above **Chapter 3.2.5** (**Figure 18**). Different sample wells were irradiated for 10 min at 0.05 W/cm^2 or 0.1 W/cm^2 power density. At 72 hours post irradiation, the cells were assessed for proliferation using the Click-iT™ EdU Cell Proliferation Kit (ThermoFisher). The steps of the assay followed the manufacturer's instructions as described above in the **Chapter 3.2.7**. These experiments were performed in triplicate and analyzed using a one-way ANOVA with posthoc Tukey.

3.2.13 Transwell Migration Assay

GFP-expressing MDA-MB-231 cells were plated at 5,000 cells/well in 96-well plates for cell migration studies. Each treatment group had replicates of 2 wells each. Cells were treated with no NPs, miR-co/NS, or miR-34a/NS and laser irradiated as described in the above **Chapter 3.2.5** and depicted in **Figure 20**. Forty-eight hours post-irradiation, the cells were lifted with trypsin, pelleted, resuspended in non-supplemented DMEM, and counted. The cells were then reseeded at 3,000 cells onto the tops of black transwell inserts (Corning) in 24-Well Glass Bottom Black Walled Plates (CellVis); non-supplemented DMEM was in the top of the insert and complete media was in the bottom of the wells. The cells were left to migrate across the 8.0 µm polyester membranes over 120 hours. The cells were imaged at 24, 48, 72, 96, and 120 hours using the GFP filters and tile imaging on an Axioobserver Z1 Inverted Fluorescent Microscope (Zeiss). These experiments were performed in triplicate and analyzed using a one-way ANOVA with posthoc Tukey.

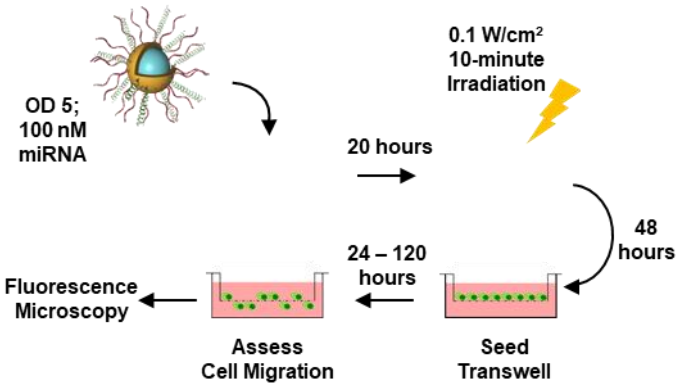

Figure 20. Schematic of NP Treatment and NS-Pulsed Laser Irradiation to Assess Cell Migration 48 Hours Post Irradiation. GFP expressing cells were reseeded into transwell inserts with a porous membrane to assess the numbers of cells that migrated across the membrane.[124]

3.3 Results and Discussion

3.3.1 Optimization of miRNA Loading

To maximize miRNA loading on NS, we optimized the synthesis through various parameters, including the initial amount of miRNA, Tween-20 concentration, salt aging conditions, and timing of mPEG addition (**Figure 21**). While increasing the nmol of miRNA added per mL of NS initially enhances loading, miRNA loading saturates at ~7500 miRNA/NS (**Figure 21A**). We also found that reduced concentrations of Tween-20 enable more efficient miRNA loading (**Figure 21B**). Increasing the concentration of salt during the salt aging period helps facilitate ion screening to increase the density of miRNA loading (**Figure 21C**). Lastly, the timing at which mPEG is added to passivate the NS is important because it competes with the miRNA for remaining binding sites on the NP surface (**Figure 21D**).

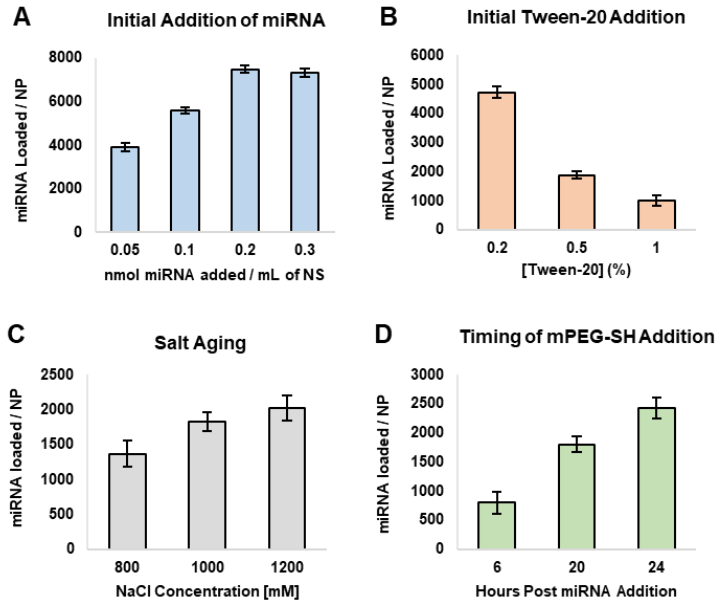

Figure 21. Optimizing miRNA Loading on Nanoshells. (**A**) Increasing amount of initial nmol of miRNA was added to a mL of NS to determine the saturation point of maximum loading. (**B**) Prepping NS with varying concentrations of surfactant Tween-20 impacts end loading of miRNA. (**C**) Increasing salt aging concentrations provide ion screening in order for miRNA duplexes to load more efficiently onto NS. (**D**) Timing of passivating NS with mPEG competes with the loading of miRNA. n = 1 (technical triplicates when quantifying loading, values shown are the average and the standard deviation of the triplicates).[124]

3.3.2 miRNA/NS Conjugate Characterization

The conjugates were visualized with electron microscopy, which confirmed the NPs were monodisperse with diameter of ~150 nm as expected (**Figure 22A**). UV-visible spectrophotometry (**Figure 22B**) provided evidence of successful miRNA conjugation to the NS, as bare NS had a peak extinction at ~810 nm that red-shifted slightly for miR-34a/NS and miR-co/NS. This was corroborated by dynamic light scattering and zeta potential measurements, which revealed the NPs' hydrodynamic diameter increased by ~20 nm and the zeta potential became more neutral following

miRNA and mPEG addition (**Figure 22C**). To quantify miRNA loading on the NS, we employed an OliGreen™ assay as previously described.[125] This revealed that miR-co/NS and miR-34a/NS had approximately 7,300 and 5,500 duplexes on their surface, respectively (**Figure 22D**).

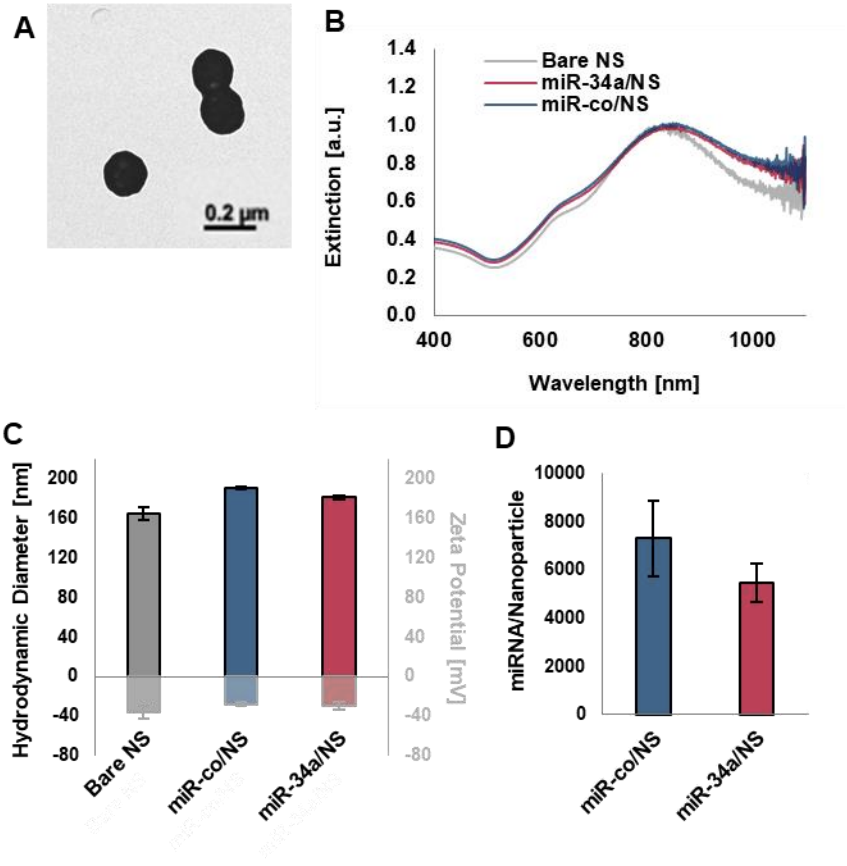

Figure 22. Synthesis and Characterization of miRNA/NS Conjugates. (**A**) Transmission electron micrograph of miR-co/NS. (**B**) Plasmon resonant extinction spectra comparing miRNA/NS conjugates to bare NS with peak extinction at 810 nm. (**C**) Hydrodynamic diameters (black outline) and zeta potential measurements (gray outline) of miRNA/NS conjugates and bare NS. (**D**) OliGreen™ analysis of miRNA loading on both miR-34a/NS and miR-co/NS. n = 12.[124]

3.3.3 miRNA/NS Stability Evaluation

The miRNA conjugates maintained similar absorbance spectrum in physiological conditions mimicked through PBS buffers at pH 5.5 and 7 from initial timepoint to 1 hour later (**Figure 23A**). Additionally, the NPs had relatively the same size in diameter between the two timepoints (**Figure 23B**).

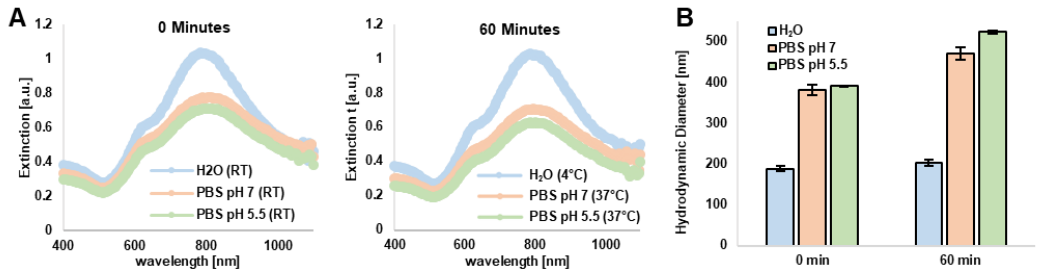

Figure 23. miRNA/NS Stability in Various Buffers. (**A**) Extinction spectra of miR-34a/NS conjugates in various buffers after 0 and 60 minutes of incubation. (**B**) Hydrodynamic diameter of miR-34a/NS conjugates in various buffer conditions after 0 and 60 minutes of incubation. n = 2.[124]

3.3.4 Characterization of miRNA Release from NS after CW and ns Pulsed Laser Irradiation

We first evaluated the thermal response of miRNA/NS irradiated with CW or ns pulsed light. Solutions of miRNA/NS at $1.5E^{10}$ NS/mL (corresponding to an optical density of 5 at the peak extinction wavelength ($OD^{810nm} = 5$)) were placed on a hotplate to bring the starting temperature to ~35°C and then irradiated with 810 nm CW or ns pulsed light at different power densities for 10 min while monitoring the maximum temperature in each sample with an FLIR thermal camera. Within 10 minutes of irradiation at 0.1 W/cm^2 with either laser mode, the temperature increased by ~1°C (**Figure 24A**), versus ~3°C for 0.2 W/cm^2 irradiation. At 0.4 W/cm^2, the temperature increased more drastically and after 10 minutes samples exposed to CW

light were ~1°C warmer than samples exposed to ns pulsed light. To quantify the amount of miRNA released from NS under these conditions, we employed an OliGreen™ Assay, wherein the number of duplexes released was determined by quantifying the number of antisense strands remaining bound to the NS post-irradiation.[125] Since the antisense strands are attached to the NS only through base-pairing to the sense strand, which is physically tethered to the NS, the number of antisense strands measured indicates the number of duplexes bound/released. After 0.1 W/cm^2 irradiation for 10 min, ~84% of miRNA duplexes remained bound to miRNA/NS exposed to CW light, compared to ~70% for those exposed to ns pulsed light (**Figure 24B**). We postulate that the increased miRNA release following ns pulsed irradiation is due to increased localized heating at the NS surface, per prior literature that states pulsed irradiation provides more efficient energy deposition allowing for cleavage of gold-thiol bonds.[140] As power densities increased, more duplexes were released under both modes of irradiation, but we selected 0.1 W/cm^2 for subsequent biological tests since 0.4 W/cm^2 irradiation increased bulk solution temperatures above the 42°C threshold where photothermal damage might occur. At these higher temperatures, duplex melting might also occur, and we aimed to achieve primarily duplex release. To confirm that miRNA/NS release primarily duplexes (rather than single-stranded oligonucleotides) upon ns pulsed irradiation, we examined released miRNA and stock miRNA duplexes and sense/antisense strands were examined by gel electrophoresis. This confirmed that miRNA/NS release primarily duplexes following ns pulsed irradiation across all power densities (**Figure 24C**).

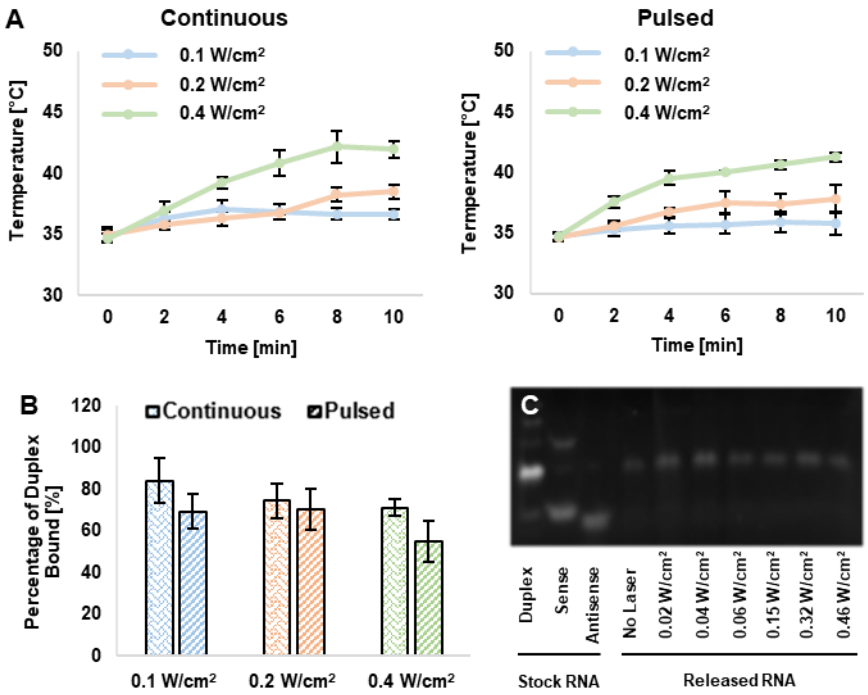

Figure 24. Characterization of miRNA release from NSs after CW and ns pulsed laser irradiation. (**A**) Heating profile of solutions of miRNA/NS conjugates irradiated at various power densities. (**B**) Percent of duplexed miRNA remaining bound to NS post-irradiation at different power densities. Results are from n = 3 different batches of NPs that were irradiated for temperature measurements and duplex quantification. (**C**) Gel electrophoresis of stock miRNA duplexes, sense strands, and antisense strands compared to miRNA released from NS upon irradiation with ns pulsed light at varying power densities. n = 3.[124]

3.3.5 Transfection of Cells Comparing Released and Native miRNA Through EdU Proliferative Analysis

Cells transfected with either native or released miR-co exhibited non-significant decreases in proliferation. Cells transfected with 100 nM of native and released miR-34a were 41% and 47% proliferative, indicating that released miR-34a is as potent as native miR-34a (**Figure 25**).

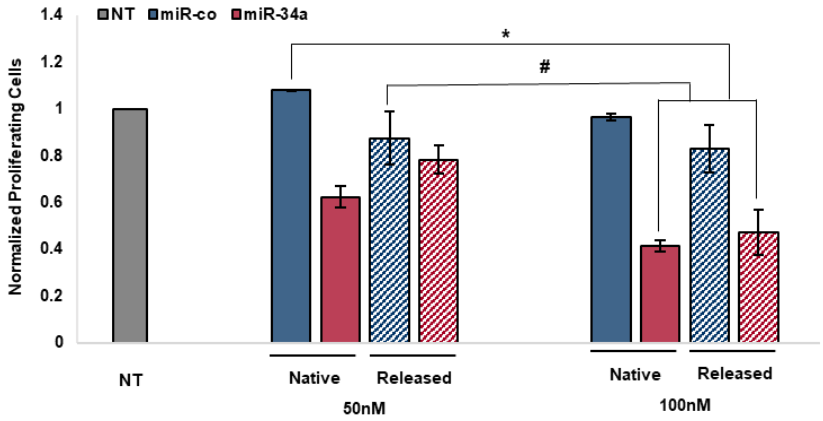

Figure 25. Function of Released miR-34a Compared to Native miR-34a. Normalized count of proliferating cells in samples transfected with native or released miRNA at 50 nM and 100 nM doses. Results are from n = 3 biological replicates with different batches of collected miRNA for transfection. *p<0.05 and #p<0.1 by one-way ANOVA with posthoc Tukey.[124]

3.3.6 Analysis of miR-34a Delivery and Target Gene Regulation in NP Treated TNBC Cells Following CW and Pulsed Laser Irradiation

For *in vitro* studies, we treated MDA-MB-231 cells with miR-co/NS or miR-34a/NS in complete medium at OD^{810nm} = 5 (~100 nM miRNA) for 20 hours, followed by sample irradiation and subsequent analysis. In initial experiments, we evaluated miR-34a expression in cells that were treated with miRNA/NS and exposed to CW or ns pulsed light at 0.1 W/cm^2 for 10 minutes. One hour and 24 hours post irradiation, the cells were lysed to collect RNA for analysis of miR-34a expression by Taqman two-step real-time quantitative reverse transcriptase-polymerase chain reaction (qRT-PCR) At 1-hour and 24-hour post-treatment, miR-34a expression was 1.2X and 1.1X higher in cells exposed to miR-34a/NS + ns pulsed light than cells exposed to miR-34a/NS + CW light (**Figure 26**). Further, miR-34a expression in samples exposed to miR-34a/NS + ns pulsed light was ~2640X higher than that of untreated cells at 1-

hour post-irradiation, and ~260X higher 24-hour post-irradiation. In the absence of irradiation, miR-34a/NS also increased miR-34a expression compared to untreated controls, but the expression at 1-hour post-treatment was 59% of that observed for miR-34a/NS + ns pulsed light. These data demonstrate miR-34a/NS can increase miR-34a expression in TNBC cells, and that the level of expression is greater following irradiation with ns pulsed light than CW light.

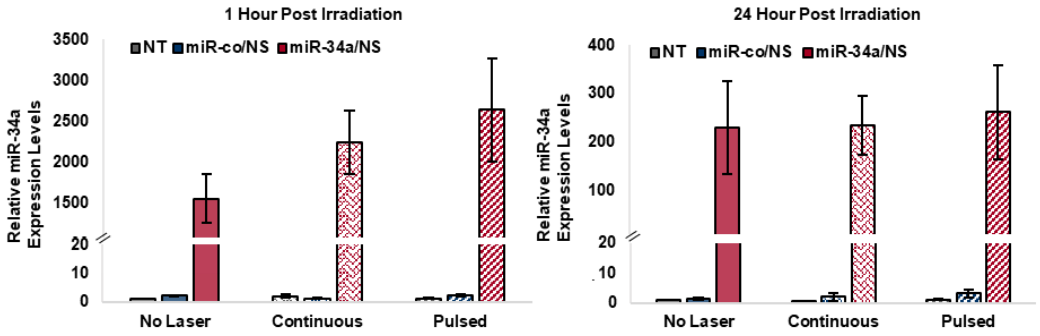

Figure 26. Relative miR-34a Expression in Cells Following Nanoparticle and CW or Pulsed Laser Treatment. Results are from n = 3 biological replicates. Not significant by one-way ANOVA with posthoc Tukey-Kramer.[124]

Knowing that ns pulsed light was more effective than CW light at promoting miR-34a expression in cells, we next evaluated the downstream expression of several known miR-34a target genes by SYBR Green One-Step qRT-PCR and Western blot 24 hours post ns pulsed irradiation. The miR-34a/NS minimally effected expression of Bcl2, CCND1, Nanog, Survivin, and Axin2 in the absence of laser irradiation (**Figure 27**). With ns pulsed laser treatment, miR-34a/NS reduced the mRNA expression of all these genes by at least 50% relative to cells that received miR-co/NS without laser irradiation (**Figure 27**).

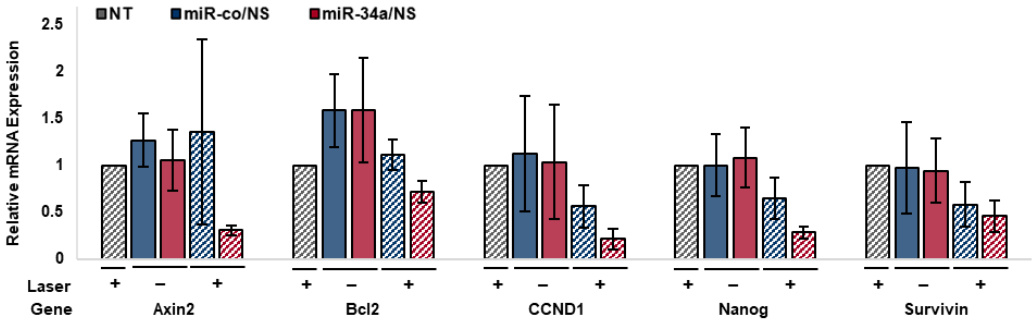

Figure 27. Relative mRNA Expression of miR-34a Target Genes. qPCR-RT assessment of mRNA expression levels in MDA-MB-231 cells following NP and ns pulsed laser treatment. Results are from n = 3 biological replicates for all genes. Not significant by one-way ANOVA with posthoc Tukey-Kramer.[124]

For comparison of gene silencing potency, the mRNA expression of each gene in cells transfected with native miR-34a or miR-co at 25 nM or 100 nM was assessed (**Figure 28**). There was a modest decrease in expression of Bcl2, CCND1, and Survivin when cells were treated with miR-co/NS + laser, which suggests the irradiated NS may have some phototherapeutic effects. However, these differences were not statistically significant versus non-irradiated cells.

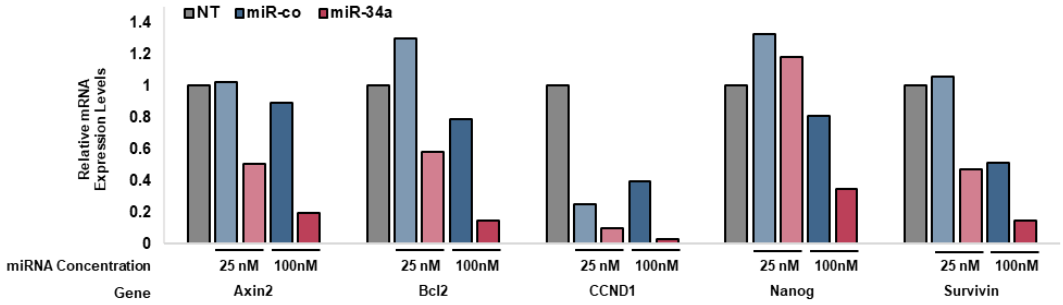

Figure 28. Validation of miRNA Transfection Effects on miR-34a Target Genes. qRT-PCR analysis of the mRNA expression of several genes in MDA-MB-231 cells that were transfected with miR-34a or miR-co for 48 hours n = 1 (technical triplicates when running PCR plates).[124]

We also evaluated the expression of Bcl2 and Sirt1 by Western Blot in treated cells, which showed that only miR-34a/NS + laser decreased protein levels of these genes (**Figure 29A**). Specifically, the expression of Bcl2 and the three Sirt1 isoforms decreased between ~1.5-fold and 2-fold relative to cells that received miR-co/NS without laser exposure (**Figure 29B**).

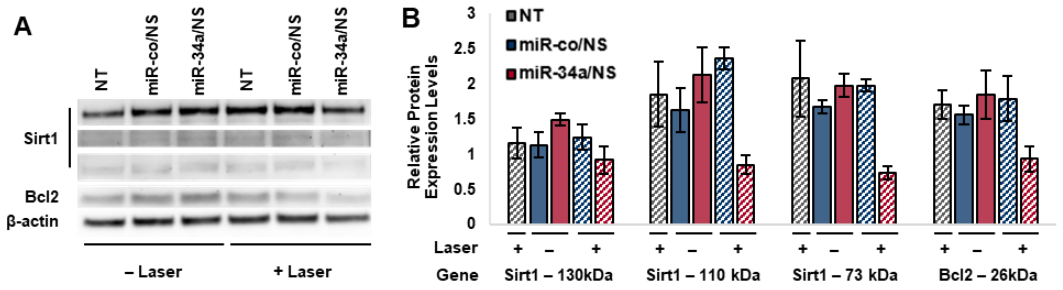

Figure 29. Analysis of Protein Expression of MDA-MB-231 Cells 24 Hours After Pulsed Laser Irradiation. (**A**) Representative Western blot showing Sirt1 (3 isoforms), Bcl2, and β-actin protein expression following NP and ns pulsed laser treatment. Results are from n = 3 biological replicates for all proteins. (**B**) Quantitative densitometry analysis of the Western blots. Not significant by one-way ANOVA with posthoc Tukey-Kramer.[124]

We also evaluated protein expression 48 hours post irradiation, and this substantiated that only miR-34a/NS + laser treatment decreased Bcl2 and Sirt1 levels, although the decrease was not as substantial as that observed 24 hours post-irradiation (**Figure 30**). In aggregate, the qRT-PCR and Western blot analyses confirm that miR-34a/NS can release their cargo upon irradiation with ns pulsed light to induce on-demand gene silencing in TNBC cells. Released miR-34a also appears to be as potent as transfected miR-34a.

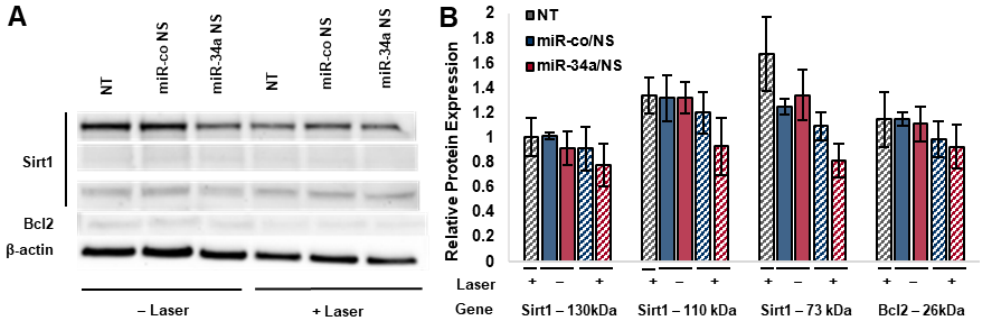

Figure 30. Analysis of Protein Expression of MDA-MB-231 Cells 48 Hours After Pulsed Laser Irradiation. (**A**) Representative Western immunoblotting showing Sirt1 (3 isoforms), Bcl2, and β-actin expression following NP and laser treatment. (**B**) Quantitative analysis of the Western blots. Not significant by one-way ANOVA with posthoc Tukey-Kramer.[124]

3.3.7 Analysis of TNBC Cell Metabolic Activity and Proliferation After Treatment with miRNA/NS and Pulsed NIR Light.

To determine whether light-triggered miR-34a release functionally impairs TNBC cells, we examined the metabolic activity and proliferation of treated cells by alamarBlue™ and EdU assays. Cells were exposed to miR-34a/NS or miR-co/NS followed by laser irradiation, then assessed for metabolic activity and proliferation 72

hours later. The miR-34a/NS reduced cellular metabolic activity by ~6% relative to non-treated cells in the absence of laser irradiation or in the presence of CW irradiation (**Figure 31A**). This difference was not statistically significant. With ns pulsed irradiation, miR-34a/NS yielded a more profound 18% decrease in metabolic activity. By comparison, miR-co/NS + ns pulsed irradiation yielded a non-significant 6% decrease in metabolic activity. To provide context to these results, we also evaluated metabolic activity of cells transfected with 25-100 nM miRNA, which revealed that transfected miR-34a reduced metabolic activity by 23%-26% (**Figure 31B**), a comparable result to that observed for miR-34a/NS + ns pulsed irradiation.

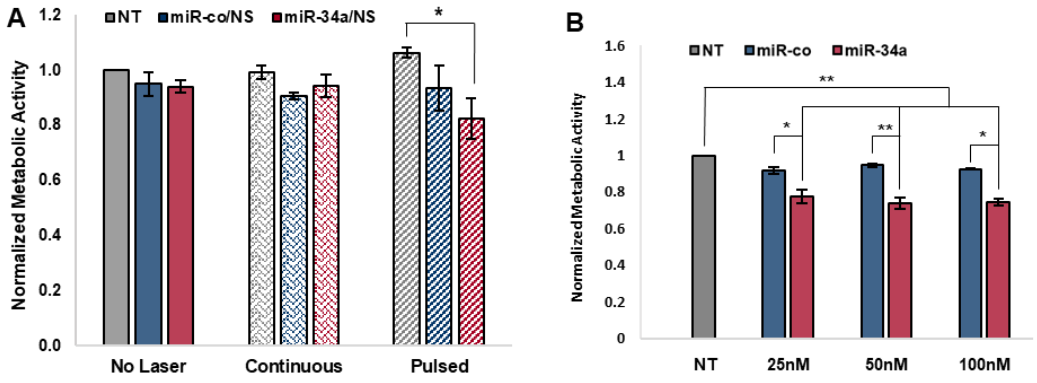

Figure 31. Cellular Metabolic Activity Assessment Following NP and Laser Treatment. Adapted graphics depicting metabolic activity assessment. (**A**) Normalized metabolic activity of MDA-MB-231 cells following NP and comparing two modes of laser treatments assessed *via* an alamarBlue™ Assay. (**B**) Functionality assessment *via* TFX. MDA-MB-231 cells were transfected with an increasing dosage of miRNA concentrations of 25, 50, and 100nM and accessed for metabolic activity following 96 hours *via* an alamarBlue™. **p<0.001 and *p<0.01 by one-way ANOVA with posthoc Tukey-Kramer.[124]

Given that miR-34a/NS activated with ns pulsed light impacted TNBC cell metabolic activity more than NPs excited with CW light, we further examined the effects of miR-34a/NS and ns pulsed light on TNBC cell proliferation by EdU assay (**Figure 32A**). In the absence of irradiation, miR-34a/NS decreased proliferation by ~22% versus non-treated controls. Comparatively, proliferation decreased by ~32% in cells exposed to miR-34a/NS and 0.05 W/cm^2 ns pulsed light, and by ~29% in cells exposed to miR-34a/NS and 0.1 W/cm^2 irradiation. The decrease observed for miR-co/NS + laser at 0.05 and 0.1 W/cm^2 was ~17% and ~19%, respectively. Cells transfected with 25-100 nM miR-34a exhibited reductions in proliferation ranging from ~30-35% (**Figure 32B**), consistent with the decrease observed for miR-34a/NS + ns pulsed light.

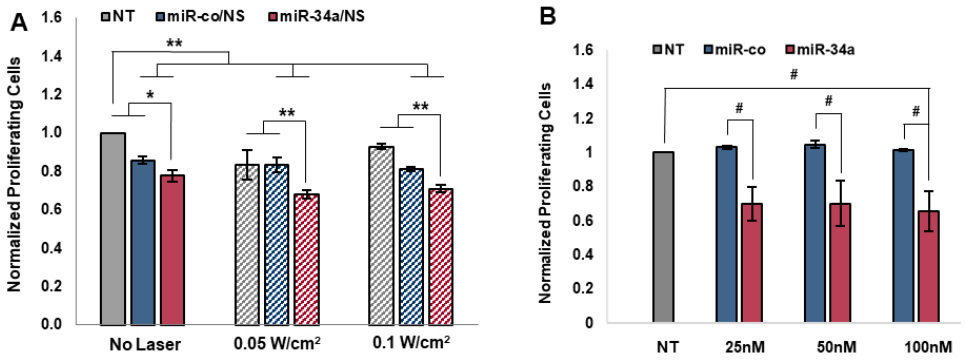

Figure 32. **Cell Proliferation Assessment Following NP and Laser Treatment.** Adapted graphics depicting cell proliferation assessment. (**A**) Normalized count of proliferating MDA-MB-231 cells following NP and ns-pulsed laser treatment at varying laser power densities assessed *via* an EdU Proliferation Assay. (**B**) MDA-MB-231 cells were transfected with an increasing dosage of miRNA concentrations of 25, 50, and 100nM and accessed for proliferation following 96 hours *via* an EdU Proliferation Assay. #$p<0.1$, *$p<0.05$, and **$p<0.01$ by one-way ANOVA with posthoc Tukey-Kramer.[124]

Overall, these assays confirm that miR-34a/NS can decrease the metabolic activity and proliferation of TNBC cells in the presence of laser irradiation, and that the decrease is greater than that observed for non-irradiated miR-34a/NS or for irradiated miR-co/NS. Moreover, light-triggered miR-34a delivery appears to be as potent as miR-34a transfection. Notably, these assays may lack sensitivity to fully evaluate the potency of the treatment, as bulk measurements do not account for potential differences in NP uptake across cells or for potential losses of cells in preparation of flow cytometry samples. Regardless, the results agree with the gene expression analyses above, as miR-34a/NS suppressed genes that regulate

proliferation (CCND1) and apoptosis (Bcl2, Sirt1, Survivin), and decreases in these functions of TNBC cells were observed in the alamarBlue^{TM} and EdU assays.

3.3.8 Analysis of MDA-MB-231 cell migration in response to light-triggered miRNA delivery.

The qRT-PCR study showed Nanog is dramatically suppressed in TNBC cells treated with miR-34a/NS + ns pulsed light, and Nanog promotes cancer stem cell motility.[141,142] Therefore, we hypothesized that miR-34a/NS + ns pulsed irradiation would reduce the migration of MDA-MB-231 cells. To test this theory, we treated GFP-expressing MDA-MB-231s with miR-34a/NS or miR-co/NS at OD^{810nm} = 5 (~100 nM miRNA) for 20 hours and irradiated the samples at 0 or 0.1 W/cm^2 for 10 minutes. Forty-eight hours later, the cells were transferred into transwell inserts at 3,000 cells per insert. Cell migration through the insert was monitored over the subsequent 120 hours by fluorescence microscopy. At 96 hours, we noted a distinct difference in the number of cells that migrated across the transwell membrane in each treatment group (**Figure 33A and B**). In the absence of irradiation, miR-co/NS had no effect on cell migration, whereas miR-34a/NS decreased migration by ~22%. When the laser was applied, miR-co/NS decreased migration by ~25%, while miR-34a/NS yielded an impressive ~65% decrease in migration (**Figure 33A and B**).

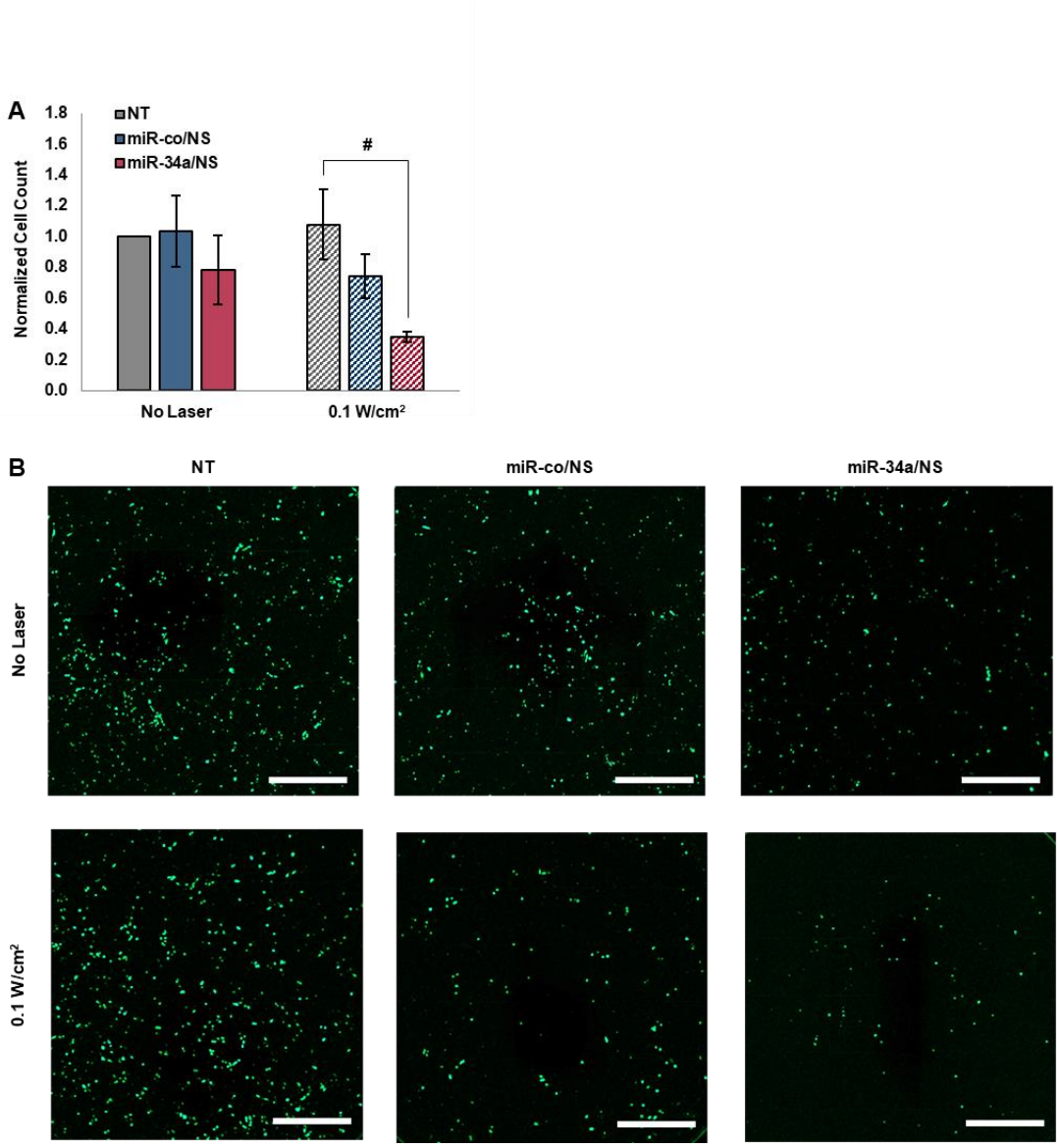

Figure 33. Analysis of MDA-MB-231 Cell Migration in Response to Light-Triggered miRNA Delivery. (**A**) Normalized count of migrated MDA-MB-231 cells following NP and laser treatment assess. (**B**) Zoomed in sections of representative fluorescent images of the migrated GFP cells. #p<0.1 by one-way ANOVA with posthoc Tukey. Scalebar = 1 mm.[124]

Similar trends in the number of migrated cells were observed when samples were imaged at 48, 72, 96, and 120 hours (**Figure 34**). Given the long timeframe, the differences observed at later timepoints may be partially due to decreases in cell migration and partially due to decreases in survival or proliferation of cells that migrated through the membrane. Overall, these results demonstrate that miR-34a/NS excited with ns pulsed light can impair cell migration *via* controlled gene regulation.

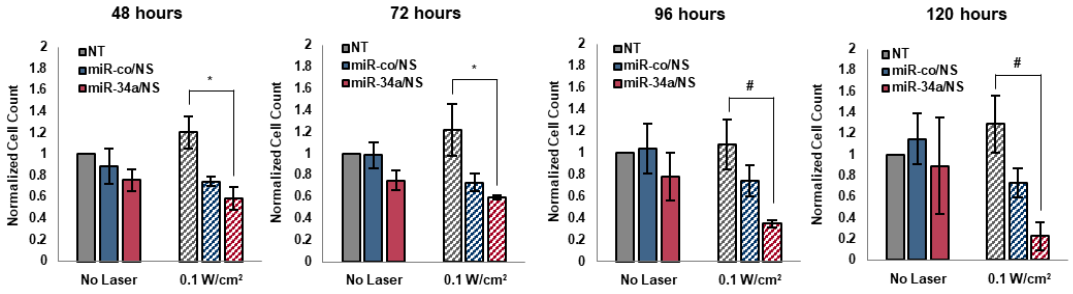

Figure 34. Qualitative Analysis of Migrated GFP-cells. Migration assay at timepoints 48, 72, 96, and 120 hours reseeding. *p<0.05 and #p<0.1 by one-way ANOVA with posthoc Tukey-Kramer.[124]

3.4 Conclusions

In summary, these studies demonstrate that NS can be activated with a clinically relevant ns pulsed NIR laser to yield light-triggered release of miR-34a, resulting in gene regulation and functional impairment of TNBC cells. While prior work has primarily studied the release of DNA[95,96,143] or siRNA[91,136,144] from plasmonic NPs using femtosecond pulsed irradiation, here we evaluated the release of miRNA triggered by ns pulsed light. Relative to DNA and siRNA, which suppress only a single target gene, miRNA is advantageous as therapeutic cargo because it can suppress multiple downstream targets, potentially resulting in more profound effects

on targeted diseased cells.[145] However, caution must be taken when delivering miRNA therapeutics, because their non-specific delivery to healthy cells could result in unintended gene silencing and off-target effects. The use of plasmonic nanocarriers to hold miRNA inactive until it is released from the NPs in the desired cells with light is a promising strategy to increase the safety and efficacy of miRNA therapeutics.

Here, we used NS as a plasmonic carrier to deliver miR-34a into TNBC cells. We demonstrated that ~30% of the miRNA is released from the NS upon 0.1 W/cm^2 ns pulsed irradiation, that this level of release is greater than that observed with CW irradiation, and that the released miRNA is primarily in duplex form. We also showed that the bulk solution temperature did not rise substantially upon irradiation with ns pulsed or CW light at 0.1 W/cm^2. When miR-34a/NS were applied to TNBC cells in combination with NIR light, they increased miR-34a expression in the cells (with greater expression observed in samples exposed to ns pulsed light than CW light) and reduced the expression of several miR-34a target genes that are implicated in cell proliferation (CCND1), survival (Bcl2, Sirt1, Survivin), and motility (Nanog). This prompted us to evaluate the effect of light-triggered miR-34a delivery on TNBC cell metabolic activity, proliferation, and migration, which confirmed that miR-34a/NS + ns pulsed laser treatment yielded the greatest effects. The miR-34a/NS did have some effect on cells in the absence of laser irradiation, which suggests either some cargo is releasing from the NS in the intracellular environment or that RISC is interacting with the miRNA while it remains tethered to the NS. In previous work evaluating siRNA/NS conjugates for on-demand gene regulation,[143] we did not observe any gene silencing in the absence of laser irradiation, so there may be subtle differences in the use of siRNA versus miRNA as cargo. Future studies could aim to minimize the effect

of miR-34a/NS on TNBC cells in the absence of laser irradiation, or to increase the percentage of duplexes that are released from the surface upon laser irradiation. Such changes would maximize the therapeutic ratio.

Overall, these studies demonstrate miR-34a/NS can enable light-triggered gene regulation using a clinically relevant ns pulsed laser to impair the proliferation and migration of TNBC cells. These studies should be validated in additional cell lines and animal models in future work. These conjugates offer precise control over miRNA delivery, which overcomes the lack of specificity of other nanocarrier systems. With additional development, light-triggered miR-34a delivery facilitated by NS may offer a promising new arsenal in the fight against TNBC and other cancers characterized by loss of miR-34a.

Chapter 4

ANTIBODY AND siRNA NANOCARRIERS FOR WNT SIGNALING INHIBITION IN TRIPLE-NEGATIVE BREAST CANCER

4.1 Introduction

As introduced earlier, TNBC is an aggressive disease that lacks targeted treatment options.[127] The backbone of targeted therapies is monoclonal antibodies, which bind specific antigens on diseased cells, allowing them to bring conjugated drugs directly to the cell or regulate cell signaling by blocking ligand/receptor interactions. The first antibody-drug conjugate for metastatic TNBC, composed of anti-trophoblast cell surface antigen 2 (Trop-2) antibodies coupled to the topoisomerase I inhibitor SN38, was only recently approved by the FDA in 2020.[ref] This was followed by the approval of two PARP inhibitors, Talazoparib and Olaparib, for patients with BRCA1/2 mutations.[refs] While these developments are exciting, the therapeutic utility of freely delivered antibodies is limited by high production costs, low efficacy, dose-limiting toxicities, and inability to cross the cellular membrane (which hinders antibodies against intracellular targets).[37] To overcome these limitations, researchers have begun to develop nanocarriers that can improve antibodies' delivery efficiency, safety profile, and clinical potential. Compared to freely delivered antibodies, antibody-NP conjugates have improved efficacy and reduced toxicity owing to the carriers' ability to protect their cargo *in vivo*, provide multivalent binding effects, and more.[98] This chapter exploits multivalent binding,

where antibodies on nanocarriers can engage multiple receptors simultaneously to increases overall binding strength/avidity compared to freely delivered antibodies.

Suppressing Wnt signaling is a promising therapeutic strategy for TNBC as this hyperactive pathway drives disease progression and lung metastasis through the activation of various oncogenes.[53] External Wnt ligands bind to cell surface FZD7 receptors leading to stabilization, cytoplasmic accumulation, and nuclear translocation of intracellular β-catenin molecules. This initiates the transcription of multiple genes including Axin2, cyclin D1, and c-Myc.[54] Axin2 is a universal indicator of Wnt activity while cyclin D1 and c-Myc are downstream Wnt targets that promote cell proliferation, migration, and invasion.[23,24] Many other oncogenes are also regulated by Wnt signaling, making this signaling pathway a critical target for therapeutic manipulation. The Day Lab has previously shown that FZD7 antibody nanocarriers can suppress intracellular β-catenin and Axin2 expression more potently than freely delivered FZD7 antibodies, which is attributed to their multivalent binding effects.[57,113] In this chapter, the increased binding avidity of FZD7 nanocarriers is exploited not only for antibody-mediated signaling inhibition, but also for targeted delivery of small interfering RNA (siRNA) molecules to enable dual regulation of the Wnt signaling pathway.

Beyond FZD7, intracellular β-catenin molecules are a critical therapeutic target within the Wnt signaling pathway. However, β-catenin is considered undruggable due to lack of an effective binding site for small molecule therapeutics. One potential way to suppress β-catenin inside cells would be through delivery of siRNA. siRNAs are double stranded RNA duplexes around 20 base pairs in length that can silence target gene expression through RNA interference (RNAi). In RNAi, exogenously delivered

siRNA molecules bind the RNA induced silencing complex (RISC) in the cell cytosol, and then unwind. The strand remaining bound to RISC guides it to perfectly complementary messenger RNA (mRNA) molecules, marking them for degradation, thereby hindering protein translation. While freely delivered siRNAs are not suitable for clinical utility owing to their nuclease susceptibility, poor pharmacokinetics, and limited cellular uptake, numerous studies have shown that siRNA-coated NPs can increase RNA stability, circulation, and cellular uptake to enable *in vivo* gene regulation.[refs] Therefore, we postulated that we could coat NPs with both FZD7 antibodies and β-catenin siRNA duplexes to suppress Wnt signaling in TNBC cells at both the receptor and effector level, providing a potentially additive or synergistic effect, or a way to circumvent cellular resistance to inhibition of this pathway. In this Chapter, we report the synthesis of NS coated with both FZD7 antibodies and β-catenin siRNAs to enable multi-level Wnt inhibition (**Figure 35**). First, we fine-tuned the loading of siRNAs and antibodies on the NS such that there was equal loading between NS coated with both antibodies and siRNAs (combo-NS) or coated with only one of the molecules (FZD7-NS and βcat-NS). Then, we evaluated the impact of each NS formulation on TNBC cells *in vitro*, including examination of cellular uptake, proliferation, migration, and sphere formation capacity. The results presented below demonstrate that both mono-therapies and combo-NS hold potential as TNBC therapeutics.

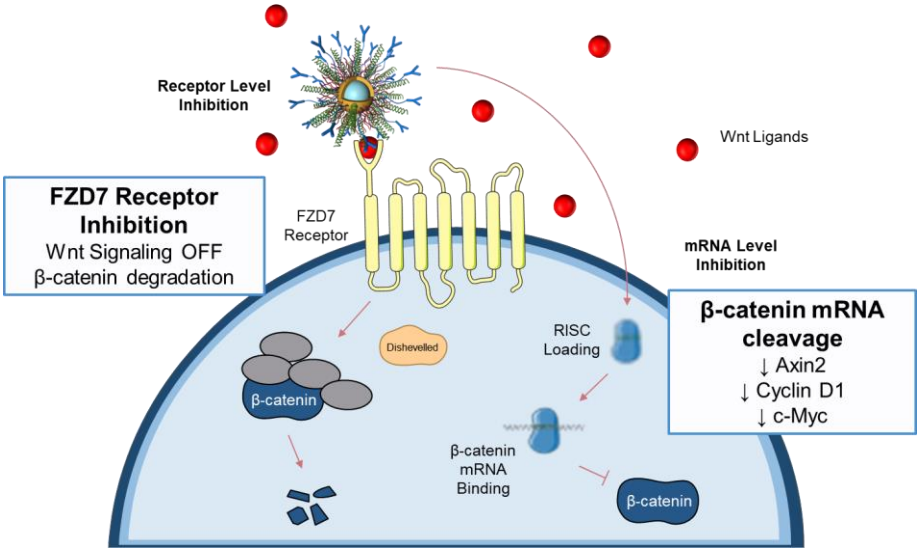

Figure 35. Scheme of NPs for Regulation of the Wnt Signaling Pathway. Wnt inhibitory NPs designed to target the signaling pathway at multiple levels including extracellularly through receptor inhibition and intracellularly through mRNA cleavage.

4.2 Materials and Methods

4.2.1 Nanoshell Synthesis and Coating with Antibodies and siRNA

NS were synthesized according to published methods which were described in detail in **Chapter 2.2**. FZD7 antibodies were purchased at 1 mg/mL from LSBio and PEGylated in house with a 5kDa OPSS-PEG-SVA linker. β-catenin siRNA oligonucleotides were purchased as single strands from Integrated DNA Technologies (**Table 4**). The sense strands were modified with thiol groups on the 3′ end for ease of functionalization to the surface of the gold NS. Complementary sense and antisense strands were mixed in equimolar amounts and duplexed. NS were diluted to 4.4×10^9 NS/mL ($OD^{810\ nm} = 1.5$) in milliQ water and incubated with 1,000 or 1,200 antibodies per NS initially (Combo-NS or FZD7-NS, respectively). Afterwards, NS were

incubated with 0.2% Tween-20 and incubated in increasing amounts of NaCl to a final salt concentration of 300 or 1000 mM (βcat-NS or Combo-NS, respectively) for 5 minutes. Then, 0.1 or 0.25 nmol of siRNA (βcat-NS or Combo-NS, respectively) and 10 μM of mPEG-SH were added as described in more detail in **Chapter 2.3.3**. The FZD7 antibody only NPs (FZD7-NS) were not salt aged, but were passivated with mPEG-SH. In optimizing equivalent loading of the monotherapeutic nanocarriers to the dual biomolecule NP, we determined how final antibody and siRNA loading on the NS is impacted by various parameters, including the biomolecule order, salt aging conditions, mPEG concentrations, and initial number of biomolecules added as detailed in **Chapter 4.2.1.1 – 4.2.1.4**. Each NP type (Combo-NS, βcat-NS, and FZD7-NS) was purified *via* centrifugation 1X at 500 g for 15 minutes and 2X for 10 minutes. Between each centrifugation step the NPs were suspended in 1XPBS. The final material was then diluted in 1XPBS at 100X less volume than the starting NS volume. NP concentration was determined *via* the extinction spectrum using the Cary 60 UV-visible spectrophotometer as described in **Chapter 2.4.1.**

siRNA	Sequence
β-catenin sense	5’ – AGC UGA UAU UGA UGG ACA GTT / iSp18//iSp18//3ThioMC3-D/ -3’
β-catenin antisense	5’ – CUG UCC AUC AAU AUC AGC UTT – 3’
β-scramble sense	5’ – GAA UGC GAA UGA UGC GUU ATT / iSp18//iSp18//3ThioMC3-D/ -3’
β-scramble antisense	5’ – UAA CGC AUC AUU CGC AUU CTT – 3’

Table 4. siRNA sequences utilized.

4.2.1.1 Optimizing Loading Based on Biomolecule Order of Addition, Salt Concentration, and mPEG-SH Concentration

We initially examined how the order of biomolecule addition would impact the loading of antibodies and siRNAs on Combo-NS. **Figure X** displays the synthesis conditions. Briefly, NS were diluted to OD^{800}=1.5 in preparation for conjugation. For the antibody first conjugation, FZD7 antibodies were added at ~1000 – 1200 antibodies / NS followed by 1 hour rocking at 4°C. The NS then incubated with 0.2% tween, salt aging up to either a low (xxx nM) or high (yyy nM) concentration, and 0.2 nmol siRNA / mL NS was added and samples rocked at 4°C for six hours. Every 1.5 hours the NPs were briefly vortexed and bath sonicated to promote conjugation and prevent aggregation. Every 3 hours the NaCl was added in increments. For the siRNA first conjugation, NS were incubated with 0.2% tween, salt aged to either a low (xxx nM) or high (xxx nM) concentration, and 0.2 nmol siRNA / mL NS added prior to rocking at 4°C. After 1 hour, FZD7 antibodies were added at a ratio of ~1000 – 1200 antibodies / NS and samples then rocked at 4°C for six hours. Every 1.5 hours the NPs were briefly vortexed and bath sonicated to promote conjugation and prevent aggregation. Every 3 hours the salt was added in increments. Following the 6 hours of initial rocking and the last salt addition, both antibody first NPs and siRNA first NPs were rocked for an additional 12 – 14 hours at 4°C. The following day the NPs were passivated with either a low or high concentration of mPEG-SH. After 4 hours of passivation, the NPs were purified *via* centrifugation as described in **Chapter 4.2.1**. siRNA and antibody loading were quantified using OliGreen™ and ELISA assays, respectively, as described in **Chapter 2.4.4** and **Chapter 2.4.5**.

4.2.1.2 Optimizing Loading Based on Salt Concentrations

Secondly, we tested how the salt aging conditions impacted biomolecule loading while keeping the biomolecule addition order and concentrations consistent. Briefly, NS were diluted to OD=1.5 in preparation for conjugation. FZD7 antibodies were added at ~1000 – 1200 antibodies / NS then samples rocked for 1 hour at 4°C. Next, NS were incubated with 0.2% tween, salt aged to final concentrations ranging from 200 – 1200 mM, and then 0.2 nmol siRNA / mL NS was added and samples left to rock at 4°C for six hours. Every 1.5 hours the NPs were briefly vortexed and bath sonicated to promote conjugation and prevent aggregation. Every 3 hours the salt was added in increments. Following the 6 hours of initial rocking and the last salt addition, NPs were rocked for an additional 12 – 14 hours at 4°C. The following day the NPs were passivated with 5 μM mPEG-SH. After 4 hours of passivation, the NPs were purified *via* centrifugation as described in **Chapter 4.2.1**.

4.2.1.3 Optimizing Loading Based on mPEG-SH Concentration

Next, we examined how mPEG-SH concentration affects biomolecule loading when the biomolecule addition order and salt concentrations are held constant. Briefly, NS were diluted to OD 1.5 in preparation for conjugation. FZD7 antibodies were added at 1000 – 1200 antibodies / NS and samples rocked 1 hour at 4°C. Subsequently, NS were incubated with 0.2% tween and salt aged to either 300 or 1000 mM (βcat-NS and Combo-NS, respectively) for 5 minutes. Then, 0.1 or 0.25 nmol of siRNA (βcat-NS or Combo-NS, respectively) was added and left to rock at 4°C for six hours. Every 1.5 hours the NPs were briefly vortexed, and bath sonicated to promote conjugation and prevent aggregation. Every 3 hours NaCl was added in increments. Following the 6 hours of initial rocking and the last salt addition, NPs were rocked for

an additional 12 – 14 hours at 4°C. The following day the NPs were passivated with mPEG-SH at either 5, 10, or 20 μM. After 4 hours of passivation, the NPs were purified *via* centrifugation as described in **Chapter 4.2.1.**

4.2.1.4 Optimizing Loading Based on Initial Number of Antibodies Added

Lastly, the number of antibodies initially added to the NS was adjusted to maintain equivalent antibody loading between Combo-NS and the corresponding FZD7-NS control. The biomolecule order, salt aging conditions, and mPEG-SH concentrations were kept constant. Briefly, NS were diluted to OD 1.5, FZD7 antibodies added at ~1000 or 1200 antibodies / NS (Combo-NS and FZD7-NS, respectively), and samples rocked 1 hour at 4°C. Then, NS were incubated with 0.2% tween, salt aged to 300 or 1000 mM (βcat-NS and Combo-NS, respectively) over 5 minutes, and 0.1 or 0.25 nmol of siRNA (βcat-NS or Combo-NS, respectively) added and samples left to rock at 4°C for six hours. Every 1.5 hours the NPs were briefly vortexed and bath sonicated to promote conjugation and prevent aggregation. Every 3 hours the salt awas added in increments. Following the 6 hours of initial rocking and the last salt addition, the NPs were rocked for an additional 12 – 14 hours at 4°C. The following day the NPs were passivated with mPEG-SH at either 5, 10, or 20 μM. After 4 hours of passivation, the NPs were purified *via* centrifugation as described in **Chapter 4.2.1**.

4.2.2 Antibody and/or siRNA Conjugate Characterization

The hydrodynamic diameter and zeta potential of the NS conjugates and bare NS were measured using an Anton Paar Litesizer as described in **Chapter 2.4.3**. siRNA loading on NS was quantified using a Quant-iT OliGreen^{TM} ssDNA

quantification kit as described in **Chapter 2.4.4**. Antibody loading on NS was quantified using an ELISA as described in **Chapter 2.4.5.**

4.2.3 Cell Culture and NP Treatment Setup for Cell Experiments

MDA-MB-231 TNBC cells purchased from American Type Culture Collection (ATCC) were cultured in Dulbecco's Modified Eagle Medium (DMEM) (VWR) supplemented with 10% fetal bovine serum (FBS) (Gemini Bio) and 1% penicillin-streptomycin (VWR). Cells were cultured in T75 cell culture flasks (VWR), passaged with 0.25% trypsin-EDTA (VWR), and incubated at 37°C in a 5% CO2 humidified environment. Cells were cultured to 80-90% confluency prior to plating for experiments, used within passage numbers of 40 – 55, and counted using a glass slide hemocytometer for all experiments. GFP-expressing MDA-MB-231 cells (Angio-Proteomie) were cultured with the same conditions. Noncancerous MCF-10A breast epithelial cells were provided by Dr. Kenneth Van Golen and cultured in 1:1 DMEM and F12 base medium supplemented with 5% FBS (Gemini Bio), 1% penicillin-streptomycin (VWR), 10 μg/mL insulin (ThermoFisher), 0.5 μg/mL hydrocortisone (Sigma), 50 μg/mL bovine pituitary extract (ThermoFisher), 20 ng/mL epidermal growth factor (ThermoFisher), and 100 ng/mL cholera toxin (Sigma). MCF-10As were cultured in the same conditions as the cells above and were used within passage numbers of 20 – 30.

The general experimental setup used for studies to assess the impact of co-delivered NPs on TNBC cells**.** Cells were plated in well plates with complete cell culture media and placed in a humidified incubator at 37°C, 5% CO_2 for at least 20 hours. The cells were then incubated with FZD7-NS, βcat-NS, Combo-NS, or full media at $3x10^9$ NPs/mL ($OD^{810\ nm} = 1$) or $1.5X10^{10}$ NP/mL ($OD^{810\ nm} = 5$) for 1 – 24

or 24 – 96 hrs depending on the experiment. $OD^{810\ nm}$ = 1 corresponds to ~ 0.8 nM FZD7 antibodies and ~12nM siRNA. $OD^{810\ nm}$ = 5 corresponds to ~ 4 nM FZD7 antibodies and ~64nM siRNA.

4.2.4 Validation of siRNA Gene Knockdown in MDA-MB-231 Cells

To validate the ability of the siRNA duplexes to mediate RNAi, the relative expression of β-catenin and several downstream target genes were measured by qRT-PCR after MDA-MB-231 cells were transfected with 50 nM siβ-catenin or scrambled control (β-scramble) duplexes using DharmaFect1 (Dharmacon) per manufacturer recommendations. Following 48- or 72-hour treatment, RNA was extracted using the Isolate II RNA Mini Kit (Bioline). Modifications to the protocol include omitting the β-mercaptoethanol addition. RNA concentration was read by measuring sample absorbance at 260 nm on a Take3 Plate on a Synergy H1 plate reader. qRT-PCR was then performed with a concentration of 75 ng RNA/2 μL using the SensiFAST SYBR One-Step Master Mix (Bioline) on a LightCycler96 (Roche). The mRNA expression levels of each target gene were normalized to that of GUSB and further normalized to no treatment group. Primer sequences are listed in **Table 5**.

Primer	Forward Sequence Reverse Sequence
GUSB	TTTTCTTAGCGCCGCAGA GGGCCTGACTCCCACAG
β-catenin	GTACGTCCATGGGTGGGACA GGCTCCGGTACAACCTTCAACTA
Axin2	TTATGCTTTGCACTACGTCCCTCCA CGCAACATGGTCAACCCTAGAC
CCND1	CCTGTCCTACTACCGCCTCA CAGTCCGGGTCACACTTGA
C-myc	CCTACCCTCTCAACGACAG CTTGTTCCTCCTCAGAGTTG

Nanog	AACCTCAGCTACAAACAGGTGA TCTGCGTCACACCATTGCTA
Snail	ACCACTATGCCGCGCTCTT GGTCGTAGGGCTGCTGGAA
Survivin	CGGTTGCGCTTTCCTTTC TGTTCTTGGCTCTTTCTCTGTCC

Table 5. Primer sequences used for real time qRT-PCR studies, listed from 5' to 3' end.

4.2.5 Binding Avidity of Wnt Inhibitory NPs *via* Multiphoton Microscopy

To evaluate the targeting capabilities of FZD7 antibodies, target MDA-MB-231 and control MCF10A cells were seeded in Nunc Lab-Tek #1 8-well chamber slides (Thermo) at 250,000 and 100,000 cells / well respectively and left to adhere for at least 20 hours while incubating at 37°C, 5% CO_2. The next day media was removed and 300 μL NPs (PEG-NS, FZD7-NS, βcat-NS, and Combo-NS) were added at $OD^{810\ nm}$ = 1 in full supplemented media for both cell lines. The cells were then incubated at 37°C. Following an hour, the media was gently removed, and the cells rinsed thrice with warm Dulbecco's PBS (DPBS, ThermoFisher). Cells were then fixed with 4% paraformaldehyde prepared in 1X PBS for 15 minutes at RT and neutralized with 1X PBS afterwards. Next, the cell membranes were dyed using CellVue Claret Red Membrane Dye (Sigma) for 8 – 10 minutes at RT covered, with the dye prepared per manufacturer's instructions. The dye was neutralized with 1% w/v BSA in 1X PBS. The dye solution and neutralizer were than aspirated and cells covered with 1X PBS. Slides were imaged using a LSM 880 Multiphoton Microscope with a 20x/0.8 water objective, which was immersed in a droplet of water to provide the correct contrast and visualization upon connection to the slides. The NPs in the slide samples were excited by the multiphoton laser tuned to $\lambda_{excitation}$ = 800 nm with a pinhole of 1.57 AU

and a detection range $\lambda_{emission}$ of 400 – 550 nm. The cell membranes in the slide samples were visualized at $\lambda_{excitation}$ = 655 nm and $\lambda_{emission}$ of 675 nm.

4.2.6 Analysis of Cy5-Labeled NP Cellular Uptake *via* Flow Cytometry

To analyze NP uptake *via* flow cytometry, the NPs were tagged with Cy5-PEG-SH, which replaced the original mPEG-SH added to passivate the NPs. The Cy5-PEG-SH was added in the same manner but had to be adjusted for some of the NP formulations as we found that the Cy5 signal varied amongst the different NPs. Following synthesis and purification of the Cy5-tagged NPs, MDA-MD-231 and MCF10A cells were seeded in 96 well plates at 75,000 and 50,000 cells per well respectively. The following day NPs (no NP, PEG-NS, FZD7-NS, βcat-NS, and Combo-NS) were added to the wells at $OD^{810\ nm}$ = 1in full supplemented media for both cell lines. The cells were left to incubate for 1, 4, and 8 hours at 37°C. Following each incubation period, the media was gently removed, and the cells rinsed thrice with warm Dulbecco's PBS (DPBS, ThermoFisher) with thorough pipetting around the well to dislodge any unbound NPs or those that were not incorporated into the cells. Cells were then trypsinized, neutralized, and transferred to Eppendorf tubes for flow cytometry analysis performed with an Acea Novocyte 2060 Flow Cytometer. The parameters were set to 100 µL/min to a cell cut off at 10,000 cells gated for singlet cells. Cells were then further gated using the APC-Cy7 filter where cells were excited at 640 nm and detected using the 780/60 nm filter to assess the shifts in Cy5 signal. In processing the data, the raw median X value of Cy5 signal was averaged in triplicate and the no treatment group values were subtracted from each NP group to evaluate the shift from the baseline cells, which should have minimal Cy5 signal.

4.2.7 qPCR Analysis of mRNA Expression in Cells Treated with Wnt Inhibitory NPs

qRT-PCR was utilized to assess the impact of NP treatment on mRNA expression of relevant Wnt-associated genes. MDA-MB-231 cells were plated at 40,000 cells/well in 12-well plates prior to NP treatment. Cells were treated with no NP, PEG-NS, FZD7-NS, βcat-NS, and Combo-NS at $OD^{810\ nm} = 1$. Following 24 – 72 hours, RNA was extracted using the Isolate II RNA Mini Kit (Bioline). Modifications to the protocol include omitting the β-mercaptoethanol addition. RNA concentration was determined by reading the sample absorbance at 260 nm using a Take3 Plate on a Synergy H1 plate reader. qRT-PCR was then performed with a concentration of 75 ng RNA/2 uL using the SensiFAST SYBR One-Step Master Mix (Bioline) on a LightCycler96 (Roche). The mRNA expression levels of each target gene were normalized to that of GUSB and further normalized to no treatment group. Primer sequences are listed in **Table 5**. These experiments were performed in triplicate and analyzed using a one-way ANOVA with posthoc Tukey.

4.2.8 Edu Proliferation Assay

An EdU assay was employed to evaluate cell proliferation of MDA-MB-231 cells after NP treatment. MDA-MB-231 cells were plated at 10,000 cells/well in 24-well plates prior to NP treatment. Each treatment group had 2 wells to serve as technical replicates. Cells were treated with no NP, FZD7-NS, βcat-NS, and Combo-NS at OD^{810} nm = 5. Following 24 – 72 hours, the cells were assessed for proliferation using the Click-iT™ EdU Cell Proliferation Kit (ThermoFisher). The steps of the assay followed the manufacturer's instructions as described in **Chapter 3.2.7**. These experiments were performed in triplicate and analyzed by one-way ANOVA with posthoc Tukey

4.2.9 Transwell Migration Assay

A transwell migration assay was employed to evaluate the invasive and migratory capacity of MDA-MB-231 cells after NP treatment. GFP-expressing MDA-MB-231 cells were plated at 10,000 cells/well in 48-well plates for cell migration studies. Each treatment group had replicates of 2 wells each. Cells were treated with no NP, FZD7-NS, βcat-NS, and Combo-NS at OD^{810} nm = 5 (**Figure 36**). At 72 and 96 hours post incubation, the cells were lifted with trypsin, pelleted, resuspended in non-supplemented DMEM, and counted. The cells were then reseeded at 3,000 cells onto the tops of black transwell inserts (Corning) in 24-Well Glass Bottom Black Walled Plates (CellVis); non-supplemented DMEM was in the top of the insert and complete media was in the bottom of the wells. The cells were left to migrate across the 8.0 μm polyester membranes over 72 hours. The cells were imaged at 24, 48, 72, hours using the GFP filters and tile imaging on an Axioobserver Z1 Inverted Fluorescent Microscope (Zeiss). These experiments were performed in triplicate and analyzed using a one-way ANOVA with posthoc Tukey

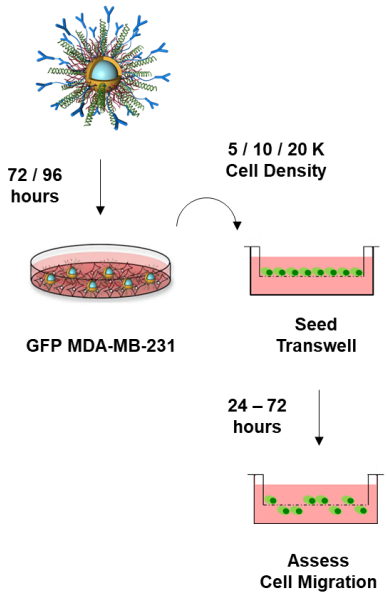

Figure 36. Schematic of NP Treatment to Assess Cell Migration. GFP-expressing MDA-MB-231 cells were incubated with NPs for 72 – 96 hours, then reseeded into transwell inserts with a porous membrane to assess the numbers of cells that migrated across the membrane over the following 24-72 hours.

4.2.10 Spheroid Formation Assay

A spheroid formation assay was employed to evaluate the self-renewal capacity of MDA-MB-231 cells after NP treatment. MDA-MB-231 cells were plated at 20,000 cells/well in 24-well plates for spheroid formation assays. Cells were treated with no NP, FZD7-NS, βcat-NS, and Combo-NS at OD^{810} nm = 5 (**Figure 37**). At 24, 48, and 72 hours post incubation, the cells were lifted with trypsin, pelleted, resuspended MammoCult Basal Medium (StemCell) supplemented with the provided MammoCult Proliferation Supplement, 4 μg/mL heparin (StemCell), and 0.48 μg/mL hydrocortisone (StemCell). The cells were then reseeded at 10,000 cells in triplicate in low adhesion U-bottom 96 well plates (BrandTech) treated for suspension tissue cultures. The cells were placed in a 37°C, 5% CO_2 humidified incubator and allowed

to form spheroids over 7 days, with brightfield imaging performed every other day using an Axioobserver Z1 Inverted Fluorescent Microscope (Zeiss) and a 10X objective. Following 7 days of spheroid formation, the metabolic activity of the spheroids was assessed *via* an alamarBlue™ assay in which 10% of alamarBlue™ was added to the spheroid containing media and left to incubate. After 24 hours, the absorbance was read at 570 nm using the Synergy H1 plate reader. These experiments were performed in triplicate and analyzed using a one-way ANOVA with posthoc Tukey.

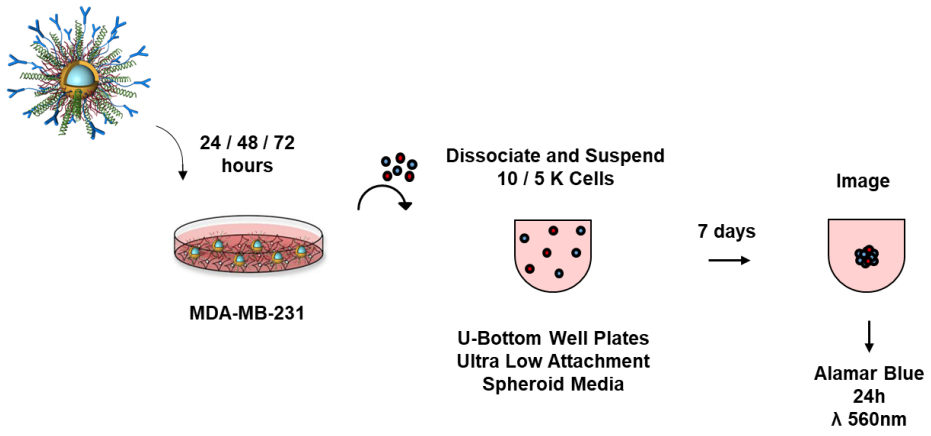

Figure 37. Schematic of NP Treatment to Assess Spheroid Formation. At 24 – 72 hours post NP incubation MDA-MB-231 cells were reseeded in spheroid forming media in U-bottom plates with ultra-low attachment surfaces to assess the ability of the cells to form loose or compact spheroids over the course of one week. At the end of this time frame, the metabolic activity of the individual spheroids was assessed using an Alamar Blue assay.

4.3 Results and Discussion

4.3.1 Wnt Inhibitory NP Loading Optimization

To maximize the delivery of both FZD7 antibodies and β-catenin siRNA using gold NS as the core nanocarrier platform, we needed to optimize the conjugation and loading of both biomolecules. Additionally, the controls for the nanocarrier platform consisted of the individual delivery of either antibodies and/or siRNA. Thus, it was imperative to control the loading of antibodies and siRNA on the co-delivery platform (Combo-NS) to deliver the same amount of corresponding biomolecule is respect to the nontherapeutic NPs (FZD7-NS and βcat-NS).

First, we evaluated the impact of biomolecule order addition as described in **Chapter 4.2.1.1**. We found that through keeping the other parameters constant the Combo-NS synthesized in this optimization step needed to be loaded with antibodies first. When siRNA was added first (solid bars) the number of antibody loading was on the order of ~20 antibodies / NS or even less (**Figure 38A**). Meanwhile when antibodies were added first (striped bars) the antibody loading was on the order of ~100 antibodies / NS or more (**Figure 38A**). Additionally, when quantifying the siRNA loading, the biomolecule order did not matter as much, and interestingly enough, adding FZD7 antibodies first yielded in more siRNA compared to adding siRNA first (**Figure 38B**).

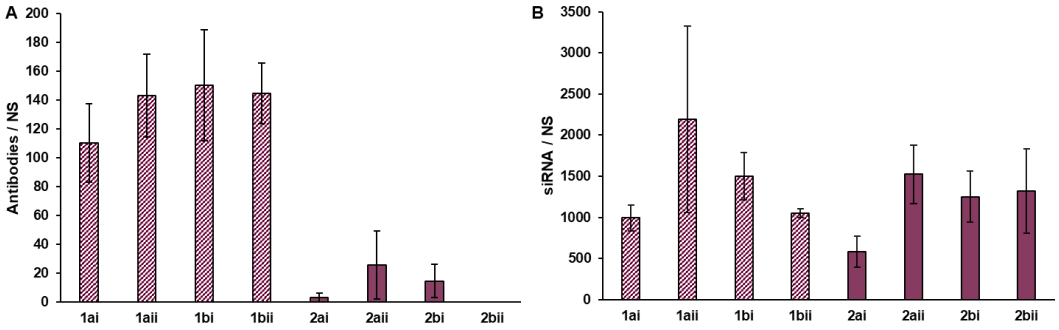

Figure 38. Optimizing Biomolecule Loading on NPs by Order of Biomolecule Addition. Optimization of (**A**) antibody and (**B**) siRNA loading onto gold NS when considering the order of molecule addition: stripes (1) = antibody added first and solid (2) = siRNA added first. (a/b) low/high NaCl concentration, (i/ii) low/high mPEG concentration. n = 2 (technical triplicates when quantifying loading).

From the above results, we moved forward with the order of adding antibodies, siRNA, and mPEG-SH. Next, we evaluated the impact of salt concentrations as described in **Chapter 4.2.1.2**. FZD7-NS were not salt aged throughout any of the synthesis formulations. Here, we mainly wanted to determine the salt concentration required for either βcat-NS or Combo-NS to yield the same number of siRNA / NS post functionalization and if it would impact the antibody loading. We found that as the salt concentration increased from 200 – 1200 mM, Combo-NS were loaded with increasing numbers of antibodies / NS from 100 – 200 (**Figure 39A**). More importantly, Combo-NS saturated at ~1500 siRNA / NS with the additional of 800 – 1200 mM NaCl (**Figure 39B**). To get the same relative loading of siRNA, βcat-NS needed nearly a third less NaCl. In general, the increase in siRNA loading corresponds with other studies in the field that have evaluated the impact of salt concentration on nucleic acid conjugation.[96,124]

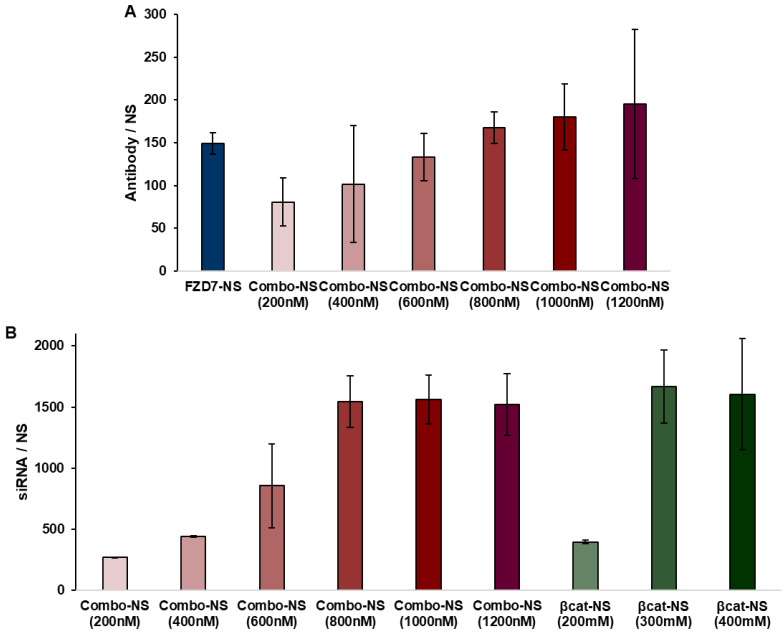

Figure 39. Optimizing Biomolecule Loading on NPs by Adjusting Salt Aging Concentrations. Comparing (**A**) antibody and (**B**) siRNA loading of FZD7-NS, Combo-NS, and βcat-NS when keeping antibody, siRNA, and mPEG concentration constant and adjusting the NaCl concentrations (in parentheses). n = 3.

After determining the necessary salt aging conditions required for the siRNA loaded NPs, we wanted to see if we could further increase antibody or siRNA loading by evaluating the impact of mPEG concentration as described in **Chapter 4.2.1.3**. We found that the increasing concentration of mPEG helped load more antibodies onto both the FZD7-NS and Combo-NS (**Figure 40A**). Interestingly, enough it the changes in loading for Combo-NS were slightly more drastic than with FZD7-NS. In regard to siRNA loading, the Combo-NS saturated out with 10 μM mPEG, while βcat-NS increased in siRNA loading with 10 μM mPEG (**Figure 40B**).

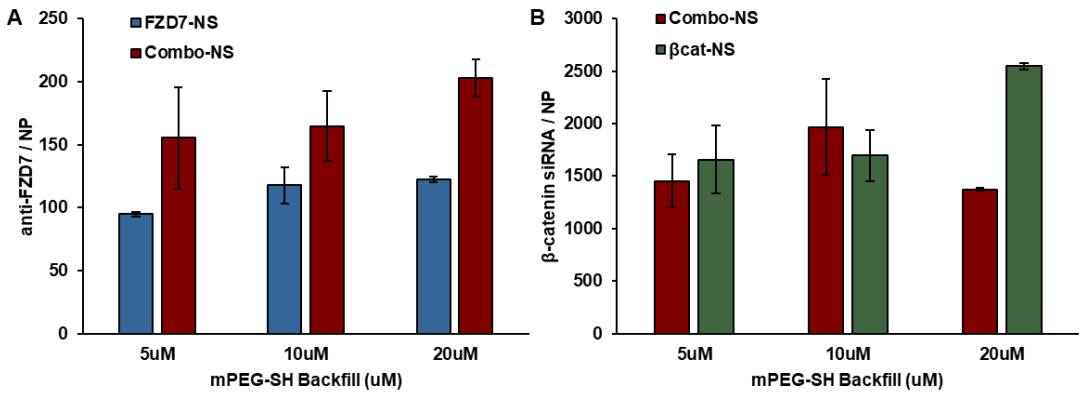

Figure 40. Optimizing Biomolecule Loading on NPs by Adjusting mPEG Concentrations. Comparing (**A**) antibody and (**B**) siRNA loading of FZD7-NS, Combo-NS, and βcat-NS when keeping antibody, siRNA, and NaCl concentration constant and adjusting the mPEG concentrations. n = 3.

From the last parameter, we moved forward with 10 μM of mPEG concentration. Through all the other optimization experiments, we noticed an even amount of antibody loading between FZD7-NS and Combo-NS. Thus, the last optimization parameter consisted with fine tuning the initial addition of antibodies as described in **Chapter 4.2.1.4**. By adding slightly more antibodies to FZD7-NS, we were able to maintain equivalent antibody loading of ~120 per NS between FZD7-NS and Combo-NS (**Figure 41A**). Additionally, this change in the synthesis did not impact the siRNA on Combo-NS which was still equivalent to ~2500 siRNA / NS (**Figure 41B**).

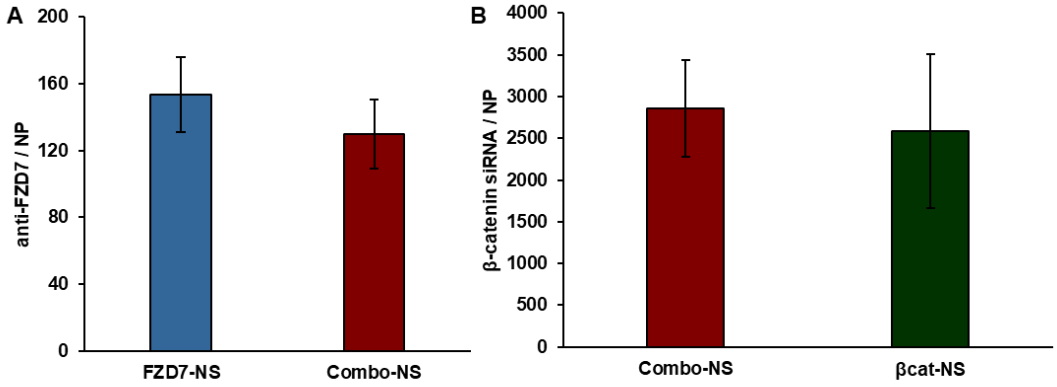

Figure 41. Finetuning Antibody Loading of FZD7-NS and Combo-NS. Anti-FZD7 loading was adjusted by increasing initial addition antibodies for FZD7-NS. Confirming equivalent (**A**) antibody and (**B**) siRNA loading with new set parameters for Combo-NS in comparison to the monotherapeutic NPs. n = 3.

4.3.2 Wnt Inhibitory NP Characterization

After the various optimization experiments to equalize antibody and siRNA on Combo-NS to the respective FZD7-NS and βcat-NS, we landed on a final functionalization protocol as described in **Chapter 4.2.1**. The NPs were characterized by DLS and Zeta potential in which we found that the NPs were larger in size by ~20 nm in diameter compared to bare NS. Additionally, the NPs were more neutral in charge (**Figure 42**). The antibody loading of Combo-NS and FZD7-NS were ~130 antibodies / NS and siRNA loading of Combo-NS and βcat-NS were ~2400 siRNA / NS (**Figure 42**). This corresponds to the following antibody or siRNA concentration for reference. $OD^{810\ nm}$ 1 = $3x10^9$ NPs/mL = ~ 0.8 nM FZD7 antibodies and ~12nM siRNA. $OD^{810\ nm}$ 5 = $1.5X10^{10}$ NP/mL ~ 4 nM FZD7 antibodies and ~64nM siRNA.

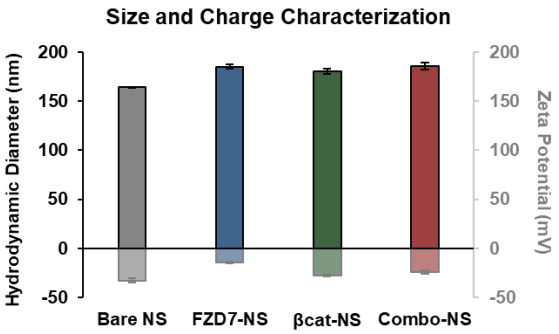

Nanoparticle Loading (per NS)		
Conjugate	FZD7 Antibody	β-catenin siRNA
FZD7-NS	127 ± 13	--
βcat-NS	--	2555 ± 397
Combo-NS	135 ± 18	2305 ± 486

Figure 42. Wnt Inhibitory NP Characterization. Final characterization of the Wnt Inhibitory NP platforms assessed *via* DLS and Zeta Potential. Additional recap of the FZD7 antibody and β-catenin siRNA loading on NS in table format. n = 11 – 19.

4.3.3 Binding Affinity of Wnt Inhibitory NPs *via* Multiphoton Microscopy

To assess the advantage of incorporating a targeting moiety to the NPs, we evaluated the binding capabilities of FZD7-loaded NPs to MDA-MB-231 versus MCF10A cells as described in **Chapter 4.2.5**. Here, we found as expected that the FZD7-loaded NPs bound more to the MDA-MB-231 cells compared to the PEG-NS and βcat-NS controls (**Figure 43**). Moreover, we saw that more Combo-NS seemed to bind to the cells compared to FZD7-NS. In regard to the control MCF10A binding, we saw minimal attachment of NPs across the board.

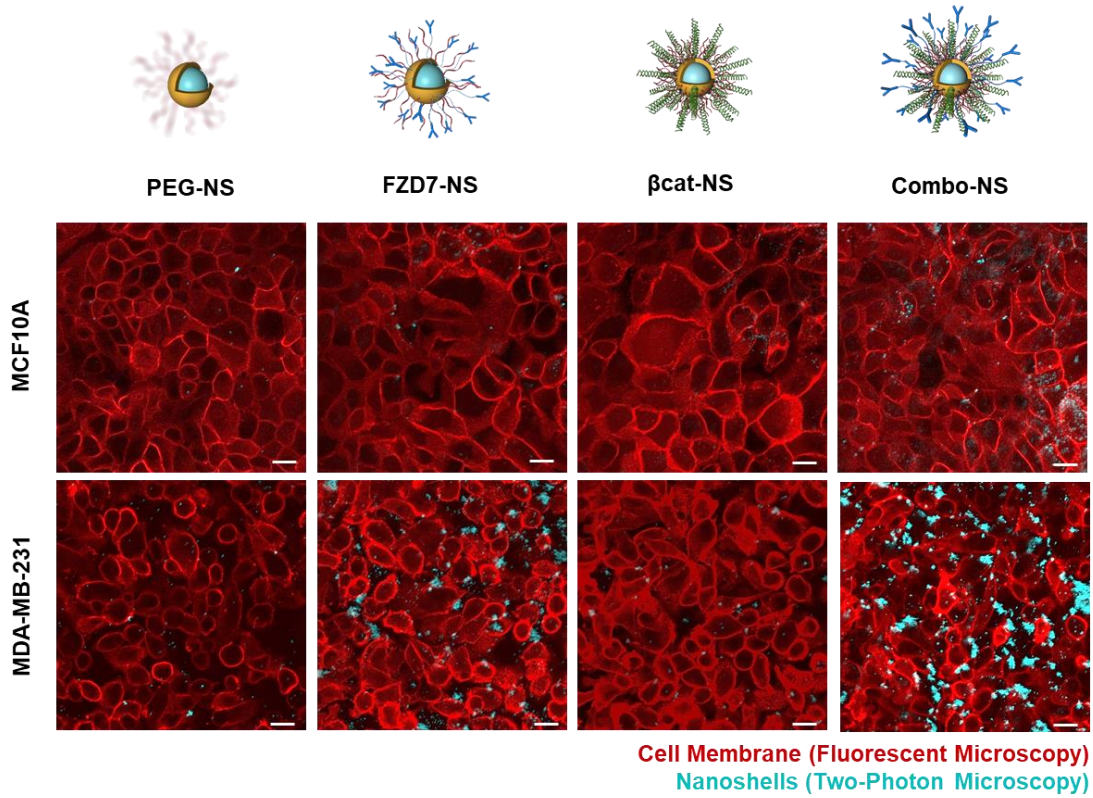

Figure 43. NP Cellular Binding Affinity. Multiphoton images of NP binding to MDA-MB-231 or MCF10A cells. Two images were taken with each biological replicate (n = 3). Scalebar = 20 μm.

4.3.4 Cellular Uptake of Cy5-labeled Wnt Inhibitory NPs

To further elucidate the cell binding capabilities and evaluate cellular uptake based on time, we shifted to evaluating the NP-cellular interactions *via* flow cytometry. To do so, we needed to tag the NPs to fluorescently activate them for analysis. We opted to replace the mPEG used in passivating the NPS with Cy5-mPEG as described in **Chapter 4.2.6**. We discovered that it was necessary to adjust the Cy5-mPEG concentrations per NP to deliver the same number of NPs and maintain equal Cy5 readings. Consequently, we found that PEG-NS and βcat-NS needed an initial

concentration of 5 μM to have the same relative Cy5 fluorescent reading as the FZD7-NS and Combo-NS (**Figure 44**).

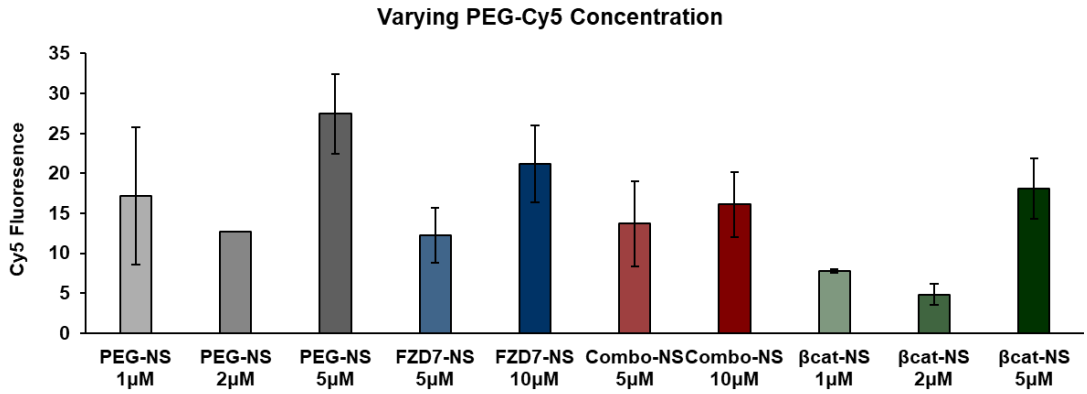

Figure 44. NP Cy5 Fluorescence. Cy5 fluorescence raw values of NPs tagged with Cy5 labeled mPEG. n = 3.

Once we optimized the Cy5 signal for the NPs, we moved forward to the flow cytometry cellular uptake studies. As with the multiphoton microscopy images taken in **Chapter 4.3.3,** we found that the antibody-loaded NPs were bound or internalized by MDA-MB-231 cells more than the PEG-NS and βcat-NS (**Figure 45A**). While the NPs signal in MDA-MB-231 were great than in MCF10A, we saw more binding or uptake in these flow experiments compared to the lack of NPs seen in MCF10As *via* multiphoton microscopy. We hypothesize that the sticky nature of the Cy5 tag on the mPEG passivation contributed to an increase in non-specific cell binding. Nonetheless the NP binding to the target MDA-MB-231 cells were ~1.5 fold more than to control MCF10A for the antibody-loaded NPs.

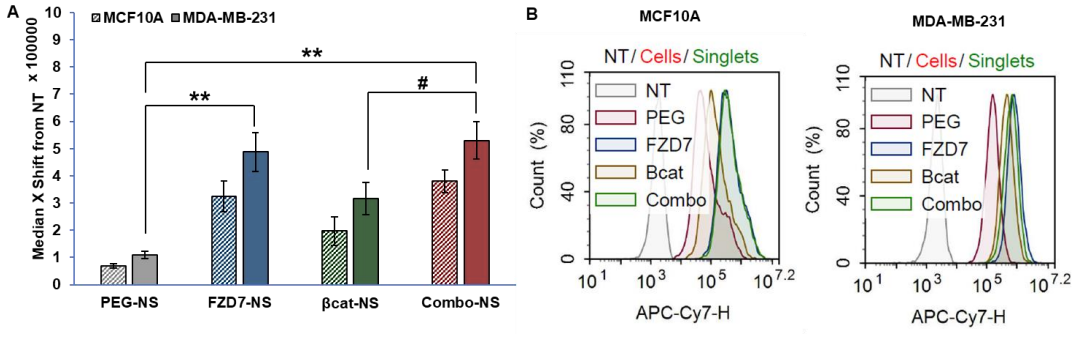

Figure 45. NP Cellular Uptake *via* Flow Cytometry. (**A**) Cellular uptake of NPs at an OD of 1 after 1 hour assessed *via* flow cytometry. (**B**) Representative flow graphs. n = 4. *p<0.1 and **p<0.01 by one-way ANOVA with posthoc Tukey-Kramer.

Additionally, we wanted to evaluate the uptake of NPs over time (**Figure 46**). From this brief assessment, we found that the NP binding and uptake in MDA-MB-231 cells saturated out at 4 hours. From 1 – 8 hours, the NP uptake in MCF10A was slower and caught up in MDA-MB-231 by 8 hours.

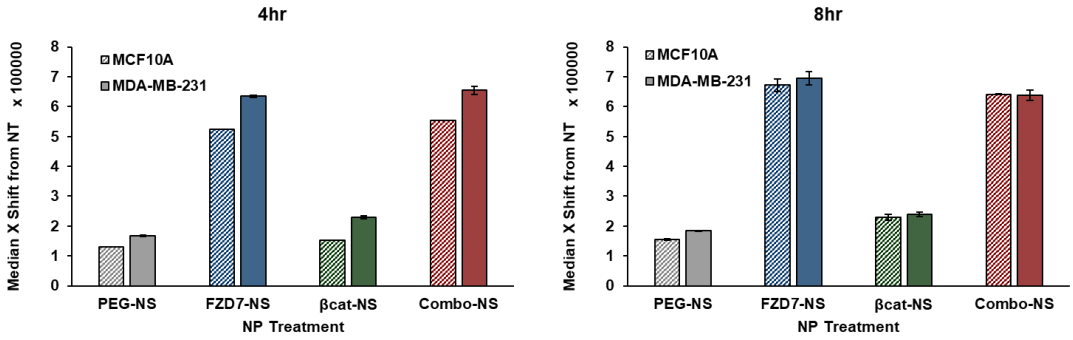

Figure 46. NP Cellular Uptake Over Time. Additional Cy5 labeled NP uptake *via* flow cytometry after 4 and 8 hours of NP incubation. n = 1 (technical triplicates when running flow samples).

In optimizing conditions for this experimental setup, we attempted to increase the initial NP concentration and evaluate the corresponding NP uptake. Here we found that the overwhelming number of NPs saturated the binding to either cell lines (**Figure 47**). We saw relatively equal binding to both cell lines regardless the NP type, and even more NP signal in MCF10A for FZD7-NS and βcat-NS. This speaks to the importance in determining NP dosage for maximal specific cellular uptake, which also translates into *in vivo* studies as evaluated by Chan *et al.* about the NP dose threshold for solid tumor delivery.[146]

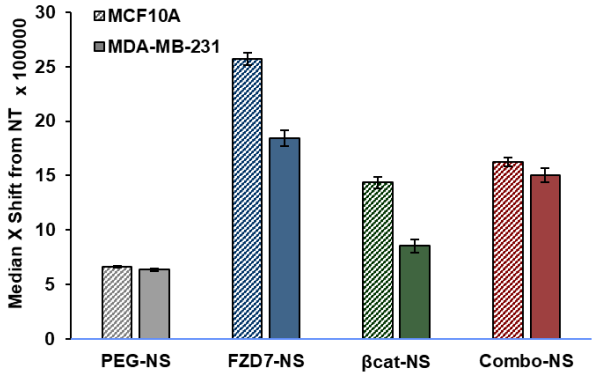

Figure 47. **NP Cellular Uptake *via* Flow Cytometry At A Higher Dose.** NP uptake when treated with twice as high concentration of NPs. n = 3.

4.3.5 Assessment of Downstream mRNA Wnt Genes *via* qPCR-RT

Following assessment of NP uptake, we moved forward with evaluating the impact on gene regulation at the mRNA level. Since the NP platform consists of delivery β-catenin siRNA, therapeutically we would expect to see gene knockdown. Additionally, in designing the NP system, we wanted to impede the Wnt signaling pathway at both receptor and mRNA levels. Consequently, there are a few other

downstream relevant Wnt genes that could be impacted by the delivery of β-catenin siRNA. We validated gene knockdown the following relevant genes (β-catenin, Axin2, CCND1, Nanog, and Snail) *via* qPCR-RT by transfecting MDA-MB-231 cells with β-catenin siRNA as described in **Chapter 4.3.7**. In comparison to β-scramble siRNA, we saw drastic knockdown in relative mRNA expression levels for β-catenin, Axin2, CCND1, Nanog, and Snail at 48 hours, which decreased further at 72 hours for β-catenin, Axin2, and Nanog (**Figure 48**). Surprisingly, the expression levels for Snail increased at 72 hours, but was still less in comparison to the β-scramble treatment.

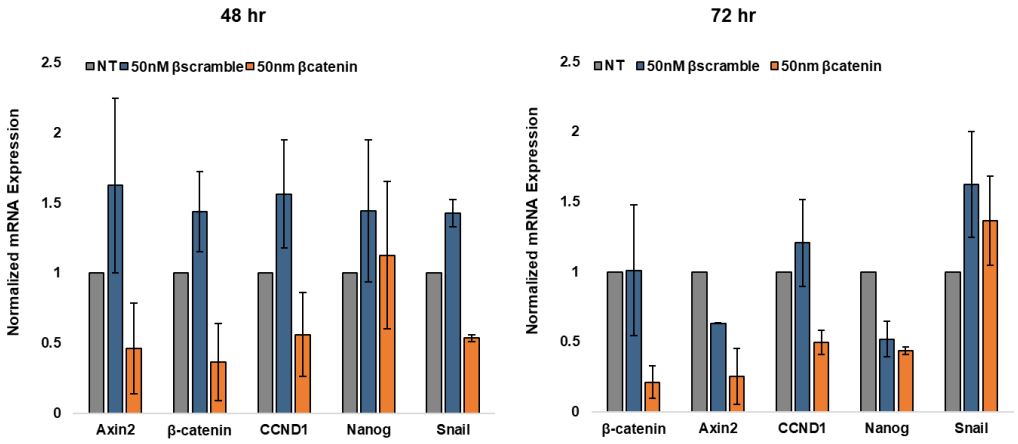

Figure 48. Validation of mRNA Knockdown in Wnt Related Genes. MDA-MB-231 cells were transfected with β-catenin siRNA at 50 nm and assessed for mRNA expression levels after 48 and 72 hours. n = 2 (technical triplicates when running PCR plates).

We then evaluated the NPs ability to knockdown β-catenin, along with other Wnt signaling and cancer suppressive relevant genes, in MDA-MB-231 cells as described in **Chapter 4.2.7.** Across the board, all the NPs had an impact on decreasing

mRNA expression levels compared to the not treatment group (**Figure 49**). Combo-NS was able to further decrease the mRNA expression levels of β-catenin, C-myc, and Snail. Impressively, the impact of the NPs was around the same order as the gene knockdown seen in the transfection validation experiments (**Figure 48**), with the siRNA-loaded NPs delivering ~4 times less RNA compared to the 50 nM transfection of β-catenin.

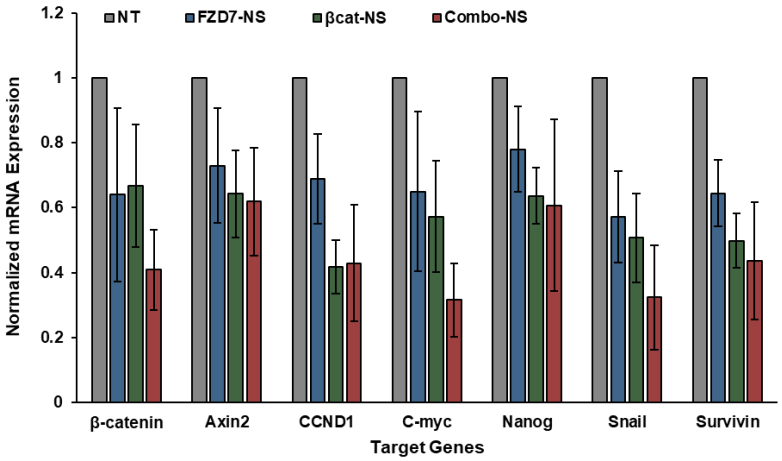

Figure 49. Relative mRNA expression of Wnt target genes in MDA-MB-231 cells following NP treatment. Results are from n = 3 biological replicates for all genes. Not significant by one-way ANOVA with posthoc Tukey-Kramer.

4.3.6 Analysis of Cellular Proliferation Following NP Treatment

Cellular proliferation is one of the hallmarks of cancer outlined in **Chapter 1.1.1** and so we evaluated the NP's impact on impeding cell proliferation using an EdU assay as described in **Chapter 4.2.8.** After 24, 48, and 72 hours of NP incubation, βcat-NS treated cells had comparable proliferation percentages as the no treatment group. Instead, the antibody-loaded NPs were able to decrease cell

proliferation at earlier times points. Furthermore, while the FZD7-NS treated cells recovered in proliferation over time, the Combo-NS treated cells were slower to recover and had statistically less proliferating cells even out to 72 hours post NP incubation (**Figure 50**). This helps validate the improvement in β-catenin siRNA delivery and therapeutic effect with the additional of FZD7 antibodies. Moving forward, it would be interesting to see the potential impact of the NPs on the various cell cycle phases (G0, G1, S, G2, M) or to evaluate the impact of multiple NP doses over a longer time, which could correlate to *in vivo* studies that typically involve multiple NP doses administered over time. The NPs may be impacting only a particular cell cycle phase and future studies will have elucidate the exacting timing of gene knockdown resulting in therapeutic effects. Additionally, siRNA silencing is transient, thus the number of doses is important to consider in developing a treatment regimen.

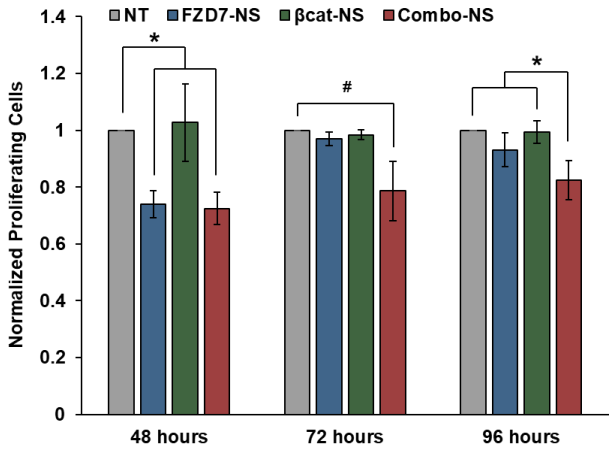

Figure 50. Assessment of Cell Proliferation Following NP Treatment. Normalized count of proliferating MDA-MB-231 cells following NP treatment assessed *via* an EdU Proliferation Assay after 96 hours. #p<0.1 and *p<0.05 by one-way ANOVA with posthoc Tukey-Kramer.

4.3.7 Analysis of Cellular Migration Following NP Treatment

Activating invasion and metastasis is another one of the hallmarks of cancer outlined in **Chapter 1.1.1**. The ability for cells to invade and migrate is an important contributing factor to cancer cell metastasis. To evaluate this on a simple level, we designed a transwell migration assay as described in **Chapter 4.2.9**. MDA-MB-231 cells are pre-treated with NPs for 96 hours and then reseeded in transwell porous membranes to evaluate their migratory behavior overtime post treatment. 6 hours post reseeding, the groups pre-treated with NPs all had less cells that migrated across the membrane compared to the no treatment group (**Figure 51A**). Moreover, the Combo-NS pre-treated cells migrated the least compared to the other NPs groups. Over time, after reseeding, the cells pre-treated with Combo-NS continued to migrate to a slower degree in comparison to the other NP groups. In fact, by 16 hours, the number of cells migrating across was relatively equal for the pre-treated FZD7-NS, βcat-NS and no treatment. Meanwhile, Combo-NS pre-treated group, maintained suppressed number of migrating cells up to 48 hours. However, at the timepoint the doubling time of the cells would need to be considered into the analysis, thus it is more accurate to consider the cells that have migrated over by 24 hours are more or less the original group of cells initially reseeded in the transwell membrane, as depicted in **Figure 51B** with representative images.

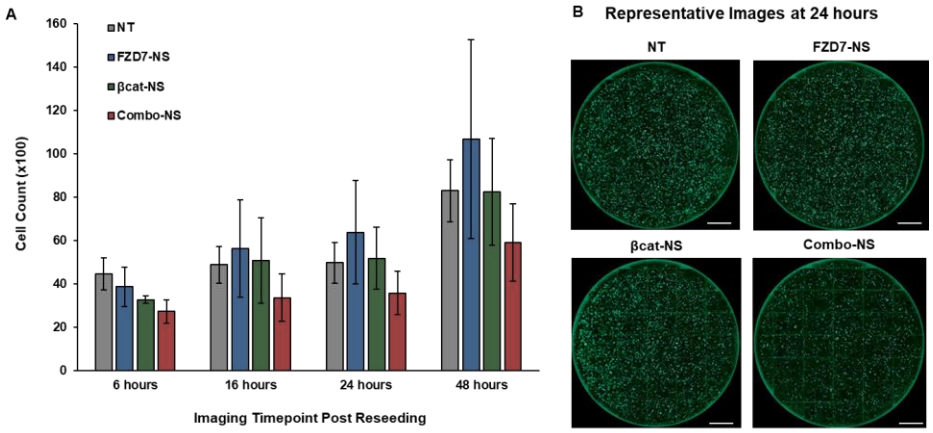

Figure 51. Analysis of MDA-MB-231 Cell Migration in Response to NP Treatment. (**A**) Normalized count of migrated MDA-MB-231 cells following NP incubation for 96 hours. (**B**) Representative fluorescent images of the migrated GFP cells. Not significant by one-way ANOVA with posthoc Tukey-Kramer. Scalebar = 1 mm**.**

Interestingly, when optimizing the conditions for the migration assay, we had also pre-treated cells for 72 hours and then reseeded them into transwell assays. Similar to the cell proliferation results in **Chapter 4.3.6**, the antibody-loaded NPs impacted cell functionality at earlier timepoints (**Figure 52**). However, longer time periods, the FZD7-NS effects wore off while the Combo-NS was able to maintain impediment of cell function when reseeding after 96 hours of NP incubation.

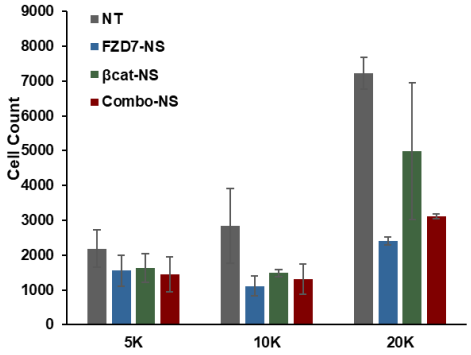

Figure 52. Optimizing Seeding Densities and Impact on Cell Migration. Normalized count of migrated MDA-MB-231 cells following NP treatment incubation for 72 hours. Not significant by one-way ANOVA with posthoc Tukey-Kramer. Scalebar = 1 mm**.**

4.3.8 Analysis of Spheroid Formation Following NP Treatment

Wnt signaling pathway is also associated with cancer stemness[147] and involves several of the genes evaluated in qPCR-RT in **Chapter 4.3.5**. Nanog and Survivin are linked to stemness and are aggressive phenotypes.[148–150] Stem-like nature of TNBC cells is also an important contributing factor to tumor initiation, treatment resistance, relapse, angiogenesis, and metastasis.[147] We evaluated the impact of treatment on self-renewal by performing spheroid formation assays as described in **Chapter 4.2.10**. Briefly, MDA-MB-231 cells were pre-treated with NPs for 24 – 72 hours and then reseeded in sphere forming media and low-adhesion u-bottom well plates to facilitate spheroid formation. After a week of formation, the metabolic activity of the spheroids was assessed *via* an Alamar Blue assay. As with the cell proliferation and migration assay results, the Combo-NS impacted the spheres more after longer incubation times. In this case, the spheres formed after 72 hours of NP incubation with decreased metabolic activity compared to the no treatment group, with that of the Combo-NS

pre-treated spheres significantly decreasing by ~34%, 21%, and ~16% compared to the no treatment, FZD7-NS, and βcat-NS groups (**Figure 53A**). Additionally, upon imaging the spheres, we found that the pre-treatment with NPs physically hindered the spheroids from forming into spheres or preventing them from being as compact as noted by the opacity of the spheres imaged (**Figure 53B**). Additionally, evaluation of adhesion genes such as E-cadherin would help elucidate if such factors are contributing to the lack of spheroid formation.

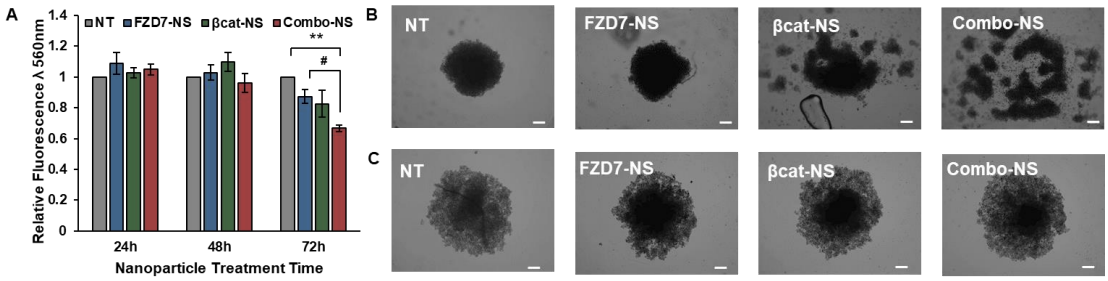

Figure 53. Analysis of MDA-MB-231 Spheroid Formation in Response to NP Treatment. (**A**) Metabolic activity assessment of spheroids after a week of formation. (**B/C**) Representative brightfield images of the spheroids formed after a week. Out of the biological replicates there were two types of spheres from. One was the lack of spheroid formation (top row) and two was the decrease in compact formation (bottom row). n = 4. #$p<0.1$ and **$p<0.01$ by one-way ANOVA with posthoc Tukey-Kramer. Scalebar = 200 μm.

4.4 Conclusions

In summary, these studies demonstrate that the dual loading of antibodies and siRNA can be carefully controlled through various parameters, including biomolecule addition order, salt aging conditions, and mPEG concentrations. Prior work has shown the delivery of FZD7-NS alone and at times with other drug inhibitors.[57,113] We

wanted to build upon this knowledge and exploit the Wnt signaling pathway which is hyperactive in TNBC. It is dysregulated by an abundance of extracellular Wnt ligands that bind to FZD7 receptors to active the signaling pathway. Consequently, this leads to the accumulation of β-catenin molecules intracellular resulting in the translation of oncogenic genes. Thus, we aimed to target two aspects of the pathway: targeting the extracellular receptor level and suppressing the intracellular mRNA level.

Here we used FZD7 antibodies and β-catenin siRNA which were co-loaded onto gold NS for treatment of TNBC through suppressing the Wnt signaling pathway. We confirmed comparable binding affinity for target TNBC cells lines for both FZD7-NS and Combo-NS through multiphoton microscopy and flow cytometry studies. The successful delivery of Wnt inhibitory NPs ensued in reducing the expression of several Wnt target genes that are implicated in cell proliferation (CCND1), survival (Survivin), and motility (Nanog). This prompted us to evaluate the effect of Wnt inhibitory NPs on proliferation, cell migration, along with spheroid formation capabilities. From these functional assays we found a trend in which at earlier time points, the antibody only NPs suppressed the aggressive characteristics of MDA-MB-231 cells. However, over time the effect of the FZD7-NS wore off, while the Combo-NS maintain some level of suppression, albeit to a lesser degree.

Overall, these studies demonstrate Wnt inhibitory NPs can enable targeting and gene regulation of TNBC cells. These conjugates provide tunable loading capabilities, which would be of value to adjust. These studies should be evaluated with varying concentrations of biomolecule loading, in addition to multiple dose administration to further understand the impact of the NPs and their clinical potential. Lastly, the platform needs to be fully studied in animal models in regard to transitional towards

the clinical pipeline. With additional development, Wnt inhibitory NPs may offer an alternative targeting therapeutic for TNBC and other cancers implicated by hyperactive Wnt signaling.

Chapter 5

DESIGNING WNT INHIBITORY NANOPARTICLES FOR TREATMENT OF TUMORS IN SPONTANEOUS METASTATIC BREAST CANCER MODEL

5.1 Introduction

Two hallmarks of cancer that will be highlighted in the following work are sustaining proliferative signaling and activating invasion & metastasis.[19,20] The proliferation of healthy breast cells is a strictly maintained mechanism to preserve homeostasis; however, in cancer, cells acquire various methods to dysregulate their proliferation capabilities to continuously divide.[151,152] This uncontrolled proliferation is due to either lack of tumor-suppressive genes, elevated levels of mutated genes, and consequently increased activity of related oncogenes.[153,154] Furthermore, part of TNBC's aggressive nature is attributed to the development of metastasis in secondary organs, which typically involve the lungs, brain, and bone.[27,149,155] This presents a significant clinical issue as the metastatic spread is the primary cause of death for TNBC patients.[27] Statistically, even after initial treatment of primary breast cancer, the 5-year relative survival rate for distant breast cancer is 27%.[156] While the exact mechanism behind metastasis is still being understood, several primary steps must occur. Initially, cancer cells in the primary breast location initiate local invasion within the local region followed by entry into the lymphatic system surrounding the breast anatomy. From here, the circulating cancer cells can extravasate into distant tissues to form secondary or metastatic tumors.[157,158] The rates of metastasis are dependent on several features but in we are focused on using gene regulation to inhibit the formation

of metastasis by reducing metastatic formation through inhibition of overactive oncogenic signaling which impacts other metastatic activities. Specifically, Wnt signaling has been implicated with EMT and higher metastasis rates.[155] Overall, the resistance of sustained proliferation and activating invasion & metastasis are crucial to the purpose of this dissertation, in which both are examined in the gene regulatory components of two different methods and multiple evaluation of various functional assessments.

Prior work has been done to evaluate the impact of Wnt inhibitory NPs for treatment of experimental lung metastasis. However, in experimental murine models, immune-compromised nu/nu mice are typically used. While this model is a simpler model to evaluate the impact of NP delivery and any therapeutic effects, the model lacks the sophisticated, complex microenvironment of the tumor site and even more importantly the influence of the immune system in combating the disease or interacting with the NPs. Here, we will investigate the NPs in a more aggressive tumor model that forms in immunocompetent mice, as this will provide a more accurate depiction of their anti-metastatic potential. Additionally, this model will allow us to preliminarily assess the safety of the Wnt inhibitory NPs in immune competent animals. We aim to use a similar design of FZD7 antibody and β-catenin siRNA functionalized NS for targeting of FZD7 in murine 4T1 cell lines. The *in vitro* studies presented below validate the rationale behind using this platform for treatment of TNBC. The *in vivo* studies thoroughly characterize a working spontaneous metastatic model using immune competent mice inoculated with orthotopic tumors at the mammary fat pad. We wrap up these studies with two different therapeutic studies

with different dose regimens and evaluating the NP's ability to slow down primary and recurrent tumor growth, along with prevention of metastatic spread.

5.2 Materials and Methods

5.2.1 Cell Culture and Experimental Setups

4T1 murine TNBC cells purchased from American Type Culture Collection (ATCC) were cultured in Roswell Park Memorial Institute (RPMI) 1640 Medium (ATCC) supplemented with 10% fetal bovine serum (FBS) (Gemini Bio) and 1% penicillin-streptomycin (VWR). Cells were cultured in T75 cell culture flasks (VWR), passaged with 0.25% trypsin-EDTA (VWR), and incubated at 37°C in a 5% CO2 humidified environment. Cells were cultured to 80-90% confluency prior to plating for experiments, used within passage numbers of 20 – 30, and counted using a glass slide hemocytometer for all experiments. Noncancerous EpH4-Ev murine breast epithelial cells were purchased from ATCC and cultured in DMEM modified with 1mM sodium pyruvate and supplemented with 10% bovine calf serum (Cytiva) and 1.2 mcg/mL puromycin (ThermoScientific). MCF-10As were cultured in the same conditions as the cells above and were used within passage numbers of 15 – 20.

The general experimental setup used for studies to assess the impact of co-delivered NPs on TNBC cells. Cells were plated in well plates with complete cell culture media and incubated for at least 20 hours. The cells were then incubated with FZD7-NS, βcat-NS, Combo-NS, or full media at $3.0x10^9$ NPs/mL ($OD^{810\ nm} = 1$), $1.5X10^{10}$ NP/mL ($OD^{810\ nm} = 5$), $3.0X10^{10}$ NP/mL ($OD^{810\ nm} = 5$) or for 12 – 48 hrs depending on the experiment. $OD^{810\ nm} = 1$ corresponds to ~ 1.2 nM FZD7 antibodies

and ~11nM siRNA , $OD^{810\ nm}$ = 5 corresponds to ~ 6 nM FZD7 antibodies and ~53nM siRNA, $OD^{810\ nm}$ = 10 corresponds to ~ 12 nM FZD7 antibodies and ~107 nM siRNA.

5.2.2 Validating FZD7 and β-catenin Expression Levels in 4T1

FZD7 expression levels were assessed on murine cell lines *via* immunocytochemical (ICC) staining. 4T1 and EpH4-Ev cells were detached from cell culture flasks with 0.25% trypsin-ETDA, plated in 24-well plates at 10,000 and 20,000 cells per well respectively, and incubated overnight. Then, cells were fixed with 4% formaldehyde and rinsed 3X with 1XPBS. Endogenous peroxidases were blocked with 3% hydrogen peroxide diluted in 1XPBS for 10 min and on specific protein interactions were blocked with 3% PBSA for 60 min. Rabbit anti-mouse FZD7 antibodies (LSBio) diluted in 3% PBSA to 0.5 μg/mL were added to each well and samples incubated overnight at 4 °C. Anti-FZD7 antibodies were removed, samples were rinsed 3X in 1XPBS rocking at RT for 5 minutes, and then HRP-anti-rabbit IgG (HRP-AR, Seracare Life Sciences) diluted to 3 μg/mL was added for 60 min at RT. Samples were again rinsed 3X in 1XPBS rocking at RT for 5 minutes. 3-amino-9-ethylcarbazole (AEC, Sigma-Aldrich) was added for 20 min covered to stain bound HRP secondary antibodies. To stop the reaction, Samples were again rinsed 3X in 1XPBS rocking at RT for 5 minutes. Stained cells were imaged on a Zeiss Axioobserver Z1 inverted fluorescence microscope using bright-field settings and a color camera. To confirm successful gene knockdown upon delivery of β-catenin siRNA in murine cells lines, 4T1 cells were transfected with therapeutic β-catenin and control β-scramble siRNA at 50 nM for 48 hours. mRNA was extracted following transfection for qPCR-RT analysis for β-catenin mRNA expression levels. The mRNA

expression levels were normalized to that of GAPDH and further normalized to no treatment group. Primer sequences are listed in **Table 6**.

Primer	Forward Sequence Reverse Sequence
GAPDH	TCAAGAAGGTGGTGAAGCAGA CCACTCTTCCACCTTTCGATGC
β-catenin	CCTTTTTGGTCGAGGAGTAA GGGATAAAAGGCATTCTGGTA

Table 6. Primer sequences used for real time qRT-PCR studies.

5.2.3 Nanoshell Synthesis and Coating with Antibodies and siRNA

NS were synthesized according to published methods which were described in detail in **Chapter 2.2**. FZD7 antibodies were purchased at 1 mg/mL from LSBio and PEGylated in house with a 5kDA OPSS-PEG-SVA linker. β-catenin siRNA oligonucleotides were purchased as single strands from Integrated DNA Technologies (**Table 7**). The sense strands were modified with thiol groups on the 3′ end for ease of functionalization to the surface of the gold NS. Complementary sense and antisense strands were mixed in equimolar amounts and duplexed. NS were diluted to $4.4x10^9$ NS/mL ($OD^{810\ nm}$ = 1.5) in milliQ water and incubated with 1000 or 1200 antibody per NS initially (Combo-NS or FZD7-NS, respectively). Afterwards, NS were incubated with 0.2% tween and salt aged to 300 or 1000 mM (βcat-NS or Combo-NS, respectively) for 5 minutes. Then, 0.1 or 0.25 nmol of siRNA (βcat-NS or Combo-NS, respectively) and 20 μM of mPEG-SH were added which was described in more detail in **Chapter 2.3.3**. The FZD7 antibody only NPs (FZD7-NS) were not salt aged. In

optimizing equivalent loading of the monotherapeutic nanocarriers to the dual biomolecule NP, we determined how final antibody and siRNA loading on the NS is impacted increasing mPEG concentrations. For all synthesis the NPs were purified *via* centrifugation 1X at 500 g for 15 minutes and 2X for 10 minutes. Between each spin step the NPs were suspended in 1XPBS. The final stock solution was then diluted in 1X PBS at 100X less volume than the starting NS volume. NP concentration was determined *via* the absorbance spectrum using the Cary 60 UV-visible spectrophotometer as described in **Chapter 2.4.1.**

siRNA	Sequence
β-catenin sense	5' – GCU GAU AUU GAC GGG CAG UAU / iSpPC/iSpPC//3ThioMC3-D/ -3'
β-catenin antisense	5' – AUA CUG CCC GUC AAU AUC AGC – 3'
β-scramble sense	5' – GUC AGA UGU AGG GCG AUU ACU UU – 3'
β-scramble antisense	5' – AGU AAU CGC CCU ACA UCU GAC UU – 3'

Table 7. siRNA sequences utilized.

5.2.4 Antibody and/or siRNA Conjugate Characterization

The hydrodynamic diameter and zeta potential of the miRNA/NS conjugates and bare NS were measured using an Anton Paar Litesizer as described in **Chapter 2.4.3**. siRNA loading on NS was quantified using a Quant-iT OliGreen^{TM} ssDNA

quantification kit as described in **Chapter 2.4.4**. Antibody loading on NS was quantified using an ELISA assay as described in **Chapter 2.4.5**.

5.2.5 Analysis of Cellular Proliferation Following NP Treatment

For studies to assess cell proliferation, 4T1 cells were plated at 2,000 cells/well in 48-well plates prior to NP treatment. Each treatment group had 2 wells each to serve as technical replicates. Cells were treated with no NP, FZD7-NS, βcat-NS, and Combo-NS at OD 1, 5, and 10. Following 12 – 48 hours, the cells were assessed for proliferation using the Click-iT^{TM} EdU Cell Proliferation Kit (ThermoFisher). The steps of the assay followed the manufacturer's instructions as described above in the Chapter **3.2.7**. These experiments were performed in triplicate and analyzed using a one-way ANOVA with posthoc Tukey.

5.2.6 Modeling Spontaneous Metastatic Tumor Growth

To design a therapeutic study for treatment of primary and metastatic tumor growth we needed to prove the ability to model a spontaneous metastatic tumor model derived from an orthotopic primary tumor in the mammary fat pad. This murine model involves inoculating Balb/C mice with 4T1 murine cells in the 4th inguinal mammary fat pad *via* surgical exposure of the fat pad. After initial growth, the primary tumor is surgically removed, and recurrent tumor and metastatic lesion growth occurs. Prior to the initial cell inoculation procedure Balb/C mice anesthetized and hair surrounding the 4th inguinal mammary gland were removed with topical removal cream, Nair (**Figure 54**).

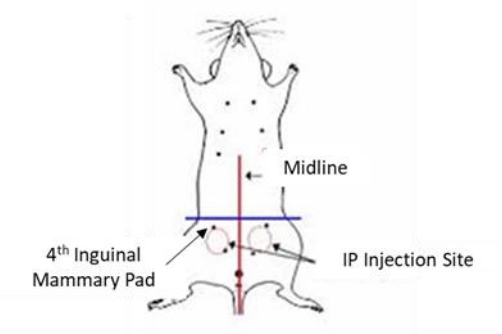

Figure 54. **4th Inguinal Mammary Fat Pad.** Simplified mice anatomy for visualization of the 4th inguinal mammary fat pad, surgical site, and IP injection site.

In preparation for initial cell inoculation, luciferase-expressing 4T1-Luc2 cells (ATCC) were expanded in T300 flasks to ~60 – 80% confluency at passages 8 – 12. Cells were lifted, collected in RPMI supplemented media, and pelleted at 200g for 5 minutes. The supernatant was aspirated and the pellet was resuspended in 1X PBS (without magnesium and calcium). The stock cell suspension was diluted down in 1X PBS for cell counting. Cell suspensions were diluted in 1X PBS to the following cell count per injection volume: 5, 10, 20, 50, and 100K cells / 50uL. Cells dilutions were left on ice until prepared for inoculation before each surgery.

During the cell inoculation surgical procedure, mice were anesthetized and maintained warm on a heating pad. Buprenorphine was prepared at 0.1mg/kg dose based on mice weight and injected intraperitoneal with a 1cc x 29G x ½'' (MedLabSupply) syringe on the opposite side of the surgical site. Ophthalmic ointment was applied to the mice eyes and the surgery site was sterilized with povidone-iodine swabsticks and isopropanol 3X. Prior to starting the surgery, all tools used were sterilized in a bead sterilizer between each surgery and the mouse was checked for reflex responses using a firm toe pinch to ensure full anesthetic state.

Before each surgery, the cell suspension was prepared by suspending the cells and aspirating up 50uL of cells in a 1cc x 29G x ½'' (MedLabSupply) syringe.

To proceed with cell inoculation a longitudinal incision with a #15 feather scalpel blade (MidWestVetSupply) was made ~0.5 cm from the 4th inguinal to the midline (**Figure 55**). A sterile cotton swab soaked in sterile 1X PBS created a pocket at the incision opening. The skin flap was lifted with curved serrated forceps (Roboz surgical instrument) to open the incision site and blunt serrated forceps (Roboz surgical instrument) were used to pull out the fad pat (opaque in color). The base of the fat pad was secured by switching from the curve tweezers to the teeth tipped forceps (BrainTree Scientific). The prepared cell suspension was injected into the base of the fat pad secured in the square tip tweezers and the fat pad was released upon successful inoculation. The incision site area was dried with sterile gauze. Lastly, the incision site was sealed using the curved forceps to pull the opening taut and applying vetbond along the seam. The mouse was placed in individual holding cages maintained warmed with a heating pad until awaken from the anesthesia. The mice were monitored for signs of discomfort or pain in which additional amounts of buprenorphine can be administered.

When the primary tumor has grown to around 200 mm^3 in volume (details on monitoring methods in **Chapter 5.2.7**), the mice was prepared for primary tumor surgical removal. The mice are prepared for surgical as detailed prior to the cell inoculation surgery. To expose the primary tumor, a longitudinal incision was made along the length of the tumor with a scalpel blade. Using curve forceps the skin was pulled back gently and detached from the tumor by using the blade to carve along the underside of the skin. Blunt forceps were used to slowly rotate the tumor to slide the

scalpel to the backside of the tumor. Upon full detachment, the tumor was placed in 1X PBS for further downstream processing as detailed below. The incision site was sealed with the same methods as described in the cell inoculation procedure and the mice were placed in individual soft bedding housing to recover for at least a week. From here, the mice were monitored for regrowth of tumors at the primary site along with any spread of metastatic lesions (details on monitoring methods in **Chapter 5.2.7**).

5.2.7 Monitoring Tumor Growth *via* Caliper Measurements and IVIS Imaging

Monitoring of tumor growth is done with physical caliper measurements and IVIS imaging of bioluminescent cells. For the measurements, a digital caliper was used to measure the length (longer) and width (shorter) of the tumor mass. The tumor volume was calculated with the following equation: (length x width^2)/2. For IVIS imaging of the tumors and any metastatic lesions, the mice were injected intraperitoneally (IP) with 150 mg/kg of D-luciferin (Biotium) diluted in saline. 10 minutes after injection, the mice were anesthetized and placed belly up into the IVIS Lumina III In Vivo Imaging System (fitted with an additional field of view lens) to read the exposure with the following parameters: imaging mode(s) = luminescence and photograph, exposure time = auto, binning = medium, F/stop = 1, excitation filter = closed, emission filter = open, overlay = checked, field of view = E, subject height = 1.5 cm, focus = use subject height, and bin = medium. Acquisition of the primary tumors are typically taken first. The chest area were imaged next with the primary tumors being hidden by a black cover.

5.2.8 Designing Therapeutic Study to Treat Primary Tumor and Metastatic Growth

Based on the results of the preliminary spontaneous tumor growth model, we designed a therapeutic study in which Balb/C were first inoculated with 100K 4T1-Luc2 cells in the 4th mammary fat pad. Following a projected 17 – 24 days in which the tumors would grow to ~100 mm^3 in volume a therapeutic regimen started as outlined below (**Figure 55**). NPs were injected *via* tail vein in 100 µL volumes at a concentration of 1.9x10^{11} NS/mL (OD$^{810\ nm}$ = 60) which corresponds to ~ 73 nM FZD7 antibodies and ~640nM siRNA. After two weekly NPs injections, the primary tumors were removed on Day 13. Two dose schedules were evaluated in this dissertation, in which the first consisted of 5 weekly NP injections and the second consisted of 2 weekly NP injections followed by 4 biweekly injections.

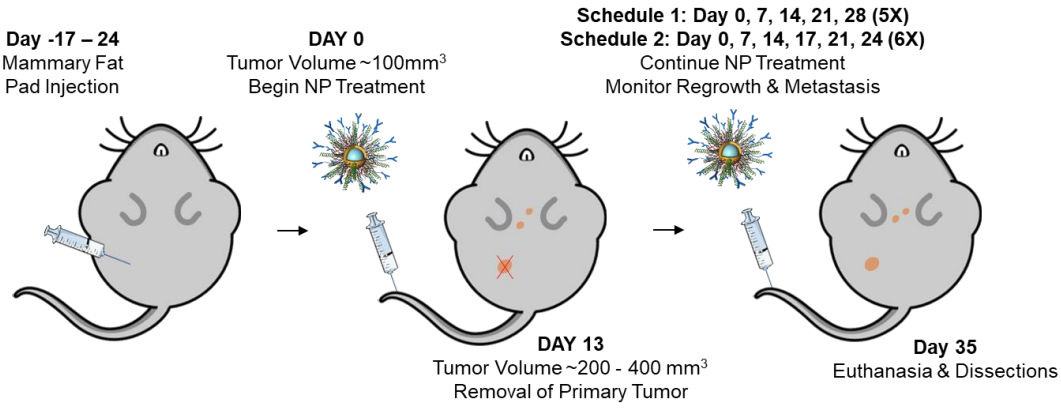

Figure 55. NP Regimen for Treatment of Spontaneous Metastatic Tumor Model. Scheme depicting the initial tumor inoculation, start of NP treatment, removal of the primary tumor, two different therapeutic dose regimens, and the end dates of the study.

5.2.9 Quantifying Gold Content in Tissue Samples *via* ICPMS

Inductively Coupled Plasma Mass Spectrometry (ICPMS) was used to assess gold content in the excised primary tumors and organs dissected at the end of the study (blood, heart, lungs, small intestine, spleen, kidney, liver, brain, and recurrent tumor). Following surgery and dissections, a quarter of each excised organ was placed into 15 mL conical tubes that were weighted beforehand for a tare weight. A wet weight was recorded with the organ in the tubes. The tubes were then frozen overnight at -80°C, lyophilized, and the dry weight of the tissues in tubes was recorded. The dried samples were digested in 97% trace metal grade nitric acid (Fisher) and 3% trace metal grade hydrochloric acid (Fisher) solution (volume varied depending on the tissue) in a heat block at 60°C in a fume hood for 1 – 2 hours (time varied depending on the tissue). Next the samples were diluted in an acid matrix containing 2% nitric acid and 2% hydrochloric acid in MilliQ water (dilution volume varied depending on the tissue), and a standard curve containing 0 – 750 parts per billion (ppb) gold using TraceCert Gold Standard for ICP (Sigma) was prepared. An internal baseline of 5 parts per million (ppm) was added to each standard and sample. Samples were analyzed on an Agilent 7500c ICP-MS instrument and the gold content in ppb was recorded for each sample. The gold content per gram of dried tissue was calculated based on the raw gold ppb values, accounting for the dilution factors throughout the sample preparation, and the dry weight of the organ (subtracting out the tare weight of the tubes).

5.2.10 Assessing mRNA Gene Knockdown in Extracted Tumor Samples *via* qPCR-RT

qPCR-RT was used to evaluate the mRNA expression levels of β-catenin in the primary and secondary organs excised partway and dissected at the end of the study. Following surgery or dissections, a quarter of each excised tumor was set aside of

RNA extraction using the Isolate II RNA Mini Kit (BioLine). The mRNA expression levels were normalized to that of GAPDH and further normalized to the saline group. Primer sequences are listed in **Table 6**.

5.3 Results and Discussion

5.3.1 Validating FZD7 Receptor and β-catenin Expression Levels in TNBC Murine Cell Lines

In shifting our target from human to murine cell lines, we needed to confirm FZD7 expression levels in murine 4T1 cells to make use of the Wnt Inhibitory NPs designed in **Chapter 4**. We validated the relative FZD7 expression of murine cancerous 4T1 cells versus noncancerous MCF10A cells by ICC staining as described in **Chapter 5.2.2**. We found that 4T1 cells expressed higher levels of FZD7 relative to EpH4 cells, as indicated by the positive red stain in the ICC samples (**Figure 56A**). We then validated gene knockdown of β-catenin by transfecting MDA-MB-231 cells with β-catenin siRNA as described in **Chapter 5.2.2**. In comparison to β-scramble siRNA, we saw drastic knockdown in relative mRNA expression levels for β-catenin (**Figure 56B**). With confirmation of both receptor and mRNA expression in 4T1, we moved forwarded to synthesizing another NP formation for Wnt targeting in murine cells lines, with antibodies and siRNA designed for murine cell line targeting and gene regulation.

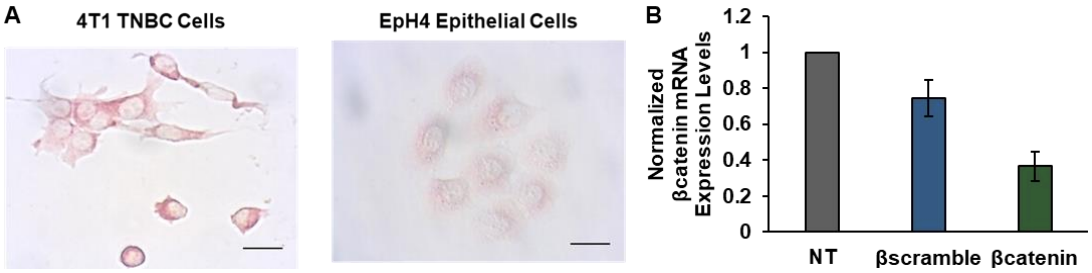

Figure 56. Validation of FZD7 Receptor and β-catenin mRNA Expression Levels in 4T1 Cells. (**A**) Immunocytochemistry analysis of cancerous 4T1 and breast epithelial cell line EpH4-Ev were evaluated for extracellular FZD7 expression levels. n = 3. Scalebar = 25μm. (**B**) Validation of β-catenin mRNA Knockdown. 4T1 cells were transfected with β-catenin siRNA *via* transfection delivery for qPCR-RT analysis of mRNA expression levels. n = 3.

5.3.2 Wnt Inhibitory NP Loading Optimization

From the results in **Chapter 4.3.1** we had a basis on what to expect in terms of optimizing antibody and siRNA loading on NS. To test if the loading could be increased, we evaluated the impact of mPEG concentration as described in **Chapter 5.2.3**. We found that the increasing concentration of mPEG helped load more antibodies onto both the FZD7-NS and Combo-NS (**Figure 57A**). Regarding siRNA loading, the Combo-NS saturated out with 10 μM mPEG, while βcat-NS increased in siRNA loading with 20 μM mPEG (**Figure 57B**).

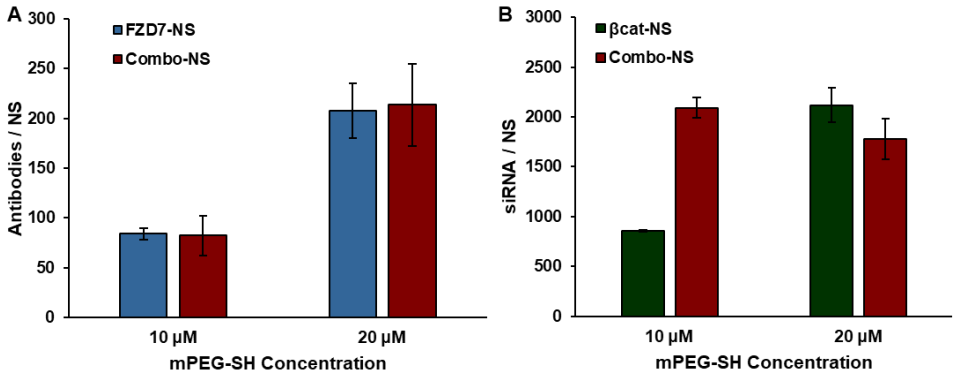

Figure 57. Loading Optimization of Multiple Wnt Biomolecules on NPs. Optimization of (**A**) antibody and (**B**) siRNA loading on gold NS depending on mPEG-SH concentration added. n = 3.

5.3.3 Wnt Inhibitory NP Characterization

After the optimizing the impact of mPEG passivation on antibody and siRNA loading of NS, we landed on a final functionalization protocol as described in **Chapter 5.2.3**. The NPs were characterized by DLS and Zeta potential in which we found that the NPs were larger in size by ~10 nm in diameter compared to bare NS. Additionally, the NPs were more neutral in charge (**Figure 58**). The antibody loading of Combo-NS and FZD7-NS were ~230 antibodies / NS and siRNA loading of Combo-NS and βcat-NS were ~2000 siRNA / NS (**Figure 58**). This corresponds to the following antibody or siRNA concentration for reference. OD^{810} nm 5 = $1.5X10^{10}$ NP/mL ~ 6 nM FZD7 antibodies and ~53nM siRNA. OD^{810} nm 60 = $1.9x10^{11}$ NPs/mL = ~ 74 nM FZD7 antibodies and ~640nM siRNA.

NP	DLS & Charge		Loading / NP	
	Hydrodynamic Diameter [nm]	Zeta Potential [mV]	Antibody	siRNA
Bare NS	175 ± 3	-24 ± 3	--	--
FZD7-NS	187 ± 6	-15 ± 1	225 ± 24	--
βcat-NS	185 ± 6	-19 ± 3	--	2094 ± 201
Combo-NS	186 ± 4	-18 ± 2	241 ± 35	1901 ± 198

Figure 58. Wnt Inhibitory NP Characterization. Final characterization of the Wnt Inhibitory NP platforms assessed *via* Litesizer measurements and loading assays for biomolecule loading. n = 12 – 16.

5.3.4 Analysis of Cellular Proliferation Following NP Treatment

Similar to the impact of the Wnt inhibitory NPs on human TNBC cells evaluated in **Chapter 4.3.6**, we evaluated proliferation in murine 4T1 cells (described in **Chapter 5.2.5**) and saw that the antibody-loaded NPs inhibited cell proliferation of 4T1 cells at earlier timepoints (**Figure 59**). This experiment was purposely set to evaluate NP impact at earlier timepoints than when evaluating in MDA-MB-231 cells, because of the faster doubling time of the 4T1 cells. As we evaluated NP impact on cell proliferation overtime, we saw that Combo-NS reduced cell proliferation by ~17% at 48 hours in comparison to the other NPs and no treatment group. Additionally, Combo-NS sustained a low level of proliferating cells over time compared to the other NP groups, which recovered more quickly. However, the impact of the Wnt inhibitory NPs on 4T1 cell proliferation is not as profound as we had seen in the MDA-MB-231 cell line.

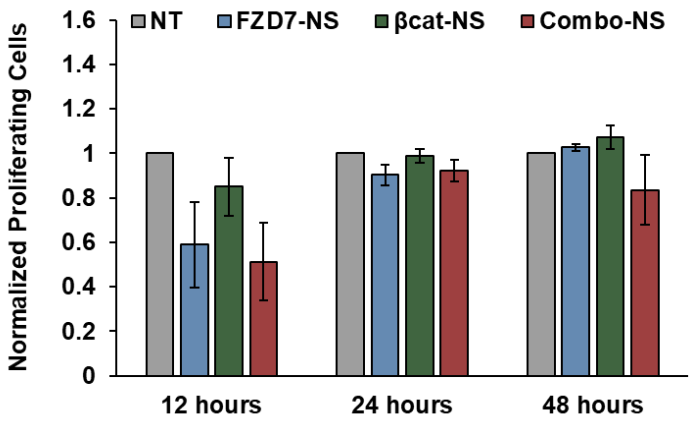

Figure 59. Assessment of Cell Proliferation Following NP Treatment. Normalized count of proliferating 4T1 cells following NP treatment at OD1 assessed *via* an EdU Proliferation Assay after 48 hours**.** n = 3. Not significant by one-way ANOVA with posthoc Tukey-Kramer.

5.3.5 Monitoring Primary and Metastatic Tumor Growth in Balb/C Mice

After validating the ability to target Wnt sigaling at the receptor level, regulate β-catenin mRNA expression levels, and reduce cell proliferation to an extent, we wanted to evaluate the NP platform on treatment of spontaneous lung metastasis. Prior work in the Day Lab has explored using the exact nanocarrier platform designed in **Chapter 4** to treat lung metastasis in nude mice induced by cell inoculation *via* IV injections. This was a pilot study spearheaded by a Day Lab alumnus in which data is not shown in this dissertation. We wanted to move into evaluating the NP's capabilities in an immune competent mouse model and thus needed to validate the ability to replicate a spontaneous lung metastatic model as described in **Chapter 5.2.6**. We first evaluated primary tumor growth at the mammary fat pad following cell inoculation of 5, 10, 50, and 100K cells (**Figure 60**) with caliper measurements and IVIS imaging as described in **Chapter 5.2.7.** The primary tumor initial was removed

on day 16 following initial cell inoculation. And tumor regrowth was monitored. The tumors inoculated at higher cell densities (50 and 100K) reached ~600 mm^3 by around day 40. The 10K group grew at a slow pace reaching the same size around day 60. Surprisingly, the 5K group grew at a faster pace reaching the same size around day 50.

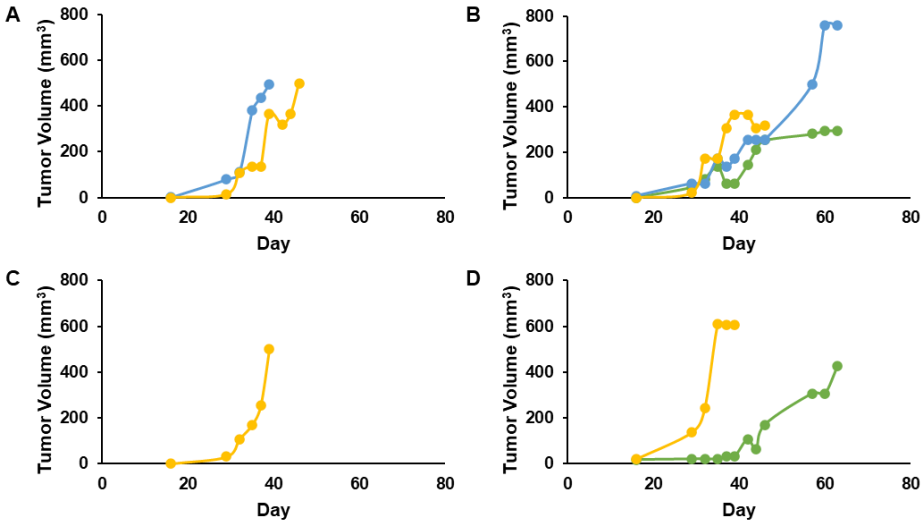

Figure 60. Primary Tumor Growth Overtime in the Mammary Fat Pad. Tumor volumes were recorded *via* caliper measures after initial cell inoculation of **(A)** 5K **(B)** 10K **(C)** 50K **(D)** 100K into the mammary fat pad. n = 1 – 3 mice per group (several mice did not take tumors – each color within the graphs indicates an individual mouse of the same experimental group).

Following the results of the preliminary tumor growth, we realized that the primary tumor needed and could be removed at a later timepoint. This would also be important for lung metastasis to form, as there no metastatic signal was detected *via* IVIS imaging throughout the 60 days.[159–161] We then redesigned the synergistic orthotopic tumor model to first inoculate the mice, remove the primary tumor when at

~200 mm^3 in volume, and monitor tumor regrowth and metastatic spread. Based on the preliminary tumor growth study, we decided to inoculate the mice at 10, 20, and 50K cell densities (**Figure 61**). The 20K group's primary tumors were removed around day 50 and the 50K group's tumors were removed around day 40. Surprisingly, the 10K group's tumors were also excised on day 40 which did not follow the trends when comparing to the 20 and 50K group data. Following this lung metastatic signal was detected for the 10K group around days 7 – 20 after the primary tumor removal. For the 20K and 50K groups they were 11 – 13 days and 6 – 7 days. Based on seeing the initial tumor growth and the timeline at which the metastatic lungs start to appear, we estimated that with 100K cells inoculated the primary tumors could be removed around day 30 with metastatic formation starting around 6 – 7 days following excision.

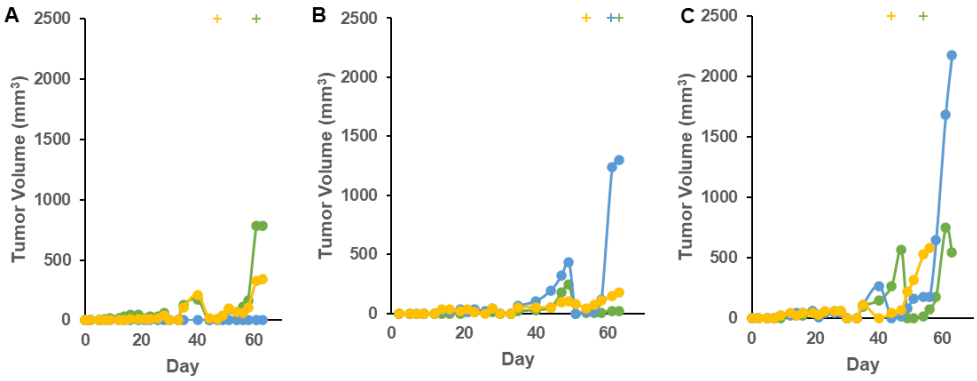

Figure 61. Evaluation of Primary Tumor and Lung Metastatic Growth.
Monitoring tumor growth following initial cell inoculation of **(A)** 10K **(B)** 20K **(C)** 50K in the mammary fat pad. Primary tumors were removed at around 200 – 400 mm^3 and lung metastatic signal was monitored *via* IVIS imaging. (+) = start date of lung metastatic signal. n = 3 mice per group.

5.3.6 Evaluation of Therapeutic Impact on Primary, Recurrent, and Metastatic Tumor Burden

After deciding on the initial cell inoculations and designing a therapeutic regimen plan around the anticipated tumor growth and metastatic spread we evaluated the impact on the Wnt inhibitory NPs in Balb/C mice with a synergistic tumor model as described in **Chapter 5.2.8.** Two different treatment schedules were conducted over two separate studies. The two schedules had the same NP treatment plan for the primary tumor growth. After the primary tumor was remove, the schedules were different in dose frequency and amounts as outlined in **Figure 55**. Since the treatment of the primary tumors were the same, the datasets across both studies were compiled together. We found that overall, the NPs were able to reduce primary tumor growth significantly (**Figure 62A**). The differences between the NPs groups were statistically insignificant, but the treatments were able to reduce the primary tumor growth by ~33 % compared to the saline group **(Figure 62B**).

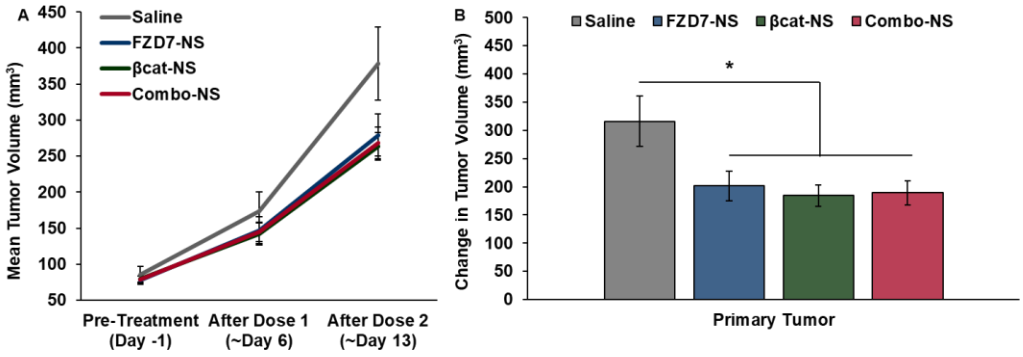

Figure 62. Primary Tumor Growth in the Mammary Fat Pad. (**A**) Change in tumor volume over time. (**B**) Change in primary tumor volume upon removal starting from initial NP injection. *p<0.05 by one-way ANOVA with posthoc Tukey. n = 12 – 14.

Following primary tumor removal, tumor regrowth and lung metastatic spread was monitored *via* IVIS imaging calculated by average radiance. From here on out the datasets from the two treatment schedules were kept separated. We expected the schedule 2, which had more NP doses at a higher frequency, to slow down the regrowth of tumors, however we found no differences in the change in recurrent tumor signal (**Figure 63**). However, during the schedule 2 study, the tumor regrowth from the start was more aggressive in comparison to during the schedule 1 study. Consequently, to compare the two treatment schedules more accurately, they would need to be conducted side by side with the same cohort of inoculated mice.

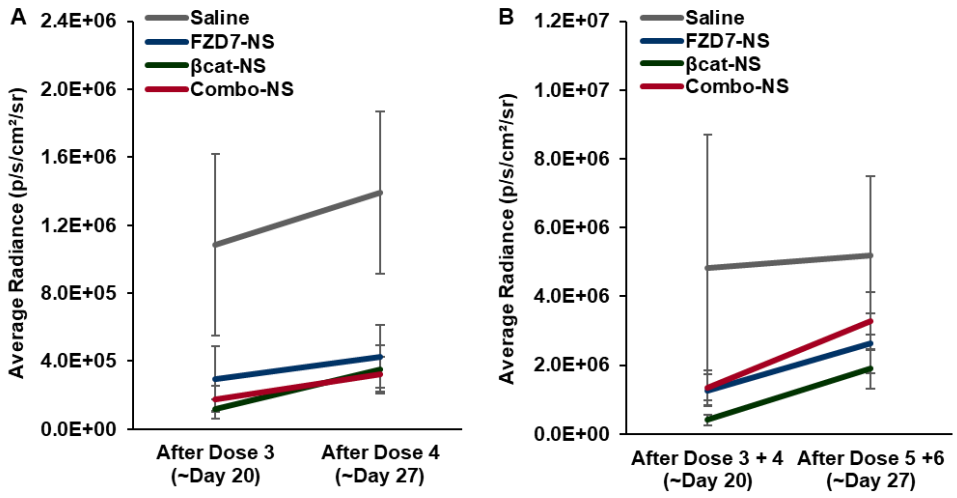

Figure 63. Change in Recurrent Tumor Growth. Primary tumors were surgically removed on day 14 and tumor regrowth was monitored starting a week after for treatment (**A**) schedule 1 (**B**) schedule 2. n = 6 – 7.

The lung metastatic spread showed more differences between the NP treatment groups and treatment schedules (**Figure 64**). For both schedules, the lung metastasis

spread was slower with the NP treatment versus the saline group (**Figure 64 Ai, Bi**). Interestingly, enough in the schedule 1 study the saline group grew lung metastases more aggressively compared to that of schedule 2, which was the opposite of what was seen above in the recurrent tumor growth. We further probed the lung metastatic data and found that between both schedules the NPs slowed down the start of metastatic growth (**Figure 64 Aii, Bii**), in which the NP groups didn't have metastatic signal appear until around ~25 days after the primary tumor removal compared to the ~20 days of the saline group. Lastly, all the NP treatments had a fraction of mice that did not form any lung metastases by the end of schedule 1. With schedule 2, only the antibody-loaded NPs had any prevention of metastatic spread. Again, it is difficult to directly compare the two schedules, but from these results, it seems to be important to remove the primary at an earlier stage and start NP treatment to help prevent metastases.

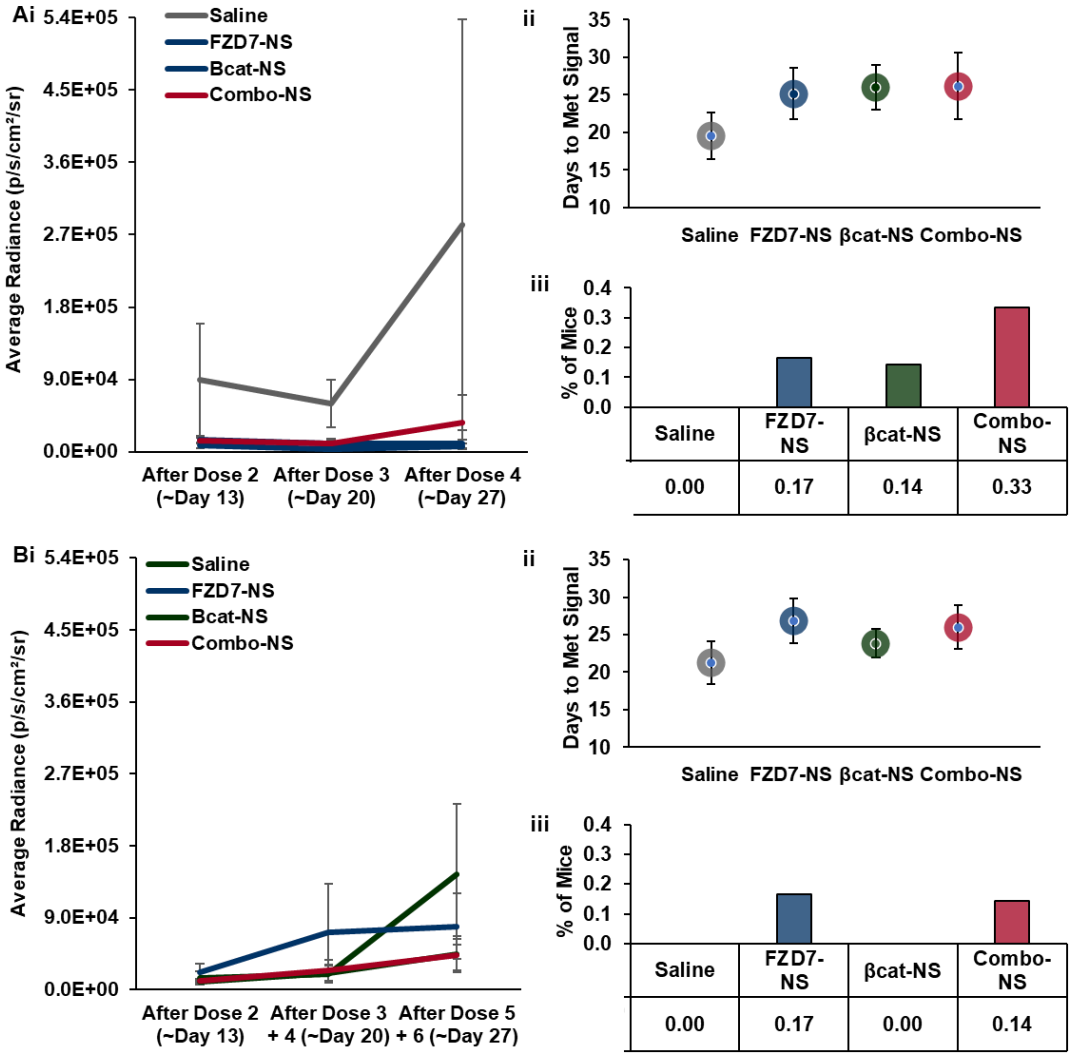

Figure 64. Lung Metastatic Analysis *via* IVIS Imaging. Comparison of treatment (**A**) schedule 1 and (**B**) schedule 2 with (**i**) average radiance taken, (**ii**) days until lung metastases signal appears, and (**iii**) percentage of mice that did not form metastasis by the end of the study. n = 6 – 7.

5.3.7 Biodistribution Quantification of Gold Content

Biodistribution of the gold NPs were assess *via* ICP-MS as described in **Chapter 5.2.9.** As expected, the antibody-loaded NPs facilitated increased delivery of

NPs to the primary (1°) tumors (**Figure 65A**). At the end of the studies, overall gold content was analyzed in all major organs. In the lungs, schedule 2 dosage accumulated more corresponding NPs than in schedule 1, except for Combo-NS (**Figure 65B**). While in the recurrent (2°) tumors, schedule 2 dosage accumulated more NPs than in schedule 1. Additionally, there was more biodistribution of the antibody-loaded NPs to the recurrent tumors compared to βcat-NS by at least 2X or more.

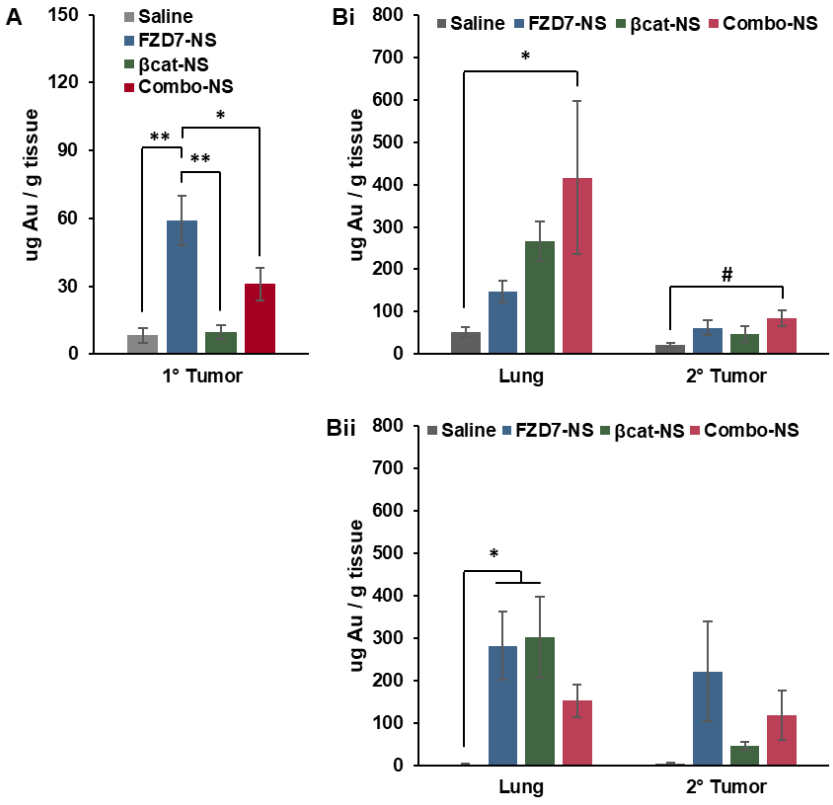

Figure 65. ICP-MS Quantification of Gold Content in Tumors and Metastatic Organs. (**A**) Primary Tumor (**B**) Lungs and Recurrent Tumors of treatment (**i**) schedule 1 and (**ii**) schedule 2. #p<0.1, *p<0.05, **p<0.01 by one-way ANOVA with posthoc Tukey. n = 12 – 14 (primary tumor) ; 6 – 7 (lungs and secondary tumor).

As expected between schedules 1 and 2, the clearance organs had increased accumulation of NPs from schedule 2, which had 6 total injections versus 5 from schedule 1 (**Figure 66**). Accumulation of all other organs were minimal compared to the clearance organs and relevant disease inflicted organs and tissues (**Figure 67**). Surprisingly, the small intestine had higher NP accumulation that the other organs (blood, heart, kidney, brain). Since historically, gold NPs, such as gold nanoshell conjugates have low excretion following NP administration there are many concerns about long-term effects despite gold being classified as bioinert and showing biocompatibility in clinical trials.[119,162] Distribution to the intestine, shows that these NPs may have the potential of being excreted and further studies should evaluate the removal of NPs outside of the desired disease target.

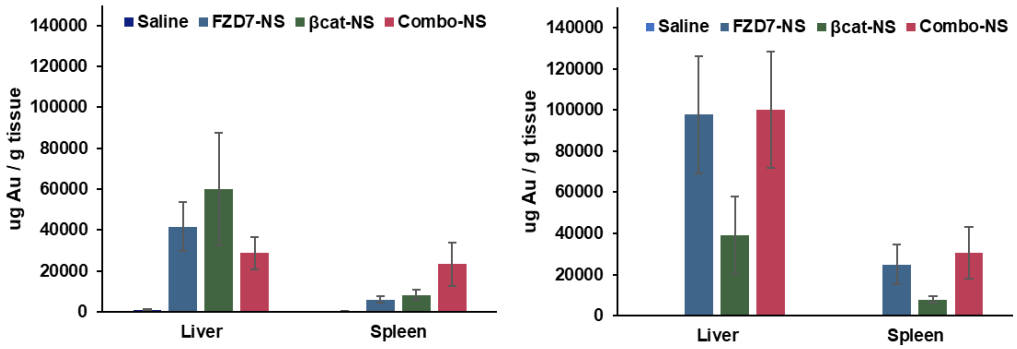

Figure 66. ICP-MS Quantification of Gold Content in Clearance Organs Liver and Spleen. Treatment (**A**) schedule 1and (**B**) schedule 2.

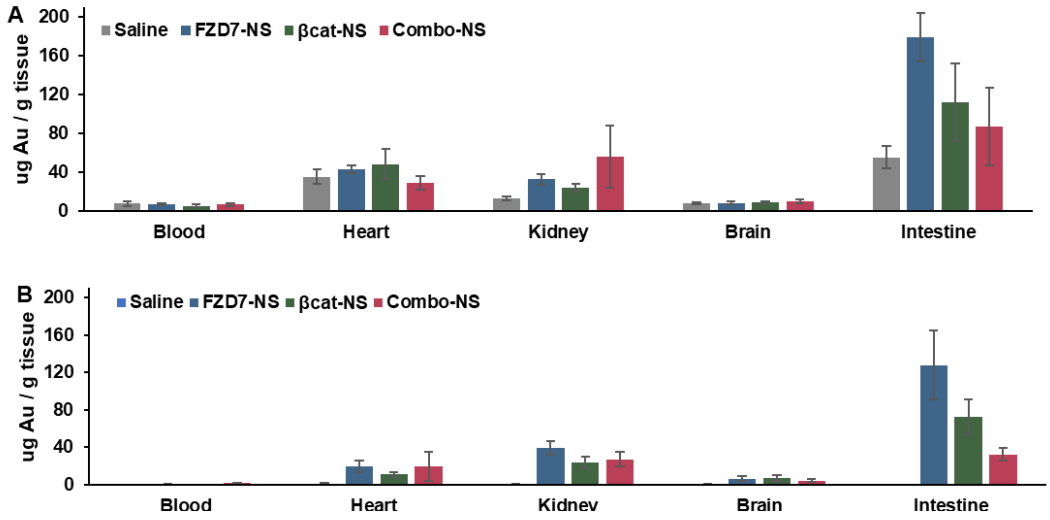

Figure 67. ICP-MS Quantification of Gold Content in Other Remaining Organs. Treatment (**A**) schedule 1and (B) schedule 2. n = 6 – 7.

In evaluating increase biodistribution of antibody-loaded NPs to the primary and recurrent tumors, we performed qPCR-RT analysis for β-catenin mRNA expression levels in the excised tumor samples as described in **Chapter 5.2.10.** Interestingly, it seems like the NP's down regulated β-catenin mRNA expression levels to some extend for both tumor types compared to the saline group (**Figure 68**). However, the knockdown does not correlate with the tumor growth progression data from above. Further evaluation of the gene knockdown would need to be done, such as sorting the 4T1 cell population from the tumor microenvironment and evaluating β-catenin mRNA on the separated cells *via* flow cytometry. Additionally, other downstream Wnt target genes, such as Axin2, CCND1, or C-myc could be assessed.

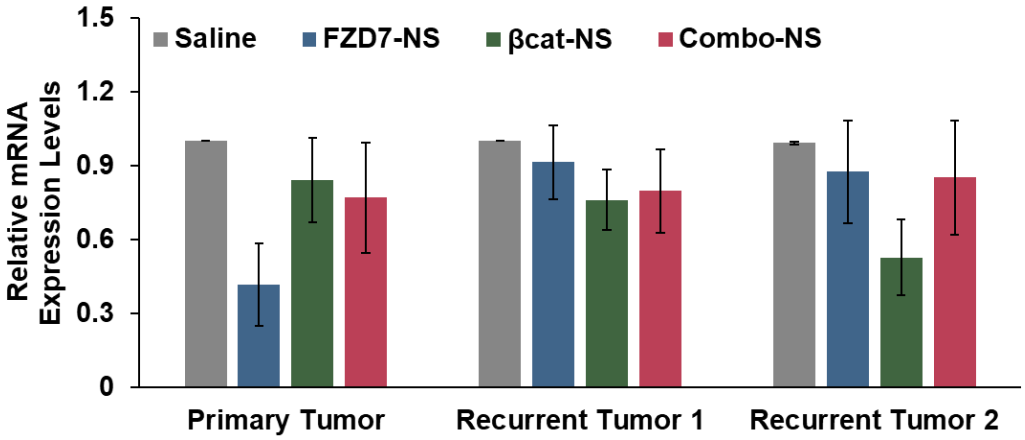

Figure 68. qPCR-RT Analysis of β-catenin mRNA Expression Levels in Excised Tumors. Assessment of β-catenin mRNA expression levels in excised primary tumors on day 14 and recurrent tumors at the end of the study. n = 6 – 7.

5.4 Conclusions

Here we used FZD7 antibodies and β-catenin siRNA which were co-loaded onto gold NS for treatment of TNBC through suppressing the Wnt signaling pathway in murine cell lines. We validated the ability to target FZD7 receptors and downregulation β-catenin mRNA levels in 4T1 cells. Following confirmation to move forward with the NP synthesis in murine cells line, we wanted to show inhibition of cell functionality before moving forward into *in vivo* studies, which was done by evaluating the impact on cell proliferation after NP treatment. We found similar results when the system was used for human TNBC cells, in which the antibody loaded NPs reduced cell proliferation earlier timepoints, but the NP effect lessened up over time. Meanwhile the dual delivery system, Combo-NS, was able to sustain the proliferation inhibition some more, albeit to a lesser extent. With these results, we started designing treatment schedules for the treatment of spontaneous lung metastatic murine models. This required thorough replication of tumor progression and metastatic growth. After

establishing the expected tumor growth and metastatic spread, we evaluated the impact of Wnt inhibitory NPs through two treatment schedules. From these studies ,we found that the NPs overall, were able to impede primary, recurrent, and metastatic tumor growth. Most excitingly, Combo-NS and FZD7-NS were capable of prevent the appearance of lungs metastases in a fraction of the studies. However, there don’t seem to be drastic difference between the two treatment regimens, in which more studies need to be done to future understand the therapeutic potential.

Chapter 6

CONCLUSIONS AND FUTURE DIRECTIONS

6.1 Introduction

This dissertation focused on the development of utilizing gold NPs, specifically gold NS, to enable NP-mediated delivery of antibodies and/or RNA for gene regulation in TNBC. First, a novel application of applying a nanosecond laser light for on-demand release of a functional miRNA for gene regulation of TNBC *in vitro*. Furthermore, the experiments involved comparing the release and impact of delivered miR-34a when released by continuous versus pulse irradiation. Second, we developed a thoroughly characterized platform that focuses on antibody-coated NS for targeted co-delivery of siRNA therapeutics. This co-delivery platform was designed to first demonstrate how multivalent NP binding can increase cellular update and secondly influence oncogenic cell signaling at multiple levels extracellularly and intracellularly *in vitro*. Lastly, the therapeutic potential of the 2nd platform was transitioned *in vivo* to evaluate its impact on a well characterized spontaneous lung metastasis murine model in immunocompetent mice. We demonstrated that the Wnt inhibitory NPs were able to reduce primary tumor growth, which extended slightly regarding tumor regrowth. While metastatic spread was not all together prevented, the Wnt inhibitory NPs were able to slow down metastatic spread and prevent metastasis to a fraction of the cohort.

Here, each chapter will be briefly recapped, and the significance, innovation, and impact of the research will be explained. This is followed by an overview of multiple approaches for the future development of these projects.

6.2 Overview of the Work Presented

In **Chapter 3**, miRNA NS conjugates were introduced as the primary therapeutic NP. Delivery of exogenous miRNA have tremendous potential in regulating under expressed gene levels. However, they are limited by a considerable number of limitations making it difficult to deliver naked miRNA and translated it towards clinical work. NP systems offer many solutions to the limitations, including early clearance, inability to cross vessel walls or being internalized in cells, encapsulation in endosomes. Even with this in mind, any miRNA tethered to or encapsulated in NPs will need a means of release mechanism. Gold NS provide photoreactive properties in which the base NP can be activated *via* light to release conjugated biomolecules. To create a precise on demand release system solely focused on delivery the miRNA, laser parameters were carefully tuned in turns of power density and duration, along with comparing the modes of irradiation, including continuous wave and pulsed. Mostly excitingly, the laser used in this application was a nanosecond laser, while is not as strong as the traditionally used femtosecond laser, had the potential to be maximized for proper RNA release. The light-triggered release platform was characterized for heating profiles and the released miRNA was examined for maintenance of structure and ability to function even after being irradiated. Here we found that through applying pulsed light irradiation onto the miRNA conjugates, the NPs had lower heating profiles, released miRNA maintained duplex structure and functionality, miR-34a miRNA expression was recovered with release from pulsed

irradiation to a greater extent than CW, and miR-34a/NS treated cells that were irradiated were able to suppress metabolic activity, cell proliferation, and migration.

In **Chapters 4 & 5,** antibody targeted co-loaded siRNA NS conjugates were introduced as the primary therapeutic NP. Similarly, to miRNA, siRNA delivery is limited by the same biological barriers. Nanocarriers have advantageous characteristics that make it easier for them to act as carriers for therapeutics such as siRNA and other nucleic acids. In designing a NP platform for co-delivery of different vastly different biomolecule, gold NS are inert for multiple reasons being they are bioinert, scalable, photoreactive, and most importantly in the context of this application they have high ease of bioconjugation. Gold chemistry is very simple and for this reason, scientists historical use gold to covalently link any type of biomolecule using any linker with a disulfide or thiol end group. In developing this co-delivery platform, it was important to tuning the loading of biomolecules to have precise concentration of molecules per NS across each of the control NPs. To do so, we adjusted a whole range of parameters including molecule addition order, salt aging, and mPEG concentration to ensure equal loading of antibody and siRNA of the Combo-NS to the corresponding nontherapeutic NP. After thorough characterization of the NP formulations, we moved forward with assessing the binding capacity of the Wnt inhibitory NPs against their antibody or siRNA only NP counterparts. We found that the antibody-loaded NPs were more efficient in binding to the target cells lines. Consequently, we next evaluated the ability of the NPs to reduce mRNA expression levels of relevant Wnt genes, in which we found that Combo-NS was able to outperform gene knockdown in comparison to the FZD7-NS and βcat-NS, but unfortunately not to a synergistic extent. Cell functionality was then assessed

following NP treatment in which we found that cells required longer incubation times for the effects of the gene regulation to initiate, reducing cell proliferation, mitigating number of migration cells, and influencing the morphology of spheroid formation. With promising *in vitro* results, the NP system was applied *in vivo* on a spontaneous lung metastatic model, in which a primary tumor was inoculated, removed, and then regrowth and metastatic spread ensues. The Wnt inhibitory NPs showed good promise in reducing the primary tumor growth. In terms of recurrent growth and metastatic spread, the NPs were able to slow down the progression of both slightly, but more work needs to be conducted to tease out a great impact from the NP treatment.

6.3 Future Directions

This work introduces utilizing gold NS to provide photoreactive therapy along with facile methods of bioconjugation to control the density and loading of biomolecules onto the NP surface. Specifically, the clinical use of a ns-pulse NIR laser for on-demand miRNA release for gene regulation of TNBC *in vitro*. The Wnt signaling pathway was targeted by designing a nanocarrier platform that would both target and impact the internal RNAi machinery to suppress Wnt signaling in a multi-level approach. Thorough characterization of dual biomolecule was performed, followed with assessment of specific cancer characteristics that contribute to the hallmarks of cancer including proliferation, migration, and self-renewal stemness behaviors *in vitro*. The nanocarrier platform for Wnt signaling was transitioned *in vivo* where we evaluated the impact the NP treatment on a spontaneous lung metastatic model. This required careful assessment of primary tumor inoculation, excision of primary tumor at the right timing, and monitoring of metastatic spread. This allowed us to more precisely design a therapeutic schedule that would be able to reduce

primary tumor growth along with reduce, and ideally, prevent metastasis spread. Future studies for improvement of these precise delivery platforms are to combine the gene therapeutics with other photoresponsive therapies, transition the light-triggered release platform *in vivo*, recharacterize the minimum number of antibody and siRNA required for therapeutic efficacy, and evaluate the NPs in various different tumor models including an experimental lung metastasis model or a rechallenged tumor model.

In short, the work presented in this dissertation provides a basis for further development on photoresponsive NP therapies along with targeted delivery of gene therapeutics in any cancers that either need (1) precise, localized treatment provided by on demand light-triggered release or (2) are dysregulated by the Wnt signaling pathway in which FZD7 antibodies offers an alternative mechanism to suppress.

6.3.1 Maximizing the Light-Triggered Release of miRNA from Nanoshells

Overall, these studies demonstrate miR-34a/NS can enable light-triggered gene regulation using a clinically relevant ns-pulsed laser for impairment of TNBC function, specifically in regard to metabolic activity, cell proliferation, and migration. These conjugates offer precise control over miRNA delivery, which overcomes the lack of specificity of other nanocarrier systems. However, with any platform there is always room for improvement. While the miR-34/NS + laser showed promising results, the miR-34/NS did have some effect on cells in absence of laser irradiation, which suggests either some cargo is released from the NS in intracellular environment or that RISC is interacting with the miRNA while it remains tethered to the NS. Studies revolving cell trafficking would help answer some of these questions. Fluorescently labeled probes for tracking of intracellular sorting organelles, such as

early endosomes, late endosomes, lysosomes, or recycling lysosomes, can be used to visualize where the miR-34a/NS are prior to irradiation and their pathway of mechanism following irradiation. Due to NS photoluminescence, live imaging could be done in parallel to the initial light-triggered release. In additional, it has been assumed that the NPs are being released from endosomes upon irradiation, which has been seen in literature. It would be interesting to reoptimize the laser conditions down from 0.1 W/cm^2 and evaluate how low of a power density is required to initiate endosomal escape. On the flip side, studies could evaluate how much can the power density increase while decreasing the irradiation duration from 10 minutes without causing additional heating effects to focus on the gene regulation aspect of this platform. Another direction this platform can be carried is repeated release of miRNA. As with all RNA therapeutics, miRNA transfection is transient. When cancer cells start to proliferate the effects of miRNA is diluted out over time. However, with this platform we showed about a ~20% release of miR-34a from the NPs after a 10 minute irradiation. Since the NPs are oversaturated with miRNA, it would be interesting to induce multiple rounds of miRNA release to provide replacement therapy of miRNA mimics when the transient effect is depleted. With the current laser conditions and overall set up, the maximal effect occurs at 72 hours post irradiation. Another round of irradiation could be conducted at the 72-hour timepoint for evaluation after an additional incubation period. Additionally, the laser parameters can be optimized to realize more than 20% of miRNA upon irradiation. These studies went up to 0.4W/cm^2 for 10 minutes, however there is some buffer space to try irradiating at higher power densities for a shorter time duration. Lastly, transitioning this platform *in vivo* would offer a new arsenal to combat TNBC, and other cancers characterized by

the loss of miR-34a. Murine models such as nu/nu would be an initial starting point, with transitioning to Balb/C models to incorporate a functioning immune response. In addition to the murine strain, dual sided tumor models, either subcutaneous or in the mammary fat pad, would be advantageous to compare no laser to laser treatments within an individual mouse. Preclinical success would be considered will full reduction or remission of tumor volumes following laser irradiation. The likelihood of translation depends not only on the therapeutic effect, but the toxicity of the delivered NPs, and laser conditions that are safe for user and patients. Additionally, Following this, the platform has many aspects that would be it primed for such as transition. The ns pulse laser from LiteCure is already a clinical available instrument being activating used, albeit for other purposes. Gold NS have made huge progress in the past decade and have been proven safe in some clinical trials. There are ongoing trials for photothermal therapies involving bare NS. And with seeing the global effects of RNA therapeutics, due to the COVID-19 vaccine, gene therapy is at the cusp of many successes to come, as more researchers pool together to work towards common goals and using similar technological designs.

6.3.2 Understanding the Impact of Wnt Inhibitory NPs in Multiple Murine Models

Overall, these studies demonstrate dual FZD7 antibody and β-catenin siRNA NS can enable gene regulation for impairment of TNBC function through the binding of FZD7 receptors and repression of Wnt signaling. To follow up on the studies evaluating the impact of these NPs on human MDA-MB-231 cells, there is a huge opportunity to transition *in vivo*. A pilot study from the lab evaluated the ability of Combo-NS to reduce metastatic burden in an experimental lung metastasis model in

nude immunocompromised mice. A study with a larger sample size (12 – 14 mice per treatment group) should be performed to support statistical analysis of biodistribution and IVIS data that showed increased antibody-loaded NP accumulation in the lungs, along with a reduction in lung metastatic signal for the Combo-NS treated mice. Further work should also evaluate the ideal antibody loading necessary for efficient NP binding and uptake, which could be done in a shorter biodistribution murine study. Studies from the Auguste Lab[109] have carefully functionalized their liposomes with a precise peptide density which resulted in higher cancer cell uptake that other formations. The density was determined from the complementing cell membrane expression to maximize the targeting cell, but not oversaturate the signaling cascade. Similar studies can be done with this platform by evaluating NP density at higher and lower concentrations impact on cellular binding *via* microscopy, or uptake *via* flow, or as mentioned briefly in a biodistribution study evaluating the different NP uptake based on the density of antibodies coating the NPs. Lastly, in the same mindset of redesigning the NP presentation, our current work uses non-directionally presented antibodies. The NPs can be redesigned with directionally oriented antibodies to help facilitate more direct receptor binding. Like the RNA therapeutics realm, targeted therapeutics is also of high interested in the nanomedicine. Regarding breast cancer, there are multiple HER2+ targeted therapies, many of which use monoclonal antibodies. TNBC has one antibody-drug conjugate available on the market, which leaves much room for other therapeutics make it through the pipeline.

To follow up on the studies evaluating the impact of these NPs on murine 4T1 cells, there is much that could be fleshed out in the context of the project along with next step experiment designs. In the scope of this dissertation, β-catenin mRNA

expression levels were evaluated in primary and recurrent tumors. However, this was done on the bulk of the tumor mass, including all the unrelated cells incorporated in the tumor microenvironment. While there was mRNA knockdown from the NP treatment groups, the data did not corroborate with the trends seen in the tumor growth and metastatic spread. β-catenin expression levels could be evaluated *via* flow cytometry or other downstream Wnt genes, such as Axin2 or C-myc, could be evaluated for knockdown. In addition to, this the lung nodules from the metastatic spread could be incorporated in the gene expression analysis of either β-catenin or any other relevant Wnt genes. Another study that would focus on preventing metastatic growth, it is evaluating how early should the NP treatment start and at what minimum size should the primary tumor be removed for maximum effect from the delivered NPs. For example, in the context of this dissertation, tumors were predicted to grow to ~200 mm^3 in volume and would be surgically removed. Prior to the removal, the mice received 2 rounds of injections. The cut off for the primary tumor could be smaller and have an impact on decreasing the aggressive characteristics that contribute to metastasis. Especially if this is done in parallel with these antibodies loaded NPs. Additionally, the dose frequency could be increased to maximize the dose schedule designed to prevent metastasis spread, but on the flip side the recurrent tumors still grew back rather quickly. Another study could focus solely on the treatment of the solid orthotopic tumors. We already saw that within 2 rounds of NP injections, the tumors were regressing in size. The dose frequency could be increased from weekly to biweekly to deliver siRNA as it starts to get diluted due to the transient delivery and aggressive proliferation of TNBC cells.

REFERENCES

1. Dai X, Gakidou E, Lopez AD. Evolution of the global smoking epidemic over the past half century: strengthening the evidence base for policy action. *Tob Control*. 2022;31(2):129-137. doi:10.1136/TOBACCOCONTROL-2021-056535
2. Siegel RL, Miller KD, Fuchs HE, Jemal A. Cancer statistics, 2022. *CA Cancer J Clin*. 2022;72(1):7-33. doi:10.3322/CAAC.21708
3. Cancer Facts & Figures 2022| American Cancer Society. Accessed July 7, 2022. https://www.cancer.org/research/cancer-facts-statistics/all-cancer-facts-figures/cancer-facts-figures-2022.html
4. Worldwide cancer data | World Cancer Research Fund International. Accessed July 7, 2022. https://www.wcrf.org/cancer-trends/worldwide-cancer-data/
5. Valcourt DM, Harris J, Riley RS, Dang M, Wang J, Day ES. Advances in targeted nanotherapeutics: From bioconjugation to biomimicry. *Nano Res*. 2018;11(10):4999-5016. doi:10.1007/s12274-018-2083-z
6. Kapadia CH, Luo B, Dang MN, Irvin-Choy N, Valcourt DM, Day ES. Polymer nanocarriers for MicroRNA delivery. *J Appl Polym Sci*. Published online November 12, 2019:48651. doi:10.1002/app.48651
7. Valcourt DM, Dang MN, Wang J, Day ES. Nanoparticles for Manipulation of the Developmental Wnt, Hedgehog, and Notch Signaling Pathways in Cancer. *Ann Biomed Eng*. Published online 2019. doi:10.1007/s10439-019-02399-7
8. Dang MN, Hoover EC, Scully MA, Sterin EH, Day ES. Antibody nanocarriers for cancer management. *Curr Opin Biomed Eng*. 2021;19:100295. doi:10.1016/J.COBME.2021.100295
9. What Is Cancer? - NCI. Accessed July 7, 2022. https://www.cancer.gov/about-cancer/understanding/what-is-cancer
10. Home | American Cancer Society - Cancer Facts & Statistics. Accessed July 7, 2022. https://cancerstatisticscenter.cancer.org/#!/
11. Cancer. Accessed July 7, 2022. https://www.who.int/news-room/fact-sheets/detail/cancer
12. Guan X. Cancer metastases: challenges and opportunities. *Acta Pharm Sin B*. 2015;5(5):402-418. doi:10.1016/J.APSB.2015.07.005
13. Triple-Negative Breast Cancer | CDC. Accessed July 7, 2022. https://www.cdc.gov/cancer/breast/triple-negative.htm
14. Triple-Negative Breast Cancer | Johns Hopkins Medicine. Accessed July 7, 2022. https://www.hopkinsmedicine.org/health/conditions-and-diseases/breast-cancer/triple-negative-breast-cancer

15. Triple-negative Breast Cancer | Details, Diagnosis, and Signs. Accessed July 7, 2022. https://www.cancer.org/cancer/breast-cancer/about/types-of-breast-cancer/triple-negative.html
16. Scott LC, Mobley LR, Kuo TM, Il'yasova D. Update on Triple Negative Breast Cancer Disparities for the United States – A Population Based Study from the United States Cancer Statistics database, 2010-2014. *Cancer*. 2019;125(19):3412. doi:10.1002/CNCR.32207
17. Female Breast Cancer Subtypes — Cancer Stat Facts. Accessed July 7, 2022. https://seer.cancer.gov/statfacts/html/breast-subtypes.html
18. Bianchini G, Balko JM, Mayer IA, Sanders ME, Gianni L. Triple-negative breast cancer: Challenges and opportunities of a heterogeneous disease. *Nat Rev Clin Oncol*. 2016;13(11):674-690. doi:10.1038/nrclinonc.2016.66
19. Hanahan D, Weinberg RA. The Hallmarks of Cancer. *Cell*. 2000;100(1):57-70. doi:10.1016/S0092-8674(00)81683-9
20. Hanahan D, Weinberg RA. Hallmarks of cancer: the next generation. *Cell*. 2011;144(5):646-674. doi:10.1016/J.CELL.2011.02.013
21. Zhong Z, Yu J, Virshup DM, Madan B. Wnts and the hallmarks of cancer. *Cancer and Metastasis Reviews 2020 39:3*. 2020;39(3):625-645. doi:10.1007/S10555-020-09887-6
22. Bommer GT, Gerin I, Feng Y, et al. p53-mediated activation of miRNA34 candidate tumor-suppressor genes. *Curr Biol*. 2007;17(15):1298-1307. doi:10.1016/J.CUB.2007.06.068
23. Clevers H, Nusse R. Wnt/β-catenin signaling and disease. *Cell*. 2012;149(6):1192-1205. doi:10.1016/j.cell.2012.05.012
24. Clevers H. Wnt/β-Catenin Signaling in Development and Disease. *Cell*. 2006;127(3):469-480. doi:10.1016/j.cell.2006.10.018
25. King TD, Zhang W, Suto MJ, Li Y. Frizzled7 as an emerging target for cancer therapy. *Cell Signal*. 2012;24(4):846-851. doi:10.1016/j.cellsig.2011.12.009
26. Slabáková E, Culig Z, Remšík J, Souček K. Alternative mechanisms of miR-34a regulation in cancer. *Cell Death Dis*. 2017;8(10):e3100. doi:10.1038/cddis.2017.495
27. Neophytou C, Boutsikos P, Papageorgis P. Molecular mechanisms and emerging therapeutic targets of triple-negative breast cancer metastasis. *Front Oncol*. 2018;8(FEB):31. doi:10.3389/FONC.2018.00031/BIBTEX
28. Jang GB, Kim JY, Cho SD, et al. Blockade of Wnt/β-catenin signaling suppresses breast cancer metastasis by inhibiting CSC-like phenotype. *Scientific Reports 2015 5:1*. 2015;5(1):1-15. doi:10.1038/srep12465
29. King TD, Suto MJ, Li Y. The Wnt/β-catenin signaling pathway: a potential therapeutic target in the treatment of triple negative breast cancer. *J Cell Biochem*. 2012;113(1):13-18. doi:10.1002/JCB.23350
30. Peng F, Setyawati MI, Tee JK, et al. Nanoparticles promote in vivo breast cancer cell intravasation and extravasation by inducing endothelial leakiness.

Nature Nanotechnology 2019 14:3. 2019;14(3):279-286. doi:10.1038/s41565-018-0356-z
31. Collignon J, Lousberg L, Schroeder H, Jerusalem G. Triple-negative breast cancer: treatment challenges and solutions. *Breast Cancer (Dove Med Press)*. 2016;8:93-107. doi:10.2147/BCTT.S69488
32. Anders C, Carey LA. Understanding and treating triple-negative breast cancer. *Oncology (Williston Park)*. 2008;22(11):1233-1239; discussion 1239-40, 1243. Accessed July 28, 2018. http://www.ncbi.nlm.nih.gov/pubmed/18980022
33. Matsumura Y, Maeda H. A New Concept for Macromolecular Therapeutics in Cancer Chemotherapy: Mechanism of Tumoritropic Accumulation of Proteins and the Antitumor Agent Smancs. *Cancer Res*. 1986;46(8):6387-6392.
34. Appelbe OK, Moynihan KD, Flor A, Rymut N, Irvine DJ, Kron SJ. Radiation-enhanced delivery of systemically administered amphiphilic-CpG oligodeoxynucleotide. *Journal of Controlled Release*. 2017;266:248-255. doi:10.1016/J.JCONREL.2017.09.043
35. Klinman DM, Shirota H. Vaccine Adjuvants. In: *Inflammation - From Molecular and Cellular Mechanisms to the Clinic*. Wiley-VCH Verlag GmbH & Co. KGaA; 2017:143-174. doi:10.1002/9783527692156.ch7
36. Nab-paclitaxel in Metastatic Breast Cancer Patients Failing Solvent Based Taxane (Tiffany) - Full Text View - ClinicalTrials.gov. Accessed November 16, 2019. https://clinicaltrials.gov/ct2/show/NCT01416558?term=nano&recrs=h&draw=1&rank=6
37. Neyt M. Cost considerations for monoclonal antibody-targeted therapy in cancer: Focus on trastuzumab. *American Journal of Cancer*. 2006;5(1):19-26. doi:10.2165/00024669-200605010-00003
38. Kulhari H, Pooja D, Shrivastava S, et al. Trastuzumab-grafted PAMAM dendrimers for the selective delivery of anticancer drugs to HER2-positive breast cancer. *Sci Rep*. 2016;6(1):23179. doi:10.1038/srep23179
39. Bardia A, Hurvitz SA, Tolaney SM, et al. Sacituzumab Govitecan in Metastatic Triple-Negative Breast Cancer. *New England Journal of Medicine*. 2021;384(16):1529-1541. doi:10.1056/NEJMOA2028485/SUPPL_FILE/NEJMOA2028485_DATA-SHARING.PDF
40. Sharma P, Retz M, Siefker-Radtke A, et al. Nivolumab in metastatic urothelial carcinoma after platinum therapy (CheckMate 275): a multicentre, single-arm, phase 2 trial. *Lancet Oncol*. 2017;18(3):312-322. doi:10.1016/S1470-2045(17)30065-7
41. Rupaimoole R, Slack FJ. MicroRNA therapeutics: towards a new era for the management of cancer and other diseases. *Nature Reviews Drug Discovery 2017 16:3*. 2017;16(3):203-222. doi:10.1038/nrd.2016.246

42. He L, Hannon GJ. MicroRNAs: small RNAs with a big role in gene regulation. *Nature Reviews Genetics 2004 5:7*. 2004;5(7):522-531. doi:10.1038/nrg1379
43. MacFarlane LA, Murphy PR. MicroRNA: Biogenesis, Function and Role in Cancer. *Curr Genomics*. 2010;11(7):537. doi:10.2174/138920210793175895
44. Kim VN. MicroRNA biogenesis: coordinated cropping and dicing. *Nature Reviews Molecular Cell Biology 2005 6:5*. 2005;6(5):376-385. doi:10.1038/nrm1644
45. Nakielny S, Dreyfuss G. Transport of proteins and RNAs in and out of the nucleus. *Cell*. 1999;99(7):677-690. doi:10.1016/S0092-8674(00)81666-9
46. Murchison EP, Hannon GJ. miRNAs on the move: miRNA biogenesis and the RNAi machinery. *Curr Opin Cell Biol*. 2004;16(3):223-229. doi:10.1016/J.CEB.2004.04.003
47. Corney DC, Flesken-Nikitin A, Godwin AK, Wang W, Nikitin AY. MicroRNA-34b and MicroRNA-34c are targets of p53 and cooperate in control of cell proliferation and adhesion-independent growth. *Cancer Res*. 2007;67(18):8433-8438. doi:10.1158/0008-5472.CAN-07-1585
48. Chang TC, Wentzel EA, Kent OA, et al. Transactivation of miR-34a by p53 broadly influences gene expression and promotes apoptosis. *Mol Cell*. 2007;26(5):745-752. doi:10.1016/J.MOLCEL.2007.05.010
49. Lodygin D, Tarasov V, Epanchintsev A, et al. Inactivation of miR-34a by aberrant CpG methylation in multiple types of cancer. *Cell Cycle*. 2008;7(16):2591-2600. doi:10.4161/cc.7.16.6533
50. Imani S, Wu RC, Fu J. MicroRNA-34 family in breast cancer: From research to therapeutic potential. *J Cancer*. 2018;9(20):3765-3775. doi:10.7150/jca.25576
51. Zhang L, Liao Y, Tang L. MicroRNA-34 family: A potential tumor suppressor and therapeutic candidate in cancer. *Journal of Experimental and Clinical Cancer Research*. 2019;38(1). doi:10.1186/s13046-019-1059-5
52. Hong DS, Kang YK, Borad M, et al. Phase 1 study of MRX34, a liposomal miR-34a mimic, in patients with advanced solid tumours. *British Journal of Cancer 2020 122:11*. 2020;122(11):1630-1637. doi:10.1038/s41416-020-0802-1
53. Polakis P. Wnt signaling in cancer. *Cold Spring Harb Perspect Biol*. 2012;4(5):9. doi:10.1101/cshperspect.a008052
54. Lustig B, Jerchow B, Sachs M, et al. Negative feedback loop of Wnt signaling through upregulation of conductin/axin2 in colorectal and liver tumors. *Mol Cell Biol*. 2002;22(4):1184-1193. doi:10.1128/mcb.22.4.1184-1193.2002
55. Moore KN, Gunderson CC, Sabbatini P, et al. A phase 1b dose escalation study of ipafricept (OMP54F28) in combination with paclitaxel and carboplatin in patients with recurrent platinum-sensitive ovarian cancer. *Gynecol Oncol*. 2019;154(2):294-301. doi:10.1016/J.YGYNO.2019.04.001

56. Jimeno A, Gordon M, Chugh R, et al. A First-in-Human Phase I Study of the Anticancer Stem Cell Agent Ipafricept (OMP-54F28), a Decoy Receptor for Wnt Ligands, in Patients with Advanced Solid Tumors. *Clin Cancer Res*. 2017;23(24):7490-7497. doi:10.1158/1078-0432.CCR-17-2157
57. Riley RS, Day ES. Frizzled7 Antibody-Functionalized Nanoshells Enable Multivalent Binding for Wnt Signaling Inhibition in Triple Negative Breast Cancer Cells. *Small*. 2017;13(26):1700544. doi:10.1002/smll.201700544
58. Hartshorn CM, Bradbury MS, Lanza GM, et al. Nanotechnology Strategies to Advance Outcomes in Clinical Cancer Care. *ACS Nano*. 2018;12(1):24-43. doi:10.1021/ACSNANO.7B05108/ASSET/IMAGES/LARGE/NN-2017-051084_0008.JPEG
59. Siamof CM, Goel S, Cai W. Moving Beyond the Pillars of Cancer Treatment: Perspectives From Nanotechnology. *Front Chem*. 2020;8:1088. doi:10.3389/FCHEM.2020.598100/XML/NLM
60. Cancer Nanotechnology Plan - NCI. Accessed August 29, 2022. https://www.cancer.gov/nano/research/plan
61. Hartshorn CM, Bradbury MS, Lanza GM, et al. Nanotechnology Strategies to Advance Outcomes in Clinical Cancer Care. *ACS Nano*. 2018;12(1):24. doi:10.1021/ACSNANO.7B05108
62. Kemp JA, Kwon YJ. Cancer nanotechnology: current status and perspectives. *Nano Convergence 2021 8:1*. 2021;8(1):1-38. doi:10.1186/S40580-021-00282-7
63. Cheng Z, Li M, Dey R, Chen Y. Nanomaterials for cancer therapy: current progress and perspectives. *Journal of Hematology & Oncology 2021 14:1*. 2021;14(1):1-27. doi:10.1186/S13045-021-01096-0
64. Azevedo C, Macedo MH, Sarmento B. Strategies for the enhanced intracellular delivery of nanomaterials. *Drug Discov Today*. 2018;23(5):944-959. doi:10.1016/j.drudis.2017.08.011
65. Bourquin J, Milosevic A, Hauser D, et al. Biodistribution, Clearance, and Long-Term Fate of Clinically Relevant Nanomaterials. *Advanced Materials*. 2018;30(19). doi:10.1002/adma.201704307
66. Walkey CD, Chan WCW. Understanding and controlling the interaction of nanomaterials with proteins in a physiological environment. *Chem Soc Rev*. 2012;41(7):2780-2799. doi:10.1039/c1cs15233e
67. Brody EN, Gold L. Aptamers as therapeutic and diagnostic agents. *Reviews in Molecular Biotechnology*. 2000;74(1):5-13. doi:10.1016/S1389-0352(99)00004-5
68. Tang Q, Ouyang H, He D, Yu C, Tang G. MicroRNA-based potential diagnostic, prognostic and therapeutic applications in triple-negative breast cancer. *Artif Cells Nanomed Biotechnol*. 2019;47(1):2800-2809. doi:10.1080/21691401.2019.1638791
69. Chakraborty A, Boer JC, Selomulya C, Plebanski M. Amino Acid Functionalized Inorganic Nanoparticles as Cutting-Edge Therapeutic and

Diagnostic Agents. *Bioconjug Chem*. 2018;29(3):657-671. doi:10.1021/acs.bioconjchem.7b00455
70. Grodzinski P, Silver M, Molnar LK. Nanotechnology for cancer diagnostics: promises and challenges. *http://dx.doi.org/101586/1473715963307*. 2014;6(3):307-318. doi:10.1586/14737159.6.3.307
71. Liang C, Wang C, Liu Z, Liang C, Wang C, Liu Z. Stem Cell Labeling and Tracking with Nanoparticles. *Particle & Particle Systems Characterization*. 2013;30(12):1006-1017. doi:10.1002/PPSC.201300199
72. Wang Y, Xu C, Ow H. Commercial Nanoparticles for Stem Cell Labeling and Tracking. *Theranostics*. 2013;3(8):544. doi:10.7150/THNO.5634
73. Ferreira L, Karp JM, Nobre L, Langer R. New Opportunities: The Use of Nanotechnologies to Manipulate and Track Stem Cells. *Cell Stem Cell*. 2008;3(2):136-146. doi:10.1016/J.STEM.2008.07.020
74. Masayuki Y, Mizue M, Noriko Y, et al. Polymer micelles as novel drug carrier: Adriamycin-conjugated poly(ethylene glycol)-poly(aspartic acid) block copolymer. *Journal of Controlled Release*. 1990;11(1-3):269-278. doi:10.1016/0168-3659(90)90139-K
75. Makadia HK, Siegel SJ. Poly Lactic-co-Glycolic Acid (PLGA) as biodegradable controlled drug delivery carrier. *Polymers (Basel)*. 2011;3(3):1377-1397. doi:10.3390/polym3031377
76. Tietjen GT, Bracaglia LG, Saltzman WM, Pober JS. Focus on Fundamentals: Achieving Effective Nanoparticle Targeting. *Trends Mol Med*. 2018;24(7):598-606. doi:10.1016/j.molmed.2018.05.003
77. Maeda H. The enhanced permeability and retention (EPR) effect in tumor vasculature: the key role of tumor-selective macromolecular drug targeting. *Adv Enzyme Regul*. 2001;41:189-207. Accessed July 28, 2018. http://www.ncbi.nlm.nih.gov/pubmed/11384745
78. Kim SM, Faix PH, Schnitzer JE. Overcoming key biological barriers to cancer drug delivery and efficacy. *Journal of Controlled Release*. 2017;267:15-30. doi:10.1016/j.jconrel.2017.09.016
79. Greish K. Enhanced Permeability and Retention (EPR) Effect for Anticancer Nanomedicine Drug Targeting. In: *Methods in Molecular Biology (Clifton, N.J.)*. Vol 624. ; 2010:25-37. doi:10.1007/978-1-60761-609-2_3
80. Maeda H. The enhanced permeability and retention (EPR) effect in tumor vasculature: The key role of tumor-selective macromolecular drug targeting. *Adv Enzyme Regul*. 2001;41(1):189-207. doi:10.1016/S0065-2571(00)00013-3
81. Riley RS, Day ES. Gold nanoparticle-mediated photothermal therapy: applications and opportunities for multimodal cancer treatment. *Wiley Interdiscip Rev Nanomed Nanobiotechnol*. 2017;9(4):e1449. doi:10.1002/wnan.1449
82. Sudhakar S, Santhosh PB. Gold Nanomaterials: Recent Advances in Cancer Theranostics. *Advances in Biomembranes and Lipid Self-Assembly*. 2017;25:161-180. doi:10.1016/BS.ABL.2017.01.003

83. Guo J, Rahme K, He Y, Li LL, Holmes JD, O'Driscoll CM. Gold nanoparticles enlighten the future of cancer theranostics. *Int J Nanomedicine*. 2017;12:6131-6152. doi:10.2147/IJN.S140772
84. Riley RS, Day ES. Gold nanoparticle-mediated photothermal therapy: applications and opportunities for multimodal cancer treatment. *Wiley Interdiscip Rev Nanomed Nanobiotechnol*. 2017;9(4):e1449. doi:10.1002/wnan.1449
85. Melamed JR, Riley RS, Valcourt DM, Day ES. Using Gold Nanoparticles to Disrupt the Tumor Microenvironment: An Emerging Therapeutic Strategy. *ACS Nano*. 2016;10(12):10631-10635. doi:10.1021/acsnano.6b07673
86. Morton JG, Day ES, Halas NJ, West JL. Chapter 7 Nanoshells for Photothermal Cancer Therapy. *Cancer Nanotechnology: Methods in Molecular Biology*. Published online 2010:101-117. doi:10.1007/978-1-60761-609-2_7
87. Valcourt DM, Dang MN, Day ES. IR820-loaded PLGA nanoparticles for photothermal therapy of triple-negative breast cancer. *J Biomed Mater Res A*. Published online April 9, 2019:jbm.a.36685. doi:10.1002/jbm.a.36685
88. Wang J, Potocny AM, Rosenthal J, Day ES. Gold Nanoshell-Linear Tetrapyrrole Conjugates for near Infrared-Activated Dual Photodynamic and Photothermal Therapies. *ACS Omega*. 2020;5(1):926-940. doi:10.1021/acsomega.9b04150
89. Weissleder R. A clearer vision for in vivo imaging. *Nature Biotechnology 2001 19:4*. 2001;19(4):316-317. doi:10.1038/86684
90. Lowery AR, Gobin AM, Day ES, Halas NJ, West JL. Immunonanoshells for targeted photothermal ablation of tumor cells. *Int J Nanomedicine*. 2006;1(2):149-154. doi:10.2147/nano.2006.1.2.149
91. Riley RS, Dang MN, Billingsley MM, Abraham B, Gundlach L, Day ES. Evaluating the Mechanisms of Light-Triggered siRNA Release from Nanoshells for Temporal Control Over Gene Regulation. *Nano Lett*. 2018;18(6):3565-3570. doi:10.1021/acs.nanolett.8b00681
92. Kapadia CH, Melamed JR, Day ES. Spherical Nucleic Acid Nanoparticles: Therapeutic Potential. *BioDrugs*. Published online June 29, 2018:1-13. doi:10.1007/s40259-018-0290-5
93. Lam JKW, Chow MYT, Zhang Y, Leung SWS. siRNA Versus miRNA as Therapeutics for Gene Silencing. *Mol Ther Nucleic Acids*. 2015;4. doi:10.1038/MTNA.2015.23
94. Bartel DP. MicroRNAs: Target Recognition and Regulatory Functions. *Cell*. 2009;136(2):215-233. doi:10.1016/j.cell.2009.01.002
95. Wijaya A, Schaffer SB, Pallares IG, Hamad-Schifferli K. Selective Release of Multiple DNA Oligonucleotides from Gold Nanorods. *ACS Nano*. 2009;3(1):80-86. doi:10.1021/nn800702n

96. Goodman AM, Hogan NJ, Gottheim S, Li C, Clare SE, Halas NJ. Understanding Resonant Light-Triggered DNA Release from Plasmonic Nanoparticles. *ACS Nano*. 2017;11(1):171-179. doi:10.1021/acsnano.6b06510
97. Maynard J, Georgiou G. Antibody engineering. *Annu Rev Biomed Eng*. 2000;2(2000):339-376. doi:10.1146/annurev.bioeng.2.1.339
98. Arruebo M, Valladares M, González-Fernández Á. Antibody-conjugated nanoparticles for biomedical applications. *J Nanomater*. 2009;2009. doi:10.1155/2009/439389
99. Grilo AL, Mantalaris A. The Increasingly Human and Profitable Monoclonal Antibody Market. *Trends Biotechnol*. 2019;37(1):9-16. doi:10.1016/j.tibtech.2018.05.014
100. Drugs@FDA: FDA-Approved Drugs. Accessed June 12, 2021. https://www.accessdata.fda.gov/scripts/cder/daf/index.cfm
101. Search of: monoclonal antibodies | Recruiting, Active, not recruiting Studies - List Results - ClinicalTrials.gov. Accessed March 21, 2021. https://clinicaltrials.gov/ct2/results?term=monoclonal+antibodies&Search=Apply&recrs=a&recrs=d&age_v=&gndr=&type=&rslt=
102. Lu RM, Hwang YC, Liu IJ, et al. Development of therapeutic antibodies for the treatment of diseases. *J Biomed Sci*. 2020;27(1):1-30. doi:10.1186/s12929-019-0592-z
103. Ryman JT, Meibohm B. Pharmacokinetics of monoclonal antibodies. *CPT Pharmacometrics Syst Pharmacol*. 2017;6(9):576-588. doi:10.1002/psp4.12224
104. Cui Y, Cui P, Chen B, Li S, Guan H. Monoclonal antibodies: formulations of marketed products and recent advances in novel delivery system. *Drug Dev Ind Pharm*. 2017;43(4):519-530. doi:10.1080/03639045.2017.1278768
105. Blanco E, Shen H, Ferrari M. Principles of nanoparticle design for overcoming biological barriers to drug delivery. *Nat Biotechnol*. 2015;33(9):941-951. doi:10.1038/nbt.3330
106. Silindir-Gunay M, Karpuz M, Ozturk N, Yekta Ozer A, Erdogan S, Tuncel M. Radiolabeled, folate-conjugated liposomes as tumor imaging agents: Formulation and in vitro evaluation. *J Drug Deliv Sci Technol*. 2019;50:321-328. doi:10.1016/j.jddst.2019.02.003
107. Guo P, You JO, Yang J, Jia D, Moses MA, Auguste DT. Inhibiting Metastatic Breast Cancer Cell Migration via the Synergy of Targeted, pH-triggered siRNA Delivery and Chemokine Axis Blockade. *Mol Pharm*. 2014;11(3):755-765. doi:10.1021/mp4004699
108. Guo P, Yang J, Liu D, et al. Dual complementary liposomes inhibit triple-negative breast tumor progression and metastasis. *Sci Adv*. 2019;5(3):eaav5010. doi:10.1126/sciadv.aav5010
109. Liu D, Guo P, McCarthy C, Wang B, Tao Y, Auguste D. Peptide density targets and impedes triple negative breast cancer metastasis. *Nat Commun*. 2018;9(1):1-11. doi:10.1038/s41467-018-05035-5

110. Valcourt DM, Dang MN, Scully MA, Day ES. Nanoparticle-Mediated Co-Delivery of Notch-1 Antibodies and ABT-737 as a Potent Treatment Strategy for Triple-Negative Breast Cancer. *ACS Nano*. 2020;14(3):3378-3388. doi:10.1021/acsnano.9b09263
111. Kumthekar P, Ko CH, Paunesku T, et al. A first-in-human phase 0 clinical study of RNA interference–based spherical nucleic acids in patients with recurrent glioblastoma. *Sci Transl Med*. 2021;13(584):eabb3945. doi:10.1126/scitranslmed.abb3945
112. Yang YSS, Moynihan KD, Bekdemir A, et al. Targeting small molecule drugs to T cells with antibody-directed cell-penetrating gold nanoparticles. *Biomater Sci*. 2019;7(1):113-124. doi:10.1039/c8bm01208c
113. Wang J, Dang MN, Day ES. Inhibition of Wnt signaling by Frizzled7 antibody-coated nanoshells sensitizes triple-negative breast cancer cells to the autophagy regulator chloroquine. *Nano Res*. 2020;13(6):1693-1703. doi:10.1007/s12274-020-2795-8
114. Ray M, Lee YW, Scaletti F, Yu R, Rotello VM. Intracellular delivery of proteins by nanocarriers. *Nanomedicine*. 2017;12(8):941-952. doi:10.2217/nnm-2016-0393
115. Lee YW, Luther DC, Kretzmann JA, et al. Protein delivery into the cell cytosol using non-viral nanocarriers. *Theranostics*. 2019;9(11):3280-3292. doi:10.7150/thno.34412
116. Qin X, Yu C, Wei J, et al. Rational Design of Nanocarriers for Intracellular Protein Delivery. *Advanced Materials*. 2019;31(46):1902791. doi:10.1002/adma.201902791
117. Dang MN, Gomez Casas C, Day ES. Photoresponsive miR-34a/Nanoshell Conjugates Enable Light-Triggered Gene Regulation to Impair the Function of Triple-Negative Breast Cancer Cells. *Nano Lett*. Published online December 11, 2020:acs.nanolett.0c03152. doi:10.1021/acs.nanolett.0c03152
118. Huang X, Pallaoro A, Braun GB, et al. Modular plasmonic nanocarriers for efficient and targeted delivery of cancer-therapeutic siRNA. *Nano Lett*. 2014;14(4):2046-2051. doi:10.1021/nl500214e
119. Gad SC, Sharp KL, Montgomery C, Payne JD, Goodrich GP. Evaluation of the toxicity of intravenous delivery of auroshell particles (Gold-Silica Nanoshells). *Int J Toxicol*. 2012;31(6):584-594. doi:10.1177/1091581812465969
120. Stern JM, Kibanov Solomonov V v., Sazykina E, Schwartz JA, Gad SC, Goodrich GP. Initial Evaluation of the Safety of Nanoshell-Directed Photothermal Therapy in the Treatment of Prostate Disease. *Int J Toxicol*. 2016;35(1):38-46. doi:10.1177/1091581815600170
121. Oldenburg, S.J.; Averitt, R.D.; Westcott, S.L.; Halas NJ. Nanoengineering of optical resonances. *Chem Phys Lett*. 1998;288(2-4):243-247. doi:10.1016/S0009-2614(98)00277-2

122. Jazayeri MH, Aghaie T, Nedaeinia R, Manian M, Nickho H. Rapid noninvasive detection of bladder cancer using survivin antibody-conjugated gold nanoparticles (GNPs) based on localized surface plasmon resonance (LSPR). *Cancer Immunology, Immunotherapy*. 2020;69(9):1833-1840. doi:10.1007/s00262-020-02559-y
123. Duff DG, Baiker A, Edwards PP. A New Hydrosol of Gold Clusters. 1. Formation and Particle Size Variation. *Langmuir*. 1993;9(9):2301-2309. doi:10.1021/la00033a010
124. Dang MN, Gomez Casas C, Day ES. Photoresponsive miR-34a/Nanoshell Conjugates Enable Light-Triggered Gene Regulation to Impair the Function of Triple-Negative Breast Cancer Cells. *Nano Lett*. 2021;21(1):68-76. doi:10.1021/acs.nanolett.0c03152
125. Melamed JR, Riley RS, Valcourt DM, Billingsley MM, Kreuzberger NL, Day ES. Quantification of siRNA Duplexes Bound to Gold Nanoparticle Surfaces. In: *Biomedical Nanotechnology: Methods and Protocols*. Humana Press, New York, NY; 2017:1-15. doi:10.1007/978-1-4939-6840-4_1
126. Billingsley MM, Riley RS, Day ES. Antibody-nanoparticle conjugates to enhance the sensitivity of ELISA-based detection methods. Xu B, ed. *PLoS One*. 2017;12(5):e0177592. doi:10.1371/journal.pone.0177592
127. Jerusalem G, Collignon J, Schroeder H, Lousberg L. Triple-negative breast cancer: treatment challenges and solutions. *Breast Cancer: Targets and Therapy*. 2016;8:93. doi:10.2147/BCTT.S69488
128. Denkert C, Liedtke C, Tutt A, von Minckwitz G. Molecular alterations in triple-negative breast cancer—the road to new treatment strategies. *The Lancet*. 2017;389(10087):2430-2442. doi:10.1016/S0140-6736(16)32454-0
129. Pogoda K, Niwińska A, Murawska M, Pieńkowski T. Analysis of pattern, time and risk factors influencing recurrence in triple-negative breast cancer patients. *Medical Oncology*. 2013;30(1):1-8. doi:10.1007/s12032-012-0388-4
130. DeSantis CE, Ma J, Gaudet MM, et al. Breast cancer statistics, 2019. *CA Cancer J Clin*. 2019;69(6):438-451. doi:10.3322/caac.21583
131. Li L, Yuan L, Luo J, Gao J, Guo J, Xie X. MiR-34a inhibits proliferation and migration of breast cancer through down-regulation of Bcl-2 and SIRT1. *Clin Exp Med*. 2013;13(2):109-117. doi:10.1007/s10238-012-0186-5
132. Beg MS, Brenner AJ, Sachdev J, et al. Phase I study of MRX34, a liposomal miR-34a mimic, administered twice weekly in patients with advanced solid tumors. *Invest New Drugs*. 2017;35(2):180-188. doi:10.1007/s10637-016-0407-y
133. Goyal R, Kapadia CH, Melamed JR, Riley RS, Day ES. Layer-by-Layer Assembled Gold Nanoshells for the Intracellular Delivery of miR-34a. *Cell Mol Bioeng*. Published online June 6, 2018:1-14. doi:10.1007/s12195-018-0535-x
134. Kapadia CH, Ioele SA, Day ES. Layer-by-layer assembled PLGA nanoparticles carrying miR-34a cargo inhibit the proliferation and cell cycle

progression of triple-negative breast cancer cells. *J Biomed Mater Res A*. Published online November 26, 2019:jbm.a.36840. doi:10.1002/jbm.a.36840
135. Fabbri M, Paone A, Calore F, Galli R, Croce CM. A new role for microRNAs, as ligands of Toll-like receptors. *RNA Biol*. 2013;10(2):169-174. doi:10.4161/rna.23144
136. Huschka R, Barhoumi A, Liu Q, Roth JA, Ji L, Halas NJ. Gene Silencing by Gold Nanoshell-Mediated Delivery and Laser-Triggered Release of Antisense Oligonucleotide and siRNA. *ACS Nano*. 2012;6(9):7681-7691. doi:10.1021/nn301135w
137. Riley RS, Dang MN, Billingsley MM, Abraham B, Gundlach L, Day ES. Evaluating the Mechanisms of Light-Triggered siRNA Release from Nanoshells for Temporal Control Over Gene Regulation. *Nano Lett*. Published online May 2, 2018:acs.nanolett.8b00681. doi:10.1021/acs.nanolett.8b00681
138. Rastinehad AR, Anastos H, Wajswol E, et al. Gold nanoshell-localized photothermal ablation of prostate tumors in a clinical pilot device study. *Proc Natl Acad Sci U S A*. 2019;116(37):18590-18596. doi:10.1073/pnas.1906929116
139. Paithankar D, Hwang BH, Munavalli G, et al. Ultrasonic delivery of silica-gold nanoshells for photothermolysis of sebaceous glands in humans: Nanotechnology from the bench to clinic. *Journal of Controlled Release*. 2015;206:30-36. doi:10.1016/j.jconrel.2015.03.004
140. Hatef A, Fortin-Deschênes S, Boulais E, Lesage F, Meunier M. Photothermal response of hollow gold nanoshell to laser irradiation: Continuous wave, short and ultrashort pulse. *Int J Heat Mass Transf*. 2015;89:866-871. doi:10.1016/j.ijheatmasstransfer.2015.05.071
141. Wang ML, Chiou SH, Wu CW. Targeting cancer stem cells: Emerging role of Nanog transcription factor. *Onco Targets Ther*. 2013;6:1207-1220. doi:10.2147/OTT.S38114
142. Jeter CR, Yang T, Wang J, Chao HP, Tang DG. Concise Review: NANOG in Cancer Stem Cells and Tumor Development: An Update and Outstanding Questions. *Stem Cells*. 2015;33(8):2381-2390. doi:10.1002/stem.2007
143. Poon L, Zandberg W, Hsiao D, et al. Photothermal Release of Single-Stranded DNA from the Surface of Gold Nanoparticles Through Controlled Denaturating and Au−S Bond Breaking. *ACS Nano*. 2010;4(11):6395-6403. doi:10.1021/nn1016346
144. Braun GB, Pallaoro A, Wu G, et al. Laser-Activated Gene Silencing via Gold Nanoshell−siRNA Conjugates. *ACS Nano*. 2009;3(7):2007-2015. doi:10.1021/nn900469q
145. Ahmadzada T, Reid G, McKenzie DR. Fundamentals of siRNA and miRNA therapeutics and a review of targeted nanoparticle delivery systems in breast cancer. *Biophys Rev*. 2018;10(1):69-86. doi:10.1007/s12551-017-0392-1

146. Ouyang B, Poon W, Zhang YN, et al. The dose threshold for nanoparticle tumour delivery. *Nat Mater*. Published online August 10, 2020:1-10. doi:10.1038/s41563-020-0755-z
147. Reya T, Clevers H. Wnt signalling in stem cells and cancer. *Nature 2005 434:7035*. 2005;434(7035):843-850. doi:10.1038/nature03319
148. Nagata T, Shimada Y, Sekine S, et al. KLF4 and NANOG are prognostic biomarkers for triple-negative breast cancer. *Breast Cancer*. 2017;24(2):326-335. doi:10.1007/S12282-016-0708-1
149. Lu X, Mazur SJ, Lin T, Appella E, Xu Y. The pluripotency factor nanog promotes breast cancer tumorigenesis and metastasis. *Oncogene 2014 33:20*. 2013;33(20):2655-2664. doi:10.1038/onc.2013.209
150. Wheatley SP, Altieri DC. Survivin at a glance. *J Cell Sci*. 2019;132(7). doi:10.1242/JCS.223826
151. Breast Cancer Ploidy and Cell Proliferation. Accessed August 30, 2022. https://www.cancer.org/cancer/breast-cancer/understanding-a-breast-cancer-diagnosis/ploidy-and-cell-proliferation.html
152. Mester J, Redeuilh G. Proliferation of breast cancer cells: regulation, mediators, targets for therapy. *Anticancer Agents Med Chem*. 2008;8(8):872-885. doi:10.2174/187152008786847747
153. Lee EYHP, Muller WJ. Oncogenes and Tumor Suppressor Genes. *Cold Spring Harb Perspect Biol*. 2010;2(10). doi:10.1101/CSHPERSPECT.A003236
154. Cooper GM. Tumor Suppressor Genes. Published online 2000. Accessed August 30, 2022. https://www.ncbi.nlm.nih.gov/books/NBK9894/
155. Dey N, Barwick BG, Moreno CS, et al. Wnt signaling in triple negative breast cancer is associated with metastasis. *BMC Cancer*. 2013;13(1):537. doi:10.1186/1471-2407-13-537
156. Survival Rates for Breast Cancer. Accessed July 13, 2022. https://www.cancer.org/cancer/breast-cancer/understanding-a-breast-cancer-diagnosis/breast-cancer-survival-rates
157. Leong SP, Naxerova K, Keller L, Pantel K, Witte M. Molecular mechanisms of cancer metastasis via the lymphatic versus the blood vessels. *Clinical & Experimental Metastasis 2021 39:1*. 2021;39(1):159-179. doi:10.1007/S10585-021-10120-Z
158. Feng Y, Spezia M, Huang S, et al. Breast cancer development and progression: Risk factors, cancer stem cells, signaling pathways, genomics, and molecular pathogenesis. *Genes Dis*. 2018;5(2):77. doi:10.1016/J.GENDIS.2018.05.001
159. Zhang Y, Zhang GL, Sun X, et al. Establishment of a murine breast tumor model by subcutaneous or orthotopic implantation. *Oncol Lett*. 2018;15(5):6233-6240. doi:10.3892/ol.2018.8113
160. Katsuta E, Demasi SC, Terracina KP, et al. Modified breast cancer model for preclinical immunotherapy studies. *Journal of Surgical Research*. 2016;204(2):467-474. doi:10.1016/j.jss.2016.06.003

161. Rashid OM, Nagahashi M, Ramachandran S, et al. An improved syngeneic orthotopic murine model of human breast cancer progression. *Breast Cancer Res Treat*. 2014;147(3):501-512. doi:10.1007/s10549-014-3118-0
162. PP S, V I, T S. Gold nanoshells: A ray of hope in cancer diagnosis and treatment. *Nucl Med Biomed Imaging*. 2017;2(2). doi:10.15761/NMBI.1000122

Appendix A

INSTITUTIONAL ANIMAL CARE AND USE COMMITTEE FORMS

A1. AUP Number: 1318 – 2018 – 1

University of Delaware
Institutional Animal Care and Use Committee
Annual Review

RECEIVED
JAN 2 2 2018
IACUC

Title of Protocol: Biodistribution of Functionalized Silica/Gold Nanoshells in Mice
AUP Number: 1318-2018-1 ← **(4 digits only)**
Principal Investigator: Emily Day
Common Name: mouse **Genus Species:** nu/nu mice

Pain Category: ***(please mark one)***

USDA PAIN CATEGORY: ***(Note change of categories from previous form)***

Category	Description
☐ B	Breeding or holding where NO research is conducted
☐ C	Procedure involving momentary or no pain or distress
☒ D	Procedure where pain or distress is alleviated by appropriate means (analgesics, tranquilizers, euthanasia etc.)
☐ E	Procedure where pain or distress cannot be alleviated, as this would adversely affect the procedures, results or interpretation

Official Use Only

IACUC Approval Signature: Glenn Tabler, DVM

Date of Approval: 3.1.18

A2. AUP Number: 1318 – 2020 – 0

University of Delaware
Institutional Animal Care and Use Committee
Application to Use Animals in Research
(New and 3-Yr submission)

RECEIVED
DEC 13 2019
IACUC JH

Title of Protocol: Analysis of Antibody/RNA Nanocarriers as Anti-Cancer Therapies	
AUP Number: 1318-2020-0	← (4 digits only — if new, leave blank)
Principal Investigator: Emily Day	
Common Name (Strain/Breed if Appropriate): nu/nu mice **Genus Species:** Mouse	
Date of Submission: December 12, 2019	

Official Use Only

IACUC Approval Signature: Talan, DVM

Date of Approval: 3.1.2020

Revised: 3/05/2019

Appendix B

PERMISSIONS TO SELF-AUTHORED PAPERS

B1. Advances in targeted nanotherapeutics: From bioconjugation to biomimicry

SPRINGER NATURE LICENSE
TERMS AND CONDITIONS

Aug 31, 2022

This Agreement between University of Delaware -- Megan Dang ("You") and Springer Nature ("Springer Nature") consists of your license details and the terms and conditions provided by Springer Nature and Copyright Clearance Center.

License Number	5379340530799
License date	Aug 31, 2022
Licensed Content Publisher	Springer Nature
Licensed Content Publication	Nano Research
Licensed Content Title	Advances in targeted nanotherapeutics: From bioconjugation to biomimicry
Licensed Content Author	Danielle M. Valcourt et al
Licensed Content Date	May 17, 2018
Type of Use	Thesis/Dissertation
Requestor type	academic/university or research institute
Format	print and electronic
Portion	full article/chapter
Will you be	no

translating?

Circulation/distribution	200 - 499
Author of this Springer Nature content	yes
Title	NANOPARTICLE-MEDIATED DELIVERY OF ANTIBODIES AND/OR RNA FOR GENE REGULATION IN TRIPLE-NEGATIVE BREAST CANCER
Institution name	University of Delaware
Expected presentation date	Sep 2022
Requestor Location	University of Delaware 590 Avenue 1743 Suite 442 NEWARK, DE 19713 United States Attn: University of Delaware
Total	0.00 USD

B2. Polymer nanocarriers for MicroRNA delivery

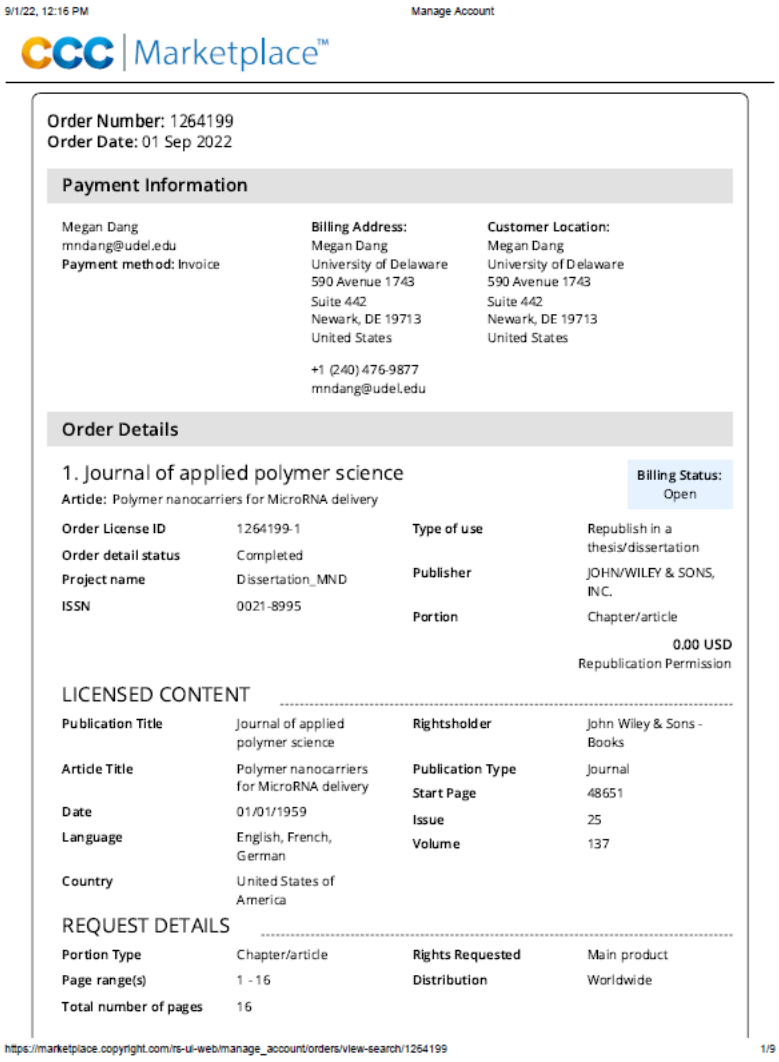

9/1/22, 12:16 PM Manage Account

CCC Marketplace™

Order Number: 1264199
Order Date: 01 Sep 2022

Payment Information

Megan Dang
mndang@udel.edu
Payment method: Invoice

Billing Address:
Megan Dang
University of Delaware
590 Avenue 1743
Suite 442
Newark, DE 19713
United States

+1 (240) 476-9877
mndang@udel.edu

Customer Location:
Megan Dang
University of Delaware
590 Avenue 1743
Suite 442
Newark, DE 19713
United States

Order Details

1. Journal of applied polymer science

Billing Status: Open

Article: Polymer nanocarriers for MicroRNA delivery

Order License ID	1264199-1	**Type of use**	Republish in a thesis/dissertation
Order detail status	Completed		
Project name	Dissertation_MND	**Publisher**	JOHN/WILEY & SONS, INC.
ISSN	0021-8995	**Portion**	Chapter/article

0.00 USD
Republication Permission

LICENSED CONTENT

Publication Title	Journal of applied polymer science	**Rightsholder**	John Wiley & Sons - Books
Article Title	Polymer nanocarriers for MicroRNA delivery	**Publication Type**	Journal
		Start Page	48651
Date	01/01/1959	**Issue**	25
Language	English, French, German	**Volume**	137
Country	United States of America		

REQUEST DETAILS

Portion Type	Chapter/article	**Rights Requested**	Main product
Page range(s)	1 - 16	**Distribution**	Worldwide
Total number of pages	16		

https://marketplace.copyright.com/rs-ui-web/manage_account/orders/view-search/1264199 1/9

Format (select all that apply)	Print, Electronic	Translation	Original language of publication
Who will republish the content?	Academic institution	Copies for the disabled?	No
Duration of Use	Life of current edition	Minor editing privileges?	No
Lifetime Unit Quantity	Up to 499	Incidental promotional use?	No
		Currency	USD

NEW WORK DETAILS

Title	NANOPARTICLE-MEDIATED DELIVERY OF ANTIBODIES AND/OR RNA FOR GENE REGULATION IN TRIPLE-NEGATIVE BREAST CANCER	Institution name	University of Delaware
		Expected presentation date	2022-09-12
Instructor name	Megan Dang		

ADDITIONAL DETAILS

The requesting person / organization to appear on the license	Megan Dang / University of Delaware

REUSE CONTENT DETAILS

Title, description or numeric reference of the portion(s)	Polymer nanocarriers for MicroRNA delivery	Title of the article/chapter the portion is from	Polymer nanocarriers for MicroRNA delivery
Editor of portion(s)	Kapadia, Chintan H.; Luo, Benjamin; Dang, Megan N.; Irvin-Choy, N'Dea; Valcourt, Danielle M.; Day, Emily S.	Author of portion(s)	Kapadia, Chintan H.; Luo, Benjamin; Dang, Megan N.; Irvin-Choy, N'Dea; Valcourt, Danielle M.; Day, Emily S.
Volume of serial or monograph	137	Publication date of portion	2020-07-05
Page or page range of portion	48651		

B3. Nanoparticles for Manipulation of the Development Wnt, Hedgehog, and Notch Signaling Pathways in Cancer

translating?

Circulation/distribution	200 - 499
Author of this Springer Nature content	yes
Title	NANOPARTICLE-MEDIATED DELIVERY OF ANTIBODIES AND/OR RNA FOR GENE REGULATION IN TRIPLE-NEGATIVE BREAST CANCER
Institution name	University of Delaware
Expected presentation date	Sep 2022
Requestor Location	University of Delaware 590 Avenue 1743 Suite 442 NEWARK, DE 19713 United States Attn: University of Delaware
Total	0.00 USD

B4. Photoresponsive miR-34a/Nanoshell Conjugates Enable Light-Triggered Gene Regulation to Impair the Function of Triple-Negative Breast Cancer Cells

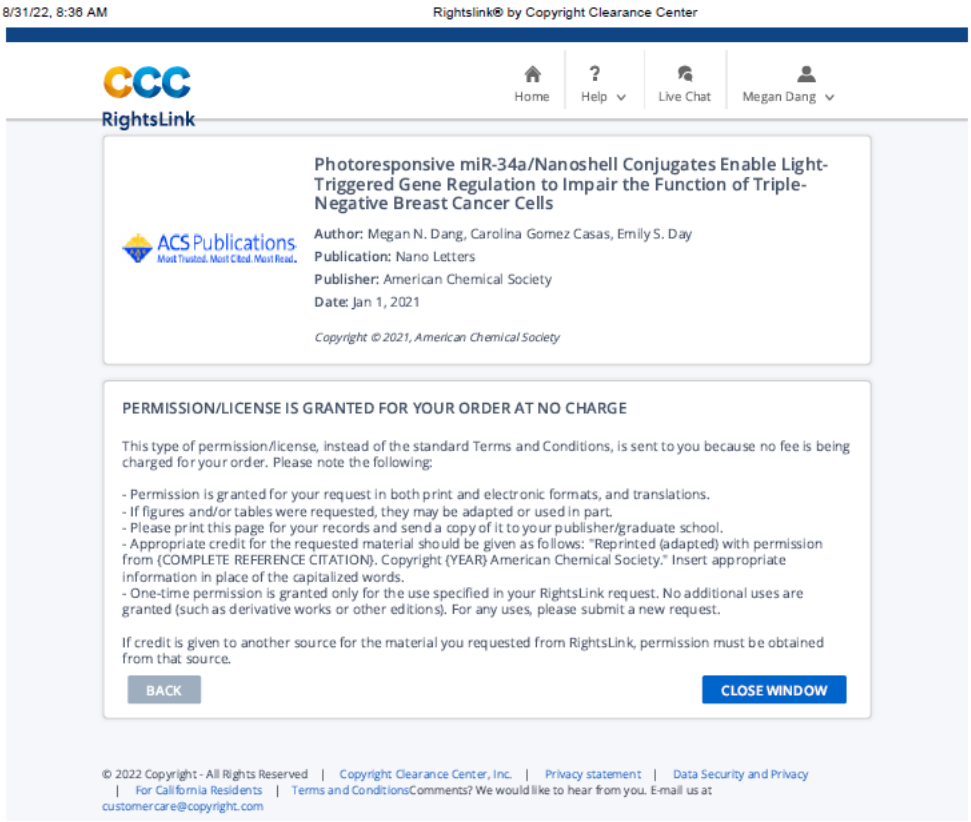

B5. Antibody nanocarriers for cancer management

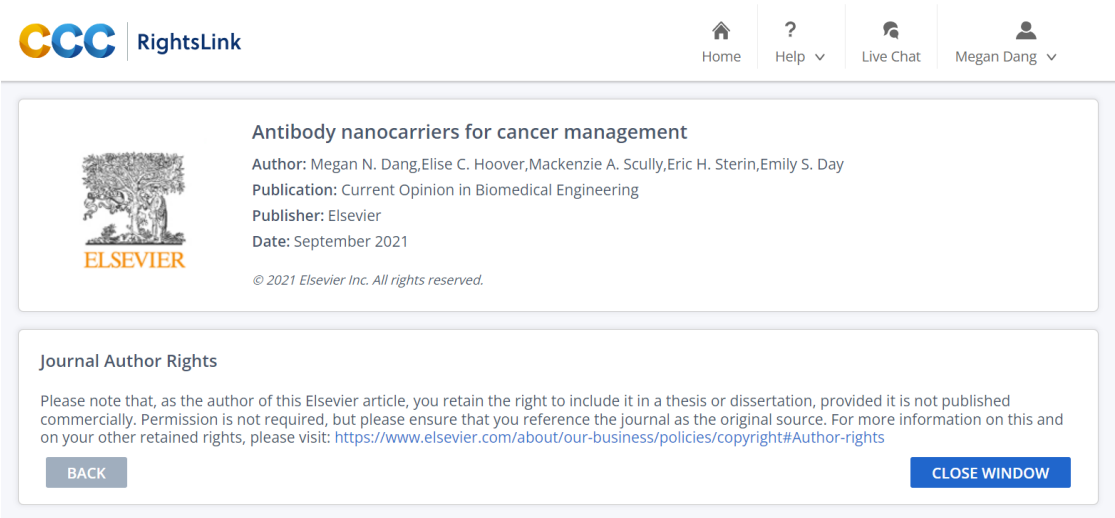

Copyright

Overview Author rights Institution rights Government rights Find out more

Overview

In order for Elsevier to publish and disseminate research articles, we need certain publishing rights from authors, which are determined by a publishing agreement between the author and Elsevier.

For articles published open access, the authors license exclusive rights in their article to Elsevier where a CC BY-NC-ND end user license is selected, and license non-exclusive rights where a CC BY end user license is selected.

For articles published under the subscription model, the authors typically transfer copyright to Elsevier. In some circumstances, authors may instead grant us (or the learned society for whom we publish) an exclusive license to publish and disseminate their work.

Regardless of whether they choose to publish open access or subscription with Elsevier, authors have many of the same rights under our publishing agreement, which support their need to share, disseminate and maximize the impact of their research.

For open access articles, authors will also have additional rights, depending on the Creative Commons end user license that they select. This Creative Commons license sets out the rights that readers (as well as the authors) have to re-use and share the article: please see here (https://www.elsevier.com/about/policies/open-access-licenses) for more information on how articles can be re-used and shared under these licenses.

This page aims to summarise authors' rights when publishing with Elsevier; these are explained in more detail in the publishing agreement between the author and Elsevier.

Irrespective of how an article is published, Elsevier is committed to protect and defend authors' works and their reputation. We take allegations of infringement, plagiarism, ethical disputes, and fraud very

Author rights

The below table explains the rights that authors have when they publish with Elsevier, for authors who choose to publish either open access or subscription. These apply to the corresponding author and all co-authors.

Author rights in Elsevier's proprietary journals	Published open access	Published subscription
Retain patent and trademark rights	√	√
Retain the rights to use their research data freely without any restriction	√	√
Receive proper attribution and credit for their published work	√	√
Re-use their own material in new works without permission or payment (with full acknowledgement of the original article): 1. Extend an article to book length 2. Include an article in a subsequent compilation of their own work 3. Re-use portions, excerpts, and their own figures or tables in other works.	√	√
Use and share their works for scholarly purposes (with full acknowledgement of the original article): 1. In their own classroom teaching. Electronic and physical distribution of copies is permitted 2. If an author is speaking at a conference, they can present the article and distribute copies to the attendees 3. Distribute the article, including by email, to their students and to research colleagues who they know for their personal use 4. Share and publicize the article via Share Links, which offers 50 days' free access for anyone, without signup or registration 5. Include in a thesis or dissertation (provided this is not published commercially) 6. Share copies of their article privately as part of an invitation-only work group on commercial sites with which the publisher has a hosting agreement	√	√
Publicly share the preprint on any website or repository at any time.	√	√